PHASE TRANSITIONS, CRITICAL PHENOMENA, AND APPLICATIONS TO RESILIENCE AND TIPPING POINTS IN COMPLEX NETWORKS

Cheng Ma

Submitted in Partial Fullfillment of the Requirements
for the Degree of

DOCTOR OF PHILOSOPHY

Approved by:
Gyorgy Korniss, Chair
Boleslaw K. Szymanski, Co-chair
Jianxi Gao, Co-chair
Vincent Meunier

Department of Department of Physics, Applied Physics, and Astronomy
Rensselaer Polytechnic Institute
Troy, New York

[May 2024]

CONTENTS

LIST OF FIGURES

ACKNOWLEDGMENT

Reflecting on my journey of study and research over the past five years at RPI, I am reminded of the challenges and hurdles I faced when embarking on my research endeavors. From the initial stages of my first research project, I recall the struggles and hours spent grappling with unexpected experimental results. However, as I near the completion of my Ph.D. studies, I am filled with a sense of accomplishment and gratitude. I recognize that I would not have made it this far without the support and guidance of my advisors, the help from friends in Troy, and also the understanding and love from my family in China.

First and foremost, I would like to thank my advisor, Dr. Gyorgy Korniss, for his invaluable mentorship and support throughout this journey. Dr. Korniss, I am truly grateful for the freedom you granted me to explore my own research interests while always being readily available to offer help and insight whenever needed. Your dedication to details and passion for science have served as a constant source of inspiration, motivating me to strive for excellence in my work. I would also like to extend my gratitude to the other members of my thesis committee. To my co-advisor, Dr. Boleslaw Szymanski, I am thankful for your lively ideas and discussions, which have encouraged me to explore new research avenues when I was inclined to settle for the outcomes already attained. To my co-advisor, Dr. Jianxi Gao, I am deeply appreciative of insightful research ideas you have shared with me, which have significantly shaped my research direction. Thank you for encouraging me to achieve high standards beyond what I initially thought possible. To Dr. Vincent Meunier, thank you for your generous help and advice from the related research field.

Further I would like to thank my lab mates, Chunheng, Omar, and Mav. Our discussions have been valuable learning experiences to me, providing me with fresh insights and inspiration for my research. I would also like to thank all my friends in Troy for helping make this journey more enjoyable than I could have imagined. Special thanks to my dear friends, Wanjing, Zerui, Shengguang, Zhizhuo, and Shuang, for providing the support and companionship that allowed me to take much-needed breaks from research. Our shared experiences have created countless cherished memories, making Troy feel like a second home to me.

Finally, I would like thank all my family in China for your understanding, love and support. In particular, I want to extend my deepest appreciation to my father, whose

unwavering encouragement has been a constant source of strength for me. You have always supported me in every endeavor I have pursued, and I am forever grateful for your belief in me. This thesis is dedicated to you!

ABSTRACT

The recognition of tipping points, where complex systems undergo abrupt shifts to distinct states, underscores the importance of understanding critical transitions in networked systems. These transitions may pose risks, as they can lead to unintended collapses, resulting in damage and losses across environmental, economic, and public health domains if timely corrective measures are not implemented. Conversely, critical transitions also present opportunities for positive change. While the surprises inherent in sudden shifts will persist, continuous efforts in this field aim to enhance our ability to foresee and respond to these pivotal moments in dynamic and interconnected systems.

Our first investigation of these focuses on critical transitions in lattice-based ecological systems. Given that many systems may shift to undesired states due to internal failures or external perturbations, with critical transitions towards degraded ecosystem states being prominent examples, resilience restoration becomes crucial. Resilience restoration focuses on the ability of networked systems and the required time to recover to their desired states under stochastic environmental conditions. Our research has shown that nucleation theory can be employed to advance the understanding of resilience restoration in spatially-embedded ecological systems, overcoming some common difficulties, such as high dimensionality, nonlinearity, and stochastic effects. We find that systems may exhibit single-cluster or multi-cluster phases based on their sizes and noise strengths. Furthermore, we also discover a scaling law governing restoration time for arbitrary system sizes and noise strengths in two-dimensional lattice systems. Importantly, this approach could extend beyond ecosystems, finding applications in various dynamical systems spanning biology to infrastructural systems.

Subsequently, our attention shifts towards the challenge of reducing the complexity and dimensionality of networks with diverse topologies. The formidable barriers posed by high dimensionality and nonlinear dynamics often impede theoretical analyses of system evolution and critical transitions in interconnected networks, a crucial aspect in comprehending the stability, resilience, and control of complex networked systems. Recent attempts at dimension reduction have sought to simplify the system by mapping it to a one-dimensional representation, allowing for the capture of macroscopic dynamics by a single effective representative. However, these approaches encounter significant limitations when applied to heterogeneous networks with multiple community structures. Our study addresses this gap

by introducing a generalized dimension reduction approach. This novel method enables the mapping of the original system to an m-dimensional system, comprising m interacting components. Noteworthy is the successful validation of this approach across various dynamical models, showcasing its ability to accurately predict the original system state and identify tipping points, if any. Numerical results further illustrate the efficacy of this approach in approximating system evolution and pinpointing critical points in the context of complex networks featuring time delays.

Finally, we turn our attention to critical transitions in social opinion dynamics, employing the Naming Game model as our framework, which is widely recognized as a classic model for examining the emergence and evolution of language within a population. Specifically, we extend the model to accommodate multiple committed opinions and analyze its dynamics on a complete graph and also random networks. Applying mean-field theory under homogeneous mixing conditions allows us to analyze the opinion evolution on a complete graph systematically. However, as the number of distinct opinions increases, the exponential growth in the number of variables describing the system presents a challenge. We concentrate our focus on a unique scenario wherein the largest group of committed agents competes with smaller committed groups, each substantially smaller than the largest one. Simultaneously, the majority of uncommitted agents initially hold another single unique opinion. This scenario is chosen for its recurrent appearance in various societies and for its inherent complexity, which can be mitigated by consolidating agents from all small committed groups into one single committed group. Our findings reveal a phase transition when the largest committed fraction dominates the system. The threshold for the size of the dominant group, triggering this transition, depends on the size of the committed group within the unified category. Furthermore, a general formula for multi-opinion evolution is derived through a recursive approach. To complement our analytical work, we utilize agent-based simulations to unveil the opinion evolution in random graphs. These results offer valuable insights into the conditions fostering the emergence of dominant opinions within a population, shedding light on the influencing factors that shape this transition.

CHAPTER 1
INTRODUCTION

In this introductory chapter, we provide an overview of fundamental concepts essential for the research presented in chapters 2-4. We start with a general exploration of networks, highlighting their mathematical properties and providing examples of regular lattice and random networks. Following this, we overview the concept of resilience and critical transitions/shifts in dynamical networks, offering some insights into a system's capacity for recovery and adaptability. Finally, we introduce the dynamics of opinion influence using the Naming Game model, which serves as an example of critical shifts in social systems.

1.1 Networks

A network (or graph in the mathematical literature) is a collection of nodes (or vertices) joined by edges (links/connections) [1]. In our exploration, we only focus on simple networks, excluding two types of edges, self-edges that connect nodes to themselves, and multiedges where more than one edge joining the same pair of nodes. The fundamental mathematical representation of a simple network is encapsulated in the adjacency matrix denoted as A. It is defined as an $N \times N$ matrix for a network with N nodes, where each element A_{ij} is set to 1 if there exists an edge between nodes i and j, and 0 otherwise [2]. Also, we only consider undirected networks, meaning that $A_{ij} = A_{ji}$ holds all time, and therefore, the adjacency matrix of such networks remains symmetric.

Another fundamental and widely used concept in network theory is degree. The degree k_i of node i is defined as the number of edges connected to it, and it can be written in the form of adjacency matrix A,

$$k_i = \sum_{j=1}^{N} A_{ij}. \tag{1.1}$$

The average degree $\langle k \rangle$ of an undirected network is then expressed as

$$\langle k \rangle = \frac{1}{N} \sum_{i=1}^{N} k_i. \tag{1.2}$$

This average degree provides insights into the network's density, indicating the sparse or dense connections. Building on the concept of node degree, we can easily derive the degree

distribution $P(k)$, which is defined as the fraction of nodes in a network with degree k, or a randomly picked node in a network has a degree of k in the probabilistic context [1],

$$P(k) = \frac{N_k}{N}. \tag{1.3}$$

Degree distribution serves as a crucial signature of network structure. While not complete, it provides rich information about the network's architecture. Next, we will cover several types of networks integral to our study, each characterized by a distinct degree distribution.

1.1.1 Regular lattice

Let us begin our exploration with the simplest network, the regular lattice, characterized by its highly ordered and symmetric structure. Such network is embedded in a Euclidean space R^n and exhibits a remarkable level of symmetry. Notably, each node in the lattice possesses an identical degree, resulting in a trivial degree distribution [3]. Furthermore, when the lattice extends infinitely in space, it attains translational invariance, ensuring that all nodes play an equal role in the network structure and its dynamics. In one of the following studies, we will investigate the dynamics and resilience within a specific instantiation of such a network, the 2D regular lattice.

1.1.2 Erdős-Rényi networks

We then introduce an element of randomness to node connections, leading us to the famous Erdős-Rényi (ER) random networks, named in honor of mathematicians Paul Erdős and Alfréd Rényi, who first systematically studied this model [4]. By fixing the number of nodes N and selecting M distinct pairs of nodes uniformly at random from all possible pairs to form M edges, we create a random graph denoted as $G(N, M)$. Alternatively, a slightly different approach involves fixing the probability of edges between N nodes instead of the number of pairs. For each possible pair of nodes, there is an independent probability p to form an edge, resulting in a random network ensemble, denoted as $G(N, p)$. One can easily show that the average degree for these two variations are $\langle k \rangle = \frac{M}{2N}$ for $G(N, M)$ and $\langle k \rangle = (N-1)p$, respectively. Here, we use the $G(N, p)$ model to show the degree distribution,

which follows a binomial distribution, given by,

$$p(k) = \binom{N-1}{k} p^k (1-p)^{N-1-k}. \tag{1.4}$$

In the scenario of a sparse large network (in the limit of $N \to \infty$, $p \to 0$), it can be demonstrated that the degree distribution approximately follows a Poisson distribution [1], expressed as

$$P(k) \approx e^{-\langle k \rangle} \frac{\langle k \rangle^k}{k!}. \tag{1.5}$$

1.1.3 Scale-free networks

For numerous real-world systems, ranging from cellular structures to societal networks and the Internet, connections between components are not completely random, rendering Erdős-Rényi (ER) networks less suitable for modeling these complex systems. Over the last two decades, empirical evidence reveal that many real networks exhibit a power-law degree distribution [5], [6], a remarkable deviation from the conventional Poisson distribution (1.5),

$$P(k) \sim k^{-\gamma}. \tag{1.6}$$

In these networks, the majority of nodes possess only a few connections, while a small number of highly connected hubs serve to link these numerous smaller nodes. Commonly referred to as scale-free networks, networks with the exponent $\gamma < 3$ exhibit infinite degree fluctuations, lacking a meaningful internal scale and characteristically being "scale-free" [2].

There are also other types of networks uncovered in real-world systems [7], including small-world network model, initially proposed by Duncan Watts and Steven Strogatz [8]. This model integrates characteristics from both regular lattices and random graphs. For instance, in a social network, most individuals have close friends nearby, forming local clusters seen in regular lattices. Simultaneously, they also maintain a few connections with people in distant locations, fostering global connectivity, a feature reminiscent of the long-range edges observed in random graphs.

1.2 Dynamics and resilience

Despite the profound diversity in the scale and purpose of networks observed in nature and technology [1], [2], [9], their topology exhibits several highly reproducible and often universal characteristics: many real networks display the small-world property [8], are scale-free [5], [6], and develop distinct community structures [10], [11]. When it comes to the dynamical processes occurring on these networks, studies on synchronization, spreading processes, and spectral phenomena have provided important insights into the interplay between network topology and dynamics. Additionally, recent efforts have explored universal patterns in the dynamics of various complex systems [12]. In this context, we will introduce a commonly used framework for exploring the resilience and simplification of complex systems in the later chapters.

1.2.1 Network dynamics

For a networked system consisting of N nodes, one can use the following mathematical framework to describe the node activity $x_i(t)$,

$$\frac{\mathrm{d}x_i}{\mathrm{d}t} = F(x_i) + \sum_{j=1}^{N} A_{ij} G(x_i, x_j). \tag{1.7}$$

The first term $F(x_i)$ on the right-hand side of Eq. (1.7) describes the self-dynamics, encompassing processes like influx, degradation or reproduction. Also, each node is influenced by its neighbouring node j, capturing by the second term $G(x_i, x_j)$, representing pairwise interactions. The adjacency matrix A is determined by the connectivity between components and the network topology. With the appropriate choice of functions $F(x_i)$ and $G(x_i, x_j)$, this framework can be mapped into many different dynamical models, including ecological systems, epidemic spreading, biological dynamics, and social influencing.

Additionally, utilizing this framework, one can investigate network dynamics in various conditions, including dynamics in the presence of perturbations, time delays, external controls, to gain insights into network resilience. For instance, in an ecological network, the introduction of a new species or the removal of a predator can be considered a perturbation. Studying how the network responds to such changes falls under this category. It also serves a backbone for network simplification, allowing one to explore the network reduction while maintaining the predictability on the original system dynamics.

1.2.2 Resilience and critical transitions

This thesis focuses specifically on the research theme of network resilience and the associated critical transitions by employing the general framework of network dynamics. Many systems on our planet shift abruptly and irreversibly from the desired state to an undesired state due to external perturbations or internal failures. Some examples of critical transitions are mass extinctions within ecosystems, cascading failures in infrastructure systems, and changes in human and animal social networks. Often, these transitions are associated with a "tipping point", where the system crosses a threshold and then it undergoes a critical transition [13].

Therefore, it is important to investigate the system resilience, as it defines a system's ability to withstand the presence of errors, adapt to disturbances, and maintain its functionality or recover quickly when faced with external perturbations [14], [15]. For instance, in ecological networks, network resilience is crucial for maintaining biodiversity and ecosystem stability. Critical transitions may occur when key species go extinct or face drastic changes in population dynamics, leading to cascading effects on other species and potentially causing the ecosystem to shift to an alternative undesired state. Understanding network resilience and critical transitions is essential for designing robust and adaptive systems across various domains, from ecology to technological networks.

1.2.3 Dimension reduction

In the realm of real-world systems, spanning from ecological webs to neuronal networks and infrastructure systems, the sheer complexity arises from a multitude of interconnected components [1], [2]. To gain a comprehensive understanding of system resilience, stability, and the emergence of spreading phenomena, it becomes imperative to quantitatively grasp the system's evolution. However, as the number of components escalates and system intricacy amplifies, such endeavors encounter increasing challenges. Analytical tools may be elusive, and computational demands may become prohibitively vast.

A promising avenue to tackle these challenges involves the application of dimension reduction. This strategy aims to transform the dynamics of an original system comprising N nodes, as defined in Eq. (1.7), into a simplified version characterized by a substantially reduced number of effective components, denoted as m (where $m \ll N$). The primary objective is to preserve key properties of the original dynamics, including global behavior

and critical transitions.

By distilling the essence of system behavior into a more manageable form, dimension reduction provides a pathway to overcome the computational hurdles and analytical complexities associated with large-scale systems. Recent studies have sought to develop the dimension reduction framework for homogeneous networks by employing methods such as mean-field theory or the eigenvalue-based approach [16], [17]. However, ongoing research is essential to develop a more general framework applicable to diverse network structures, especially heterogeneous networks.

1.2.4 Social dynamics and social influencing

Network science has also found valuable applications in comprehending social dynamics, including opinion formation, and language evolution. These complex phenomena are often modeled in terms of a small set of variables whose dynamics is determined by social interactions between a set of connected individuals/agents taking place on a networked system. Such general framework enables the exploration of social behavior, the spread of cultural norms, and the emergence of consensus [18]. The emerging tipping points and nonlinear properties, which underpin the most interesting characteristics of social systems, are investigated through an array of tools ranging from the agent-based model to mean-field theory [19].

Recent studies have increasingly involved the presence of zealots in opinion dynamics for understanding their impact on the resilience of consensus and their crucial role in critical transitions [20], [21], [22]. Often referred to as committed agents, those individuals never change their opinions while actively seeking adoption of their own opinion by others. The phenomenon of zealotry resonates across diverse disciplines, exemplified by religious zealots who maintain their faith and actively influence others to adopt their beliefs, resulting in the formation of distinct religious communities with shared values and practices. In the realm of online social networks, influencers dedicated to promoting specific ideologies, products, or lifestyles also embody zealots. Their commitment significantly shapes the opinions and behaviors of their followers, contributing to the emergence of consensus within their respective communities.

In this thesis, our focus will be specifically on the Naming Game (NG) with the presence of committed agents for understanding language formation, opinion dynamics and consen-

sus emergence. Initially designed to simulate the formation of a vocabulary from different observations, the NG model has demonstrated how a population of agents can collectively converge to a single unique word for labeling different objects or observations in their environment [23]. In the NG model, agents have only peer-to-peer pairwise interactions without central control, but nevertheless manage to reach a global consensus. Recent applications extend the NG model to explore the dynamics of social influence and the evolution of competing opinions [21], [24]. The exploration of such opinion dynamics model provides not only theoretical insights but also practical applications for understanding and navigating complex social systems.

CHAPTER 2
UNIVERSALITY OF NOISE-INDUCED RESILIENCE RESTORATION IN SPATIALLY EXTENDED ECOLOGICAL SYSTEMS

2.1 Introduction

Resilience, a system's ability to retain its basic functionality when errors and failures occur, is a defining property of many complex systems [14], [15], [16]. Theoretical models of resilience loss and transitions between alternative states are used to study unanticipated and drastic changes. In real-world systems, many critical transitions are observed, including catastrophic shifts in ecological systems [25], [26], blackouts in power grids [27], financial crises [28], climate changes [29], human depression [30]. These abrupt shifts may arise in the presence of alternative stable states. They can be modeled as critical transitions causing the resilience loss of the desired state, after which the systems switch from functional to a dysfunctional state [31], [32], [33]. Ecologists are particularly concerned about sudden critical switches between alternative stable states [25], [26]. As the system approaches the tipping point, its behavior becomes barely predictable when the gradual change of some environmental factors leads to the drastic change of the system state. Once a system loses its resilience and becomes dysfunctional, restoring the environmental conditions only to those existing before the collapse is often insufficient. Instead, environmental conditions should be recovered to the critical point where the undesired state is destabilized and then resilience restoration would occur. In this work, we study the resilience restoration in spatially-extended ecosystems, which focuses on a system's ability and required time to recover to its desired state after the transition to the undesired state. Even though various restoration methods targeted at specific systems have been proposed, stochastic perturbations receive little attention [34], [35], [36]. On the other hand, stability of stochastic dynamical systems containing only one variable has been extensively explored. Also, it has been known for a long time that noise can greatly affect the stability and resilience of the system with bistable states. In particular, it has been shown that noise can induce transitions between alternative stable states and the

Portions of this chapter previously appeared as: C. Ma, G. Korniss, B. K. Szymanski, and J. Gao, "Universality of noise-induced resilience restoration in spatially-extended ecological systems," *Commun. Phys.*, vol. 4, pp. 1–12, Dec. 2021.

required time to transition has been established by computing the mean first passage time (MFPT) [15], [37], [38], [39]. Those studies indicate that the single-variable systems can switch between alternative stable states in the presence of noise. One may expect that noise can also induce transitions in multi-variable systems. However, one should keep in mind that such noise-induced transition occurs only when the system is close to the bifurcation point where the basin of attraction of the current stable state is close to vanishing. If the system is far from this bifurcation point, noise may drive the system back and forth between alternative stable states, or even not be able to trigger any transition. Since environmental stochasticity is an inherent property of real-world ecosystems, we investigate resilience restoration after introducing stochastic perturbations into multi-variable systems, providing a theoretical understanding of critical transitions in spatially-extended systems subject to environmental stochasticity.

Despite advances in understanding the macroscopic characteristics of resilience restoration, previous research has mostly focused on single-variable or low-dimensional systems, which do not account for the exceptionally large number of variables that in reality are needed to control the state of a complex system. Indeed, many real-world systems consist of numerous components connected via a complex set of weighted, often directed, interactions [2]. The complicated interactions may lead to phenomena not arising in single-variable systems. For example, in the ecosystems, the recovery (or extinction) of a species in one location can impact the states of this species in the neighboring locations, leading to a recovery (or extinction) over the entire system [40]. Accordingly, a full understanding of the system evolution, stability, and resilience cannot be gained without considering interactions among a sufficiently large number of components. However, hindered by the high-dimensionality of interaction topology and the nonlinear evolution dynamics, few analyses of critical transitions and resilience restoration had been done directly on high-dimensional systems consisting of a great number of participants until the effective reduction theory was recently developed by Gao *et.al.* [16]. This theory enables us to effectively reduce a multi-dimensional complex system to a one-dimensional system by capturing the average activities of the original system. Furthermore, Liang *et.al.* [41] designed a universal indicator for critical transitions in complex networks and concluded that noise compensates for the structural defects of complex networks, indicating that noise may alter the critical threshold. Jiang *et.al.* [42] studied mutualistic networks through dimensional reduction and claimed that the tipping

point can be predicted accurately even in the presence of noise. Tu *et.al.* [43] developed an analytical framework for collapsing complex N-dimensional networked systems into an $M+1$-dimensional manifold as a function of M effective control parameters with $M \ll N$. Nonetheless, our study shows that noise eliminates the deterministic critical threshold, and the recovery of the entire system from the dysfunctional state is possible in the presence of perturbations as long as noise is strong enough to trigger the transition for just one component. This scenario is very likely to occur when the system is close to the deterministic threshold where the undesired state loses stability. The farther away the system is from this point, the more difficult it is for noise to induce the transition.

The time required to recover a system is a quantity of great interest but determined by many factors, including system sizes, noise strengths, and dynamical functions. Nucleation theory provides an elegant bridge between the noise-induced transition and the spread of such transition over the entire system. The classical approach to homogeneous nucleation theory was originally developed to describe phase transformation in materials [44], [45], [46], [47], in particular in ferromagnetic [48], [49] and ferroelectric systems [50], [51]. Recently, it was applied to invasion phenomena in spatial ecological systems [52], [53], [54], [55]. Korniss *et.al.* [53] and O'Malley *et.al.* [54] studied ecological invasion in spatially-extended systems with competition. They discriminate between two fundamental modes of nucleating invasive clusters (single-cluster vs. multi-cluster) and their time-evolution and stochastic features. A more recent study by Michaels *et.al.* [56] combined nucleation theory with local-scale positive feedback and offered a novel way to understand transitions and resilience in ecological systems. The theory of nucleation and growth describes how clusters are generated and spread out [48]. Our study reveals the crucial effects of noise strength and system size on transition features. Generally, the stronger noise triggers the transition faster, and the larger system takes less time to recover compared with the smaller system under the same intensity of noise. For large systems or under strong noise, there are multiple clusters nucleated simultaneously in the beginning, and these clusters spread out to their neighbors and to the whole system. Our numerical simulations reveal that the transition time is narrowly centered at an average value, signaling a deterministic feature. For small systems or under weak noise, one cluster is generated first, which expands until the entire system finishes transitions. The transition times vary stochastically for different realizations of noise, and they universally follow an exponential distribution.

2.2 Mathematical framework

The current analytical framework for noise-induced transitions is specifically targeted at the low-dimensional system consisting of only a few interacting components (or only one variable) [33], [37], [57], [58], [59]. It would be highly challenging to directly analyze the system consisting of many interacting components (for example, the square lattice). Before the investigation of multi-variable systems, it is helpful to understand the role of noise in single-variable systems and the possibility of transitions between alternative stable states.

2.2.1 Single-variable system

For a single-dimensional system, the dynamics may follow the general form as,

$$\frac{\mathrm{d}x}{\mathrm{d}t} = f(x, \beta) + \eta(t). \tag{2.1}$$

In Eq. (2.1), $f(x, \beta)$ governs the deterministic dynamics as the tunable parameter β captures the changing conditions, and $\eta(t)$ is delta-correlated noise with zero mean and variance $\langle \eta(t)\eta(t') \rangle = \sigma^2 \delta(t - t')$, where σ is the standard deviation of the noise, which is referred to as noise strength. If the system has a fixed point, x_0, it satisfies $f(x_0, \beta) = 0$. This fixed point is stable if $\frac{\partial f(x,\beta)}{\partial x}\Big|_{x_0} < 0$, defined by the linear stability condition. These two equations enable us to derive the resilience function $x(\beta)$, which represents all the possible steady states of the system as a function of β, as shown in Fig. 2.1a. This resilience function demonstrates that when the control parameter, β, is greater than β_{c_2}, the system only has one stable fixed point, denoted as x_{H}, indicating a resilient state. The system will always recover to the fixed point, x_{H}, for any state perturbations. When the parameter is less than β_{c_1}, the system also has a single fixed point, x_{L}, indicating a collapse of the system. The system is not restorable, unless we change the parameter β. In this work, we particularly focus on the parameter space where β is between β_{c_1} and β_{c_2} and close to one of the bifurcation points, such that the system has one unstable fixed point (the dashed line) and two stable fixed points, each with very different sizes of basin of attraction. In the absence of noise, to trigger the shift from x_{L} to x_{H}, the environmental conditions would need to be restored all the way to β_{c_2}, to allow for a transition back to x_{H}. However, noise of the appropriate intensity can trigger the transition without restoring the condition to β_{c_2}. For example, for a system with β_1 and the system is in the low state, this system can recover to the high state if the

noise has a chance to push the system across the unstable fixed point. Furthermore, for two systems (the system 1 and the system 2) with parameters, β_1 and β_2 ($\beta_2 > \beta_1$), respectively, it is easier to restore the system 2, because the undesired state of the system 2 is closer to the unstable fixed point. Here, we introduce a normalized variable $\rho(t)$ in Eq. (2.2) to describe the state behavior during the restoration process. Thus, the normalized stable fixed points are $\rho_{\mathrm{L}} = 0$, $\rho_{\mathrm{H}} = 1$ and the normalized unstable fixed point is ρ_{u} ($\rho_{\mathrm{u}} \in [0, 1]$),

$$\rho(t) = \frac{x(t) - x_{\mathrm{L}}}{x_{\mathrm{H}} - x_{\mathrm{L}}}. \tag{2.2}$$

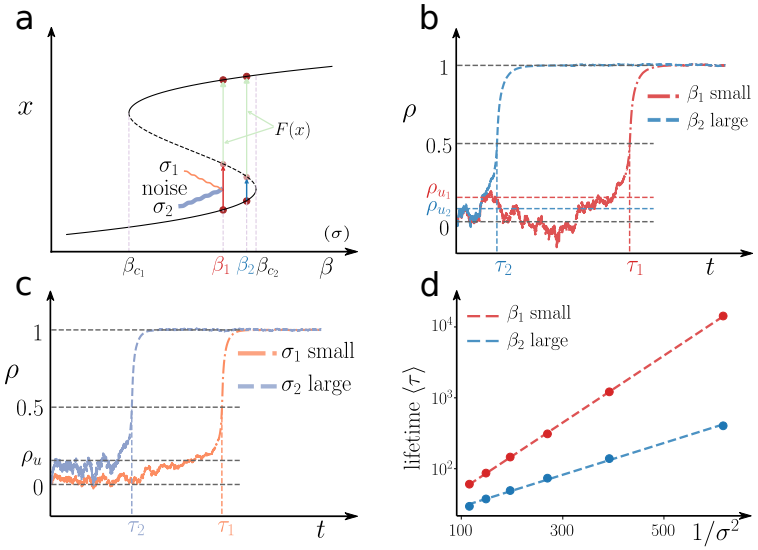

Figure 2.1: The transition in the single-variable system. (a) The resilience function of a general bistable system. For the bifurcation parameter $\beta \in (\beta_{c_1}, \beta_{c_2})$, there are two stable states (x_{L}, x_{H}) and one unstable state (x_{u}). The initial stable state (x_{L}) evolves to the unstable state (x_{u}) by the aid of noise and is then naturally attracted to the other stable state (x_{H}) by its deterministic dynamics. (b) and (c) display the evolution of the rescaled state ρ in the presence of noise. (b) As β_2 is closer to the critical value β_{c_2} than β_1, the unstable state ρ_{u_2} is lower, making the barrier in the landscape easier to cross in the presence of the same strength of fluctuations. The lifetime τ_2 is thus smaller than τ_1. (c) The parameter β is the same, leading to the same landscape. In the presence of stronger noise σ_2, it is easier to drive the system to get over the barrier, causing τ_2 to be smaller than τ_1. (d) shows the simulation results of the average lifetime $\langle\tau\rangle$ under different values of β and different noise strength. The dashed line is fitted based on Eq. (2.4).

In the following analysis, we focus on the case when the desired state ρ_{H} has a much larger basin of attraction than the undesired state ρ_{L}, suitable to examine the "one-way recovery" from ρ_{L} to ρ_{H}. Because of symmetry, the insights gained from this investigation should be readily applicable to the transition from ρ_{H} to ρ_{L} when ρ_{L} has a larger basin of attraction. In this case, the basin of attraction of the state ρ_{L} is much smaller than that of ρ_{H}, such that the value of the unstable state ρ_u is very close to ρ_{L}, increasing the chance for perturbations to push the system from the state ρ_{L} over the unstable fixed point ρ_u until the system gets attracted to the state ρ_{H}. Notably, the backward transition is highly improbable by the same level of perturbations because of the much stronger attraction of the state ρ_{H}. To quantify the time needed for the transition from ρ_{L} to ρ_{H}, the half lifetime, τ (mathematically, $\tau = \{t|\rho(t) = 0.5\}$), can be safely used as an indicator of the degree of inertia associated with the transition from the undesired state to the desired one. One can choose any value as the cutoff as long as it is sufficiently larger than the unstable state ρ_u [53], [60]. The lifetime τ is determined by the noise strength σ and the relative stability of alternative stable states controlled by β. Intuitively, larger noise strength indicates stronger fluctuations, which increases the chances of transition, making τ smaller (Fig. 2.1c). On the other hand, as β increases, the basin of attraction of the stable state ρ_{H} gets larger, making the transition from ρ_{L} to ρ_{H} easier so that τ typically decreases (Fig. 2.1b). To better illustrate the transition process, the underlying landscape picture [61] is introduced, and the effective potential energy is provided by Eq. (2.3) with zero potential energy at $x = 0$. In the landscape representation, stable states are traditionally treated as valleys, and unstable states are pictured as hills [25], [62], [63]. The transition between stable states can be viewed as the transition from one shallow valley to a deeper valley by crossing the barrier.

$$V_{\mathrm{eff}}(x) = -\int_0^x [f(x')]\, dx'. \tag{2.3}$$

The transition time from one stable state to the other is a random variable because of the stochastic fluctuations, but the average value, $\langle\tau\rangle$, presents interesting properties. Following the derivations of the Kramers formula for the escape rate over a potential barrier by particles of Brownian motion [64], [65], the average transition time $\langle\tau\rangle$ can be calculated

through the analysis of the mean first passage time (MFPT), which is given by Eq. (2.4),

$$\langle \tau \rangle = \frac{2\pi}{\sqrt{V''(x_{\mathrm{L}})|V''(x_u)|}} e^{2[V(x_u)-V(x_{\mathrm{L}})]/\sigma^2}. \tag{2.4}$$

From the quantitative predictions, one can notice that $\langle \tau \rangle$ increases exponentially with the potential energy difference $\Delta V = V(x_u) - V(x_{\mathrm{L}})$ between the low stable state and the unstable state (also interpreted as the barrier height) and decreases with noise intensity σ^2, which is numerically verified in Fig. 2.1d. The analysis of single-variable systems provides theoretical support for our intuitive assumption that the low barrier height and strong noise facilitate transitions, leading to resilience restoration, see [58], [64] for derivation). With the knowledge of the average lifetime $\langle \tau \rangle$ for single-variable systems available, we are ready to investigate transitions in multi-variable (spatially-extended) systems. Nucleation theory is utilized to analyze the generation and spread of the transition in multi-variable systems under external fluctuations.

2.2.2 Spatially-extended system

Generally, the evolution of a system that consists of N coupled components under external perturbations is described by Eq. (3.1). This study focuses on the spatially-extended ecosystem, where one type of species is considered, and its density varies in two-dimensional space and is discretized according to the square lattice topology with periodic boundaries. The deterministic dynamics of each node follows the same self-dynamics $F(x_i)$ and the same interaction dynamics $G(x_i, x_j)$, and parameters of these functions are also set uniformly for all components. The element of the adjacency matrix A is either 0 or a positive value R, which decides the coupling strength between interacting elements. Additionally, to model the external fluctuations acting on the node i, delta-correlated Gaussian noise $\eta_i(t)$ with zero mean and variance $\langle \eta_i(t)\eta_j(t') \rangle = \sigma^2 \delta_{ij} \delta(t - t')$ is introduced, which is the same as the noise applied to the single-variable systems. This general framework can be used to describe a wide range of coupling systems under external perturbations,

$$\frac{\mathrm{d}x_i}{\mathrm{d}t} = F(x_i) + \sum_{j=1}^{N} A_{ij} G(x_i, x_j) + \eta_i(t). \tag{2.5}$$

Utilizing the dimensional reduction theory [16], the deterministic evolution of multi-

variable systems can be reduced to Eq. (2.6), containing only one variable, x_{eff},

$$\frac{\mathrm{d}x_{\text{eff}}}{\mathrm{d}t} = F(x_{\text{eff}}) + \beta_{\text{eff}} G(x_{\text{eff}}, x_{\text{eff}}). \tag{2.6}$$

In the lattice, the fixed states and their stability for each component are proved to be the same as in the reduced one-dimensional system [66]. Hence, according to the analysis of single-variable systems, for the specific values of effective interaction strength ($\beta \in (\beta_{c_1}, \beta_{c_2})$), each component in this system has two stable states and one unstable state. In the presence of noise, the transition from the low state x_{L} to the high state x_{H} is possible for every component. Once the first transition occurs to the node i, its neighbors will also recover through the interaction with it. To show the overall evolution properties of the entire system, the global state $\rho(t)$ is defined in Eq. (2.7) by taking the average of the individual state value,

$$\rho(t) = \langle \rho_i(t) \rangle_N = \frac{1}{N} \sum_{i=1}^{N} \rho_i(t). \tag{2.7}$$

The spread of such transition can be well described by the theory of homogeneous nucleation and growth in *finite* systems [48], [53], [54], and this theory can also predict the spatial-clustering pattern formed during the spreading process. The transition from ρ_{L} to ρ_{H} occurs to some node at first, nucleating a cluster, and this cluster continues to expand until it fills the entire space, or the cluster's edge reaches the edge(s) of other clusters that have nucleated in the system. Homogeneous nucleation makes two assumptions [53]: nucleation occurs in a Poisson process with a constant rate I both temporally and spatially; once a cluster nucleates, it grows homogeneously with a *constant* radial velocity v. Since the interaction environments for all components are identical, and the perturbations they receive come from the same distribution, each node has the same chance to nucleate a cluster, which satisfies the assumptions of homogeneous nucleation.

As predicted by homogeneous nucleation theory, the restoration process exhibits different patterns for small systems and large systems when the nucleation rate I is fixed. Small systems exhibit the single-cluster pattern because the number of candidates is so limited that the first cluster nucleates and spreads out to the rest of the system before the second possible cluster emerges. Since the nucleation for a specific individual follows a Poisson process, the global state ρ is expected to evolve distinctly for different noise realizations. Also, the time

to nucleate the first cluster, t_n, and the lifetime, τ, are inherently random. We introduce the waiting time to quantify the time to the system recovery. Because the underlying process is modeled as the random Poisson process, the complementary cumulative probability distribution of waiting time P_{not} is derived as an exponential function, which represents the probability that the global state ρ has not exceeded 0.5 by time t. (Note that our chosen conventional cut-off value 0.5 does not affect the findings.) The distribution of waiting time P_{not} is expressed as,

$$P_{\text{not}}(t) = \begin{cases} 1, & t \leq t_g \\ e^{-(t-t_g)/\langle t_n \rangle}, & t > t_g \end{cases}, \tag{2.8}$$

where $\langle t_n \rangle$ is the average time elapsing until the first cluster nucleates (i.e., the first transition occurs); t_g represents the time required for the global state ρ to reach 0.5 after the first cluster emerges, and this time depends on the linear size of the system, $t_g \sim N^{1/2}/v$, where v is the constant radial velocity. Also, $\langle t_n \rangle \sim (IN)^{-1}$, where I is the nucleation rate per unit area. The average transition time from the initial undesired state to the desired state or the average lifetime of the initial state is expressed as $\langle \tau \rangle = \langle t_n \rangle + t_g$. For small system sizes or in the weak-noise limit, the dominant term in the lifetime is the nucleation time, hence $\langle \tau \rangle \sim (IN)^{-1}$.

In contrast, for large systems, more than one independent cluster nucleates and expands separately, leading to the multi-cluster mode. Spatial self-averaging reduces randomness of the global state ρ, making each individual τ closer to the average value and pushing P_{not} closer to a step function. In the large system-size limit, the lifetime distribution is narrowly centered about the average. Based on Avrami's Law, for sufficiently large systems [44], [45], [46], [50], [51], the evolution of ρ can be expressed in a deterministic form as $\rho = 1 - e^{-\frac{\pi v^2 I}{3} t^3}$. By setting $\rho = 0.5$ (without loss of generality), the average lifetime for the multi-cluster mode can be obtained as, $\langle \tau \rangle = (\frac{3 \ln 2}{\pi v^2 I})^{1/3}$. Then the evolution of ρ can be described by,

$$\rho = 1 - e^{-(\frac{t}{\langle \tau \rangle})^3 \ln 2}. \tag{2.9}$$

According to Avrami's Law and homogeneous nucleation in finite systems [48], [53],

[54], the average lifetime of two transition modes is summarized as,

$$\langle\tau\rangle \sim \begin{cases} \frac{1}{IN}, & N^{\frac{1}{2}} \ll R_0 \quad \text{(single-cluster mode)} \\ I^{-\frac{1}{3}}, & N^{\frac{1}{2}} \gg R_0 \quad \text{(multi-cluster mode)} \end{cases} , \tag{2.10}$$

where $R_0 \sim (\frac{v}{I})^{1/3} \sim I^{-1/3}$ is the typical distance between separate clusters (and $N^{1/2}$ is the linear size of the two-dimensional lattice). Transition patterns for different system sizes and nucleation rates are classified into two distinct cluster nucleation modes, separated by a *crossover* region centered around the curve, $N^{1/2} \sim R_0$. Small systems or low nucleation rates induce the single-cluster mode, while large systems or high nucleation rates exhibit the multi-cluster mode.

By constructing a scaling function [67] with the following asymptotic behavior,

$$S(u) \sim \begin{cases} u^2, & u \gg 1 \quad \text{(single-cluster mode)} \\ \text{const.}, & u \ll 1 \quad \text{(multi-cluster mode)} \end{cases} , \tag{2.11}$$

where $u = R_0/N^{1/2} \sim v^{1/3}/(I^{1/3}N^{1/2}) \sim I^{-1/3}N^{-1/2}$, one can capture the average lifetime of *any* system size and nucleation rate (including the *crossover* between the single-cluster and multi-cluster regimes),

$$\langle\tau\rangle = I^{-\frac{1}{3}} S(R_0/N^{\frac{1}{2}}) = I^{-\frac{1}{3}} S(I^{-\frac{1}{3}}N^{-\frac{1}{2}}) \, . \tag{2.12}$$

Motivated by the study on the average transition time $\langle\tau\rangle$ for single-variable systems [Eq. (2.4)], the relationship between local nucleation rate and noise strength in spatially-extended systems is expected to scale as

$$I \sim e^{-\frac{c}{\sigma^2}}, \tag{2.13}$$

where c is a constant specific to the given dynamics and can be empirically fitted in the weak-noise case. In turn, the average lifetime $\langle\tau\rangle$ for different system sizes and noise strength can be described by a universal scaling function: employing Eqs.(2.12) and (2.13), when plotting $\langle\tau\rangle e^{-\frac{c}{3\sigma^2}}$ vs. $e^{\frac{c}{3\sigma^2}}/N^{\frac{1}{2}}$, all curves should collapse on the same curve $S(u)$.

2.3 Resilience restoration of mutualistic systems

To verify the predictions by nucleation theory of the noise-induced transition patterns in systems with alternative stable states, we first study resilience restoration of the mutualistic system.

2.3.1 Dynamical model

We use Eq. (2.14) and Eq. (2.15) as the deterministic dynamics to track the abundance of one species distributed among a square lattice in the mutualistic system [68], [69]. The self-dynamics $F(x_i)$ describes that the growth of the species in each location follows the logistic law with the Allee effect [70], and the dynamics $G(x_i, x_j)$ accounts for the mutualistic interaction between the species in two neighboring locations i and j through the interaction strength A_{ij} defined in Eq. (2.5).

$$F(x_i) = B_i + x_i \left(1 - \frac{x_i}{K_i}\right) \left(\frac{x_i}{C_i} - 1\right) \tag{2.14}$$

$$G(x_i, x_j) = \frac{x_i x_j}{D_i + E_i x_i + H_j x_j}. \tag{2.15}$$

The parameters are node-uniform and set as $B_i = B = 0.1$, $C_i = C = 1$, $D_i = D = 5$, $E_i = E = 0.9$, $H_j = H = 0.1$, $K_i = K = 5$, and the interaction strength $R = 1$ (leading to the effective interaction strength $\beta_{\text{eff}} = 4$). At some moment, if the species in all locations are trapped in the low stable state x_{L}, they will stay at this state forever if there is no action or perturbation. It is, for sure, not desired from the ecological viewpoint. If one would like to keep the system always in the high stable state x_{H}, a straightforward approach is to increase the interaction strength to ensure that β_{eff} is larger than the critical bifurcation value β_{c2}. In this case, the system will be attracted to the high state no matter where it starts. Alternatively, noise has shown the ability to induce the transition between two stable states from the study of one-variable systems. We are particularly interested in how noise assists the resilience restoration (i.e., transferring the system from the undesirable state x_{L} to the desired state x_{H}).

2.3.2 Patterns of resilience restoration

Let us consider the case when all nodes in the system start from the low state x_{L}, indicating a collapsed state. Observed from simulations, the proper noise can excite some node to x_{H}, and such transition spreads out to its neighbors via interaction until the rest of the system completes transitions. According to homogeneous nucleation theory, for different system sizes and nucleation rates, two possible transition patterns are present. We successfully show the snapshots of two cluster modes by numerical simulations, the single-cluster and multi-cluster mode.

Notably, these two modes possess radically distinct properties. For the single-cluster mode (Fig. 2.2a), there is only one node that switches from x_{L} to x_{H} in the beginning, and the remaining nodes shift to x_{H} through the interactions with the neighbors which have already transitioned; while for the multi-cluster mode (Fig. 2.2e), there is more than one node in the separate location that transfers to x_{H} simultaneously. It is expected since for the large system, there are enough candidates to receive fluctuations, increasing the chance to induce independent transitions.

As predicted by nucleation theory, the evolution of $\rho(t)$ for the single-cluster mode and multi-cluster mode differs a lot, and numerical results confirm the difference. Fig. 2.2b and Fig. 2.2f display 100 realizations for system sizes $N = 100$ and $N = 10000$ under the same intensity of noise. For the single-cluster mode (Fig. 2.2b), the evolution varies for individual realizations, so the transition times are different, indicating the uncertain evolution feature. In contrast, for the multi-cluster mode (Fig. 2.2f), the evolution of $\rho(t)$ is similar for different realizations, implying that the evolution is deterministic in the infinite system-size limit. Following this, the waiting time distribution P_{not} for two cluster modes is also verified (Fig. 2.2c). For the single-cluster mode, P_{not} is initially constant and then decreases exponentially with respect to t verifying Eq. (2.8). The slope of the distribution gets more negative as noise becomes stronger suggesting a larger nucleation rate. For the multi-cluster mode, P_{not} gets closer to a step function (Fig. 2.2g) as noise strength increases. This is because the larger nucleation rate induces more separate clusters for a given system size and thus leads to the more deterministic evolution by self-averaging. From the theoretical analysis, the global state ρ for the multi-cluster mode evolves predictably according to Eq. (2.9). Whereas, for the finite-size system, the evolution of the multi-cluster mode (Fig. 2.2h) is not perfectly deterministic, but still much less random than the single-cluster

mode (Fig. 2.2d).

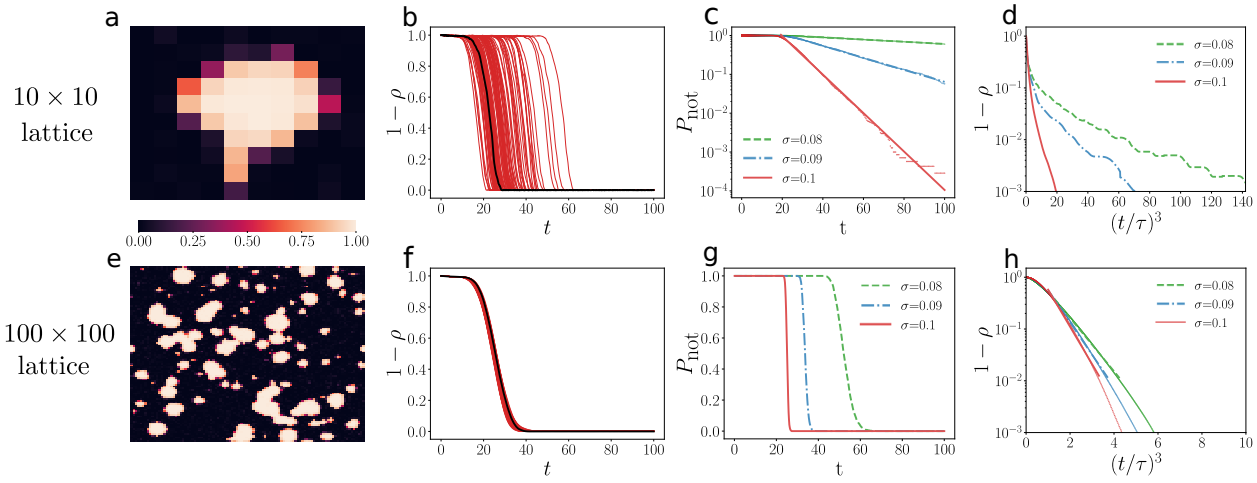

Figure 2.2: Single-cluster and multi-cluster modes in the mutualistic system. (a) One snapshot for the state ρ_i of each node under the noise of the standard deviation $\sigma = 0.1$. Initially, all of the nodes are at the low state $x_{\rm L}$. At some time later, the transition to the high state $x_{\rm H}$ occurs to one node, which is treated as a single cluster. Such transition then spreads out to its neighbors. (b) The evolution of the global state ρ for 100 realizations of the single-cluster mode (a). (c) The probability distribution of waiting time $P_{\rm not}$ for the fixed system size and the various noise strengths $\sigma = 0.08, 0.09, 0.1$. The single dots are simulation data, and different types of lines are obtained by linear fit according to Eq. (2.8). (d) The evolution of the average global state ρ using the same data as in (c). (e) One snapshot shows the state ρ_i of each node for the case when all nodes starts from $x_{\rm L}$ initially, and σ is also 0.1. Different from (a), the transition to $x_{\rm H}$ occurs at several separate nodes, and they expand independently, forming the multiple cluster. (f) The evolution of the global state ρ for 100 realizations, which are more centered around a certain value instead of being random in (b). (g) The distribution $P_{\rm not}$ for $N = 10000$ and $\sigma = 0.08, 0.09, 0.1$, which approaches the step function as σ increases. (h) The evolution of the global state ρ averaged over 100 realizations using the same data as in (g). The single dots are simulation data, and different types of lines are obtained by linear fit according to Eq. (2.9).

2.3.3 The role of system size and noise strength

The cluster mode not only depends on the system size but also relies on the nucleation rate, which is decided by noise strength. Typically, large systems under strong noise belong to the multi-cluster mode, while small systems under weak noise exhibit the single-cluster

mode. However, low nucleation rates resulting from weak noise can induce the single-cluster mode even for a very large system (Fig. 2.3a, 2.3b). Also, the average nucleation time $\langle t_n \rangle = (NI)^{-1}$ for the single-cluster mode is validated. The average lifetime $\langle \tau \rangle$ behaves differently for the two cluster modes and exhibits two regimes (Fig. 2.3c), and its value increases exponentially as σ^{-2} increases for both cluster modes as predicted by Eq. (2.10). For the given dynamics, $\langle \tau \rangle$ entirely depends on the system size N and noise strength σ (Fig. 2.3c, 2.3d), and there is a decrease as N or σ increases. One can also notice that the slope of $\ln\langle \tau \rangle$ as a function of σ^{-2} for the single-cluster mode is larger than the slope for the multi-cluster mode.

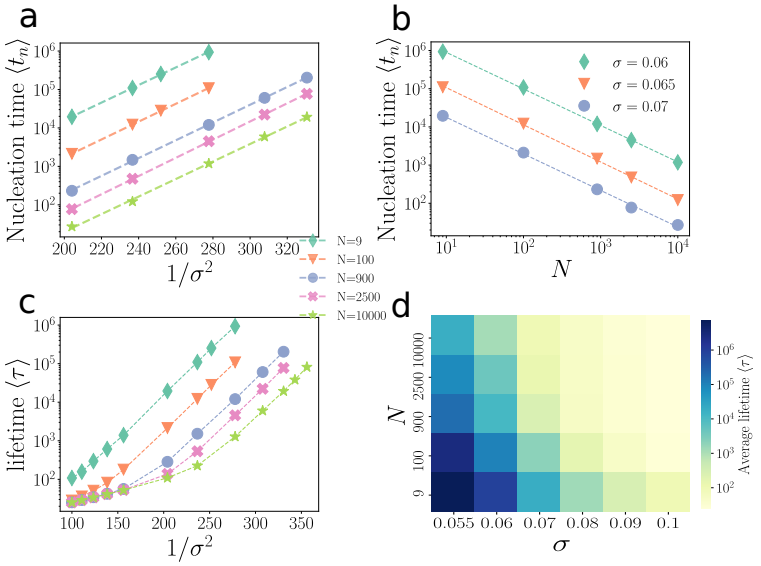

Figure 2.3: The influence of system size N and noise strength σ on transition modes and average lifetime. Initially, all of the nodes are at the low state x_{L}, and the time to switch to the high state x_{H} is measured. (a) The average nucleation time $\langle t_n \rangle$ changes with noise strength for different system sizes. (b) The linear relationship between $\langle \tau \rangle$ and N^{-1}. (c) Two regimes with different slopes of $\ln\langle \tau \rangle$ as a function of σ^{-2} corresponding to two cluster modes. (c) and (d) summarize the effects of system size N and noise strength σ on the average lifetime $\langle \tau \rangle$. The increase of noise strength lowers the average lifetime. For the single cluster mode, the larger system requires less time to complete transitions.

2.3.4 Phase diagram and finite-size scaling

In accord with the scaling theory, Eqs. (2.10)-(2.12), the two distinct cluster-growth modes are separated by a *crossover* region centered around $N^{1/2} \sim R_0$ (Fig. 2.4a). One

should note that this crossover (centered around the dashed curve in Fig. 2.4a) is not a sharp transition separating the two cluster-growth modes. The gradual change of the background color (red-white-blue) is to qualitatively illustrate the continuous nature of the crossover from the single-cluster mode to the multi-cluster mode.

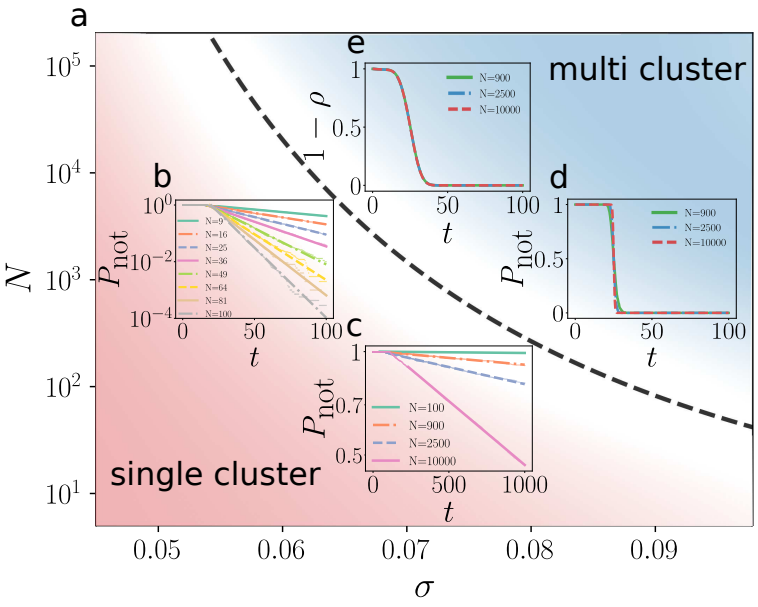

Figure 2.4: Crossover between two cluster modes for the sample mutualistic system. Initially, all of the nodes are at the low stable state $x_{\rm L}$, and they are driven to the high stable state $x_{\rm H}$ in the presence of noise. (a) According to Eq. (2.10), two cluster modes are distinguished. The dashed curve is drawn according to the equation $N^{1/2} = e^{\frac{c}{3\sigma^2}}$, where c is a fitted parameter. The gradual change of the background color (red-white-blue) is to qualitatively illustrate the continuous nature of the crossover from the single-cluster mode to the multi-cluster mode. The dashed curve corresponds to the center of the crossover region (provided by the above formula), separating the two cluster-growth modes. (b) and (c) describe the single-cluster mode (in red), while (d) and (e) display the multi-cluster mode (in blue). (b) The distribution $P_{\rm not}$ for the fixed noise strength $\sigma = 0.1$ and different system sizes $N = 9, 16, 25, 36, 49, 64, 81, 100$. (c) $P_{\rm not}$ for the fixed weak noise $\sigma = 0.06$ and $N = 100, 900, 2500, 10000$. In both (b) and (c), the single dots are simulation data, and different types of lines are obtained by linear fit according to Eq. (2.8). (d) $P_{\rm not}$ for the fixed noise strength $\sigma = 0.1$ and different system sizes $N = 900, 2500, 10000$. (e) The evolution of the global state ρ using the same data as in (d).

The small system (Fig. 2.4b) or weak noise induces (Fig. 2.4c) the single-cluster mode,

while the large system or relatively strong noise (Fig. 2.4d, 2.4e) produces the multi-cluster mode. According to the proposed scaling function Eq. (2.12), employing and plotting properly scaled variables, $\langle\tau\rangle e^{-\frac{c}{3\sigma^2}}$ vs. $e^{\frac{c}{3\sigma^2}}/N^{\frac{1}{2}}$, we expect that all numerical data would collapse onto the scaling function $S(u)$, capturing general nucleation behavior [67].

2.3.5 The universal scaling law

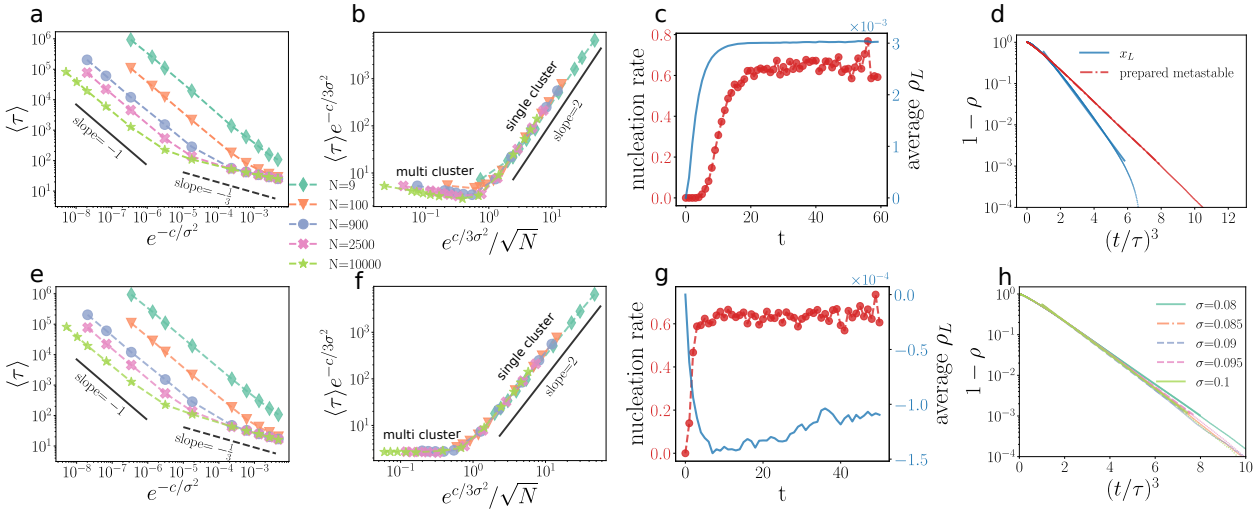

Figure 2.5: Scaling between two cluster modes in the mutualistic system. For (a) – (c), the system starts from the low state x_{L}, and the time to reach the state x_{H} is characterized by τ. (a) The relationship of $\langle\tau\rangle$ and $e^{-\frac{c}{\sigma^2}}$ differs between two cluster modes. (b) The finite-size scaling is drawn by assuming the slope of multi-cluster mode in (a) is $-\frac{1}{3}$. For (c) and (d), $N = 10000$ and $\sigma = 0.08$. (c) The nucleation rate increases before the average state of nodes which have not transitioned stabilizes. (d) The system starts to evolve from x_{L} and the prepared state, respectively. The evolution of the global state ρ for the latter case agrees better with Eq. (2.9) than the former case. For (e) – (h), the system starts from the prepared metastable state, and the time to reach the state x_{H} is recorded as τ. (e) The average lifetime $\langle\tau\rangle$ for two cluster modes. (f) The finite-size scaling is consistent with the theoretical prediction in Eq. (2.12). (g) The nucleation rate needs less time to stabilize compared with (c). (h) The evolution of the global state ρ for the multi-cluster mode when $N = 10000$ and $\sigma = 0.08, 0.085, 0.09, 0.095, 0.1$. In both (d) and (h), the single dots are simulation data, and different types of lines are obtained by linear fit according to Eq. (2.9).

Nevertheless, observed in Fig. 2.5a, for the multi-cluster mode, $\langle\tau\rangle$ is not precisely proportional to $I^{-1/3}$. Therefore, the two transition modes cannot be scaled in a satisfactory fashion as the scaled data for the multi-cluster regime is not constant (Fig. 2.5b), which contradicts the assumption of Eq. (2.11). The deviation from Avrami's Law suggests that the assumption(s) of homogeneous nucleation might be violated. For a large system subjected to relatively strong noise, which guarantees the multi-cluster mode, the nucleation rate changes in the beginning (Fig. 2.5c), defying the assumption of constant nucleation rate. The initial rise of the spatially distributed low state for the nodes which have not been driven to the high state indicates that the initial state is not a metastable state. In the presence of noise, the metastable state is a state distribution where all nodes are around the low state ρ_{L}, but some nodes are closer to the unstable state ρ_u and some are even below the state ρ_{L}. The system in the presence of noise needs time to reach a new metastable state which is different from the low stable state. To keep the nucleation rate constant, one should use the metastable configuration as the initial condition. However, as seen in Fig. 2.5c, some cluster have already emerged before the system reaches the metastable configuration indicated by the increase of the average low state and the nucleation rate, so that the preprocessing of the initial state is needed to forbid any transition before the metastable configuration is constructed. One can artificially prepare the system close to the metastable state by reverting the node back to ρ_{L} if any other sites nucleate during preprocessing.

To gain further insight into the source of this discrepancy, we carried out simulations with the initial configurations being very close to the metastable state. In such a case, the nucleation rate I stabilizes much faster (Fig. 2.5g) compared with the system without preprocessing. Afterward, the nucleation rate is roughly constant, so homogeneous nucleation theory can be reliably applied. This leads to a better agreement between the simulation and the theory, as the evolution of ρ is closer to what Eq. (2.9) postulates (Fig. 2.5d, 2.5h), and the data from the two cluster modes follows the scaling function (Fig. 2.5e, 2.5f). It is expected that the average lifetime $\langle\tau\rangle$ agrees better with Eq. (2.10) if the metastable state can be perfectly prepared.

2.4 Restoration of diffusion dynamics

To further validate the proposed theory, we adapt three well-studied ecological models exhibiting alternative stable states [71], [72] with diffusive interaction and then apply the

above theory to investigate the transition features.

2.4.1 Examples of some dynamics

The self-dynamics for three diffusion models are defined below.

The harvesting model in Eq. (2.16) describes the growing resource biomass with fixed grazing rate [31]. The first term on the right hand side of Eq. (2.16) describes logistic growth, where r is the maximum growth rate, and K is the carrying capacity. The second term is the "Holling's type 3" consumption function [73]. The system transitions from an underexploited state to overexploited state as the harvesting rate β exceeds a certain critical value.

$$F(x_i) = rx_i(1 - \frac{x_i}{K}) - \beta\frac{x_i^2}{x_i^2 + 1} \tag{2.16}$$

The eutrophication model in Eq. (2.17) describes the dynamics of nutrient concentration in the eutrophic lake [74]. The variable x_i represents the density of phosphorus mass (nutrient) in the location i of the lake. The first term a on the right hand side of Eq. (2.17) is the nutrient loading rate, the second term describes nutrient loss processes with the rate r, and the last term accounts for recycling processes following a sigmoid function. As the maximum recycling rate β increases to the critical point, the lake transfers from oligotrophic to eutrophic.

$$F(x_i) = a - rx_i + \beta\frac{x_i^8}{x_i^8 + 1} \tag{2.17}$$

The vegetation-turbidity model in Eq. (2.18) describes the vegetation dynamics considering turbidity [75]. The variable x_i represents the density of aquatic vegetation in the location i of the lake. The first term on the right hand side of Eq. (2.18) characterizes the growth of vegetation with the maximum growth rate r_v. The function E in Eq. (2.19) is an inverse Monod function and used to describe the vegetation effect on turbidity. Accordingly, the second term is a Hill function describing the sigmoidal decline of vegetation with turbidity. As the water becomes turbid, indicated by the background turbidity β, macrophytes suddenly decrease.

$$F(x_i) = r_v x_i - r_v x_i^2\frac{r^4 + E_i^4}{r^4} \tag{2.18}$$

$$E_i = \frac{h_v\beta}{h_v + x_i} \tag{2.19}$$

All three models can exhibit alternative stable states with the properly chosen bifurcation parameter β as illustrated in Fig. 2.7a, 2.7e, 2.7i. The transition from the low stable state to the high stable state is possible in the presence of noise for such single-variable systems.

2.4.2 The spatially-extended diffusion dynamics

Likewise, the underlying topology is also a square lattice with periodic boundaries. The interaction dynamics is defined in Eq. (2.20), which represents the diffusive process between adjacent neighbors, and the interaction strength R determines the uniform diffusion rate. The species density at each location varies according to the internal dynamics as defined in Eqs. (2.16) – (2.19) , and it is also influenced by dispersion to or immigration from neighbors and stochastic environmental fluctuations.

$$G(x_i, x_j) = x_j - x_i. \tag{2.20}$$

Once the system gets stuck in a malfunctioning state, resilience restoration is required. In the presence of noise, each component is likely to be driven from the undesired state to the functional stable state, and then the entire system undergoes substantial changes due to the transition of one or a few nodes. Nucleation theory can be employed as well to study the overall transition features. The results we collected from three diffusion models are similar to those obtained from the mutualistic system and thus verify the predictions by nucleation theory. We consider the case when the undesired state has a much smaller basin of attraction than the desired state so that noise can drive the system from the initial undesired state to the functional state, resulting in resilience restoration.

2.4.3 The phase diagram of harvesting system

Take the harvesting model as an example to illustrate the successful application of nucleation theory to resilience restoration. Two cluster-growth modes are observed and separated by a crossover around $N^{1/2} \sim R_0$ (Fig. 2.6a). Similar to the mutualistic system, the large system or strong noise produces multi-cluster mode; conversely, the small system or weak noise induces single-cluster mode. For the small system, there is only one cluster formed during the transition (Fig. 2.6b), and the individual lifetime τ in Fig. 2.6c varies a lot for different realizations, indicating a stochastic feature. Also, the distribution of waiting

times P_{not} follows an exponential function after a certain period t_g (Fig. 2.6d, 2.6e.

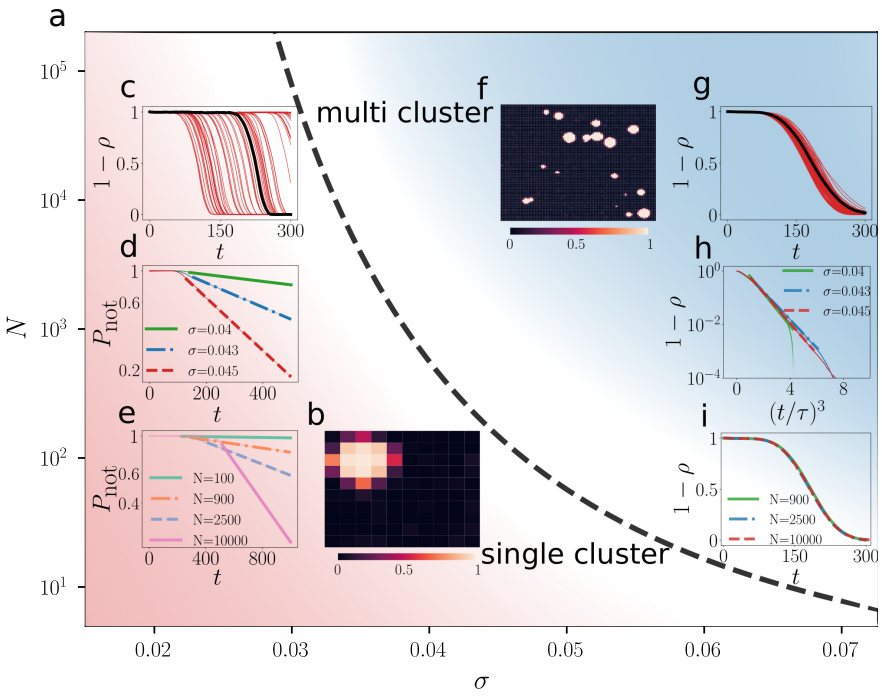

Figure 2.6: Harvesting system. The parameters are set as $r = 1$, $K = 10$, the diffusion rate $R = 0.02$, and the bifurcation parameter $\beta = 1.8$. Initially, all of the nodes are at the low stable state x_{L}, and they are driven to the high stable state x_{H} in the presence of noise. (a) Two clusters are separated according to the curve $N^{1/2} = e^{\frac{c}{3\sigma^2}}$, where c is a fitted parameter. For (b) – (d), the system size $N = 100$. (b) One snapshot shows the evolution of each node ρ_i in the presence of noise with $\sigma = 0.045$. The initial states for all of the nodes are x_{L}. Later, the transition to x_{H} occurs to one node, which is treated as a single cluster, and it spreads out to its neighbors. (c) The evolution of the global state ρ for 100 realizations, which corresponds to the single-cluster mode in (a). (d) The distribution of waiting time P_{not} for the $N = 100$ and $\sigma = 0.04, 0.043, 0.045$. (e) P_{not} for $\sigma = 0.035$ and $N = 100, 900, 2500, 10000$. In both (d) and (e), the single dots are simulation data, and different types of lines are obtained by linear fit according to Eq. (2.8). For (f) – (h), $N = 10000$. (f) The snapshot illustrates the evolution of the system starting from x_{L}, where σ is also 0.045. The transitions to x_{H} occur at several separate nodes, forming the multiple cluster. (g) 100 realizations of the global state ρ. (h) The evolution of ρ averaged over 100 realizations for $\sigma = 0.04, 0.043, 0.045$. The single dots are simulation data, and different types of lines are obtained by linear fit according to Eq. (2.9). (i) The evolution of the global state ρ averaged over 100 realizations for $\sigma = 0.045$ and $N = 900, 2500, 10000$.

If the system is exposed to weak noise which means a low nucleation rate, it is very likely to enter the single-cluster regime even the size is sufficiently large (Fig. 2.6e). For the large system (like $N = 10000$) with proper intensity of noise, more than one node in the separate location is recovered simultaneously (Fig. 2.6f), presenting a multi-cluster pattern. Spatial-averaging reduces randomness so that the individual lifetime τ is more centered about a certain value (Fig. 2.6g). The evolution is much more deterministic than the system in a single-cluster mode. The global state ρ evolves approximately as Eq. (2.9) predicts (Fig. 2.6h). If the applied noise is strong enough, the moderate-sized system can still exhibit the multi-cluster mode (Fig. 2.6i).

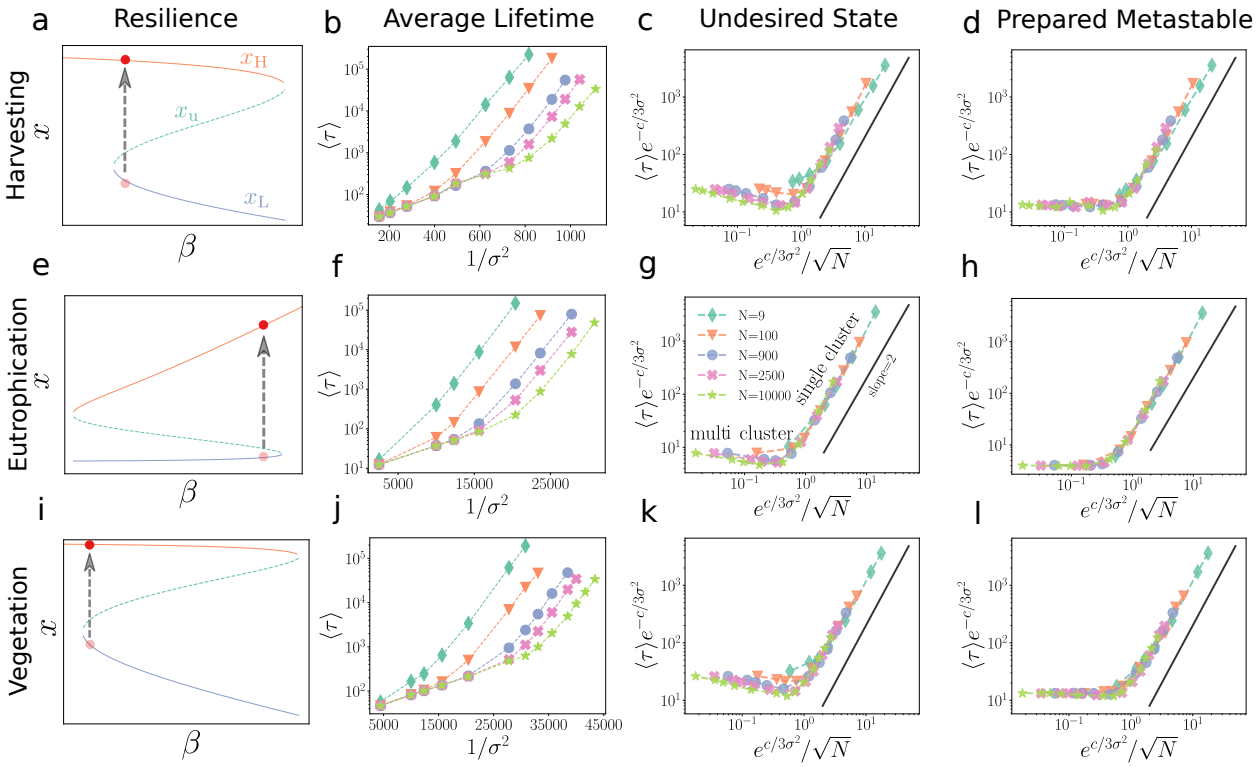

Figure 2.7: Average lifetime $\langle\tau\rangle$ and the scaling results for three diffusion models. The diffusion rate $R = 0.02$. (a) – (d) harvesting model, $r = 1$, $K = 10$; (e) – (h) eutrophication model, $a = 0.5$, $r = 1$; (i) – (l) vegetation model, $r = 1$, $r_v = 0.5$, $h_v = 0.2$. (a), (e), and (i) are the resilience diagrams with alternative stale states if β (a) $\in (1.79, 2.60)$, (e) $\in (0.86, 6.35)$, and (i) $\in (2.59, 3.64)$. In simulation, the bifurcation parameter β takes values of $1.80, 6.00, 2.60$ for (a), (e), and (i), respectively. For (b), (f), and (j), the system starts from x_L. (c), (g), and (k) show two clusters and cross-over scaling for the system starting from x_L. (d), (h), and (l) show the scaling for the system starting from the prepared metastable state.

2.4.4 The universal scaling in diffusion dynamics

As seen in Fig. 2.7, the system size and noise strength decide the recovery time and the cluster mode. Similarly, the average lifetime $\langle\tau\rangle$ of three diffusion models displays two distinct regimes. One is the single-cluster and the other is the multi-cluster regime (Fig. 2.7a, 2.7d, 2.7g). The slope of $\ln\langle\tau\rangle$ versus σ^{-2} reveals which mode is active. If the system starts from the undesired stable state, the scaling between two cluster modes deviates a little from the theoretical prediction (Fig. 2.7b, 2.7e, 2.7h). If the system starts from the prepared state, resembling the metastable configuration, the scaling agrees well with the designed scaling function (Fig. 2.7b, 2.7e, 2.7h). Overall, the conclusions of the single-cluster and multi-cluster transition are validated in three diffusion models.

2.5 Discussion

We have utilized nucleation theory to analyze the noise-induced resilience restoration in ecosystems where the desired state has a much larger basin of attraction than the undesired state has. This is a general theory, and we successfully apply it to four ecological models, revealing the transition features. During the restoration process, homogeneous nucleation theory distinguishes two different cluster modes: the single-cluster and multi-cluster transition modes. We also derive the formulas for the recovery time under different conditions and propose a scaling function that collapses all the data onto one universal line.

The two cluster modes possess quite distinct features. The individual lifetime is random for the single-cluster phase, and the waiting time before the transition follows an exponential distribution. In contrast, for the multi-cluster mode, the lifetime is less random and centered about its average value so that the evolution of the global state ρ is more deterministic. Which cluster mode the system follows is decided by its size and noise strength, and the crossover region is theoretically derived and can separate two phases. Generally, the large system subjected to strong noise presents the multi-cluster mode, and the small system with weak noise displays the single-cluster regime. One quantity of interest for resilience restoration is the recovery time, which also depends on the system size and the noise strength. The rise of noise strength increases the nucleation rate, diminishing $\langle\tau\rangle$. There is no finite-size effect when noise is strong enough; that is, $\langle\tau\rangle$ is the same for different system sizes. The decrease of noise strength reveals the size effect, where larger systems take less time to complete transitions than smaller systems on average.

Due to the distinct evolution features, the relationship between $\langle\tau\rangle$ and σ varies for two cluster modes. What can be clearly seen in Fig. 2.3 and Fig. 2.7a, 2.7d, 2.7g, is that $\langle\tau\rangle$ exhibits two distinctive regimes, corresponding to two cluster modes. The scaling between two cluster modes is proposed according to Avrami's Law. The deviation observed in numerical simulation can be corrected by preparing the initial state close to metastable configurations to satisfy two homogeneous nucleation assumptions. Employing the nucleation theory, we successfully extend the noise-induced transition in single-variable systems to spatially-extended multi-variable systems. Our framework is useful to predict critical transitions and guide the resilience restoration in the general dynamical systems presenting alternative stable states.

One may wonder how the mean-field theory works in noisy environments as the noise-induced transition in single-variable systems has been well explored. The mean-field approach makes a satisfactory prediction of the system state when the system is close to the stable states. Unfortunately, it cannot capture the transition features observed in spatially-extended systems, including the average lifetime, the dependence on the system size, and the spatial-clustering patterns. Therefore, it is still an open question whether the mean-field theory can be used to study transitions in noisy environments. One may need to develop a new dimension reduction approach for this problem.

Also, there are further questions to be addressed. For example, we analyze the transition in the lattice model. In reality, the interaction relationship in ecosystems exhibits various structures. In addition, the interaction strength between components in the real-world complex systems varies, which may add to the difficulty of analysis. Furthermore, we focus on the one-way transition, which requires that the system be close to the theoretical bifurcation point where the basin of attraction of the undesired state vanishes. For the case when two alternative stable states have basins of attraction of similar sizes, stochastic switching (namely back-and-forth switching) between states may arise, which is beyond the scope of this study. In summary, network topology (in addition to spatial structure), coupling strength, and stochastic switching are of great interest to be investigated in future studies.

CHAPTER 3
GENERALIZED DIMENSION REDUCTION APPROACH FOR HETEROGENEOUS NETWORKED SYSTEMS WITH TIME-DELAY

3.1 Introduction

The networked dynamical systems have been broadly used to study a variety of real-world systems, including ecological webs, social networks, neuronal systems, and infrastructure networks, and many of them consist of numerous components connected via complicated interactions [1], [2], [76], [77]. Advances in the understanding of system synchronization [78], dynamical spreading [79], and catastrophic shifts [25], [29] have offered important clues on the relationship between complex network topology and dynamical evolution [12]. To quantitatively investigate those collective phenomena, we often need to obtain the system's long-term evolution and equilibrium states, if any. However, as the number of components and the system complexity increase, such tasks become increasingly computationally expensive.

One common strategy to address this issue is to use the dimension-reduction approach to reduce the number of components in the system, allowing the construction of a simplified version to approximate the original system. Here, we use the term "dimension" to refer to the system size (as commonly used in control theory), i.e., the number of nodes in a networked system. The challenge is to find ways to preserve key properties of the original system and make it computationally manageable. In recent years, several dimension-reduction theories and techniques have emerged. Pecora *et.al.* [80] and Schaub *et.al.* [81] inspected network symmetry and proposed the irreducible representation to group nodes into different clusters based on their topology, which provides an exact solution to the original system, enabling the study of cluster synchronization and desynchronization. The limitation is that this framework is only applicable to networks that are extremely sparse or dense, which have nontrivial subgroups by symmetry clustering. Gao *et.al.* [13], [16] proposed a degree-weighted mean-field approach that effectively maps any N-dimensional network to its one-dimensional one. This approach was used to predict the universal resilience pattern under various types of per-

Portions of this chapter previously appeared as: C. Ma, G. Korniss, B. K. Szymanski, and J. Gao, "Generalized dimension reduction approach for heterogeneous networked systems with time-delay," Aug. 2023. arXiv:*2308.11666*.

turbations. Later, Laurence *et.al.* [17] introduced an eigenvalue-based reduction framework from the perspective of spectral analysis, opening up new perspectives on the relationship between the network topology and the approximation accuracy. Pereira *et.al.* [82], [83] applied mean-field theory to build effective networks from observations and was able to identify the interaction structure, reproduce the behavior of the original network, and predict the critical transitions. Tu *et.al.* [43] developed an analytical framework for systems with node-specific dynamics, which collapses complex N-dimensional networked system into an $S+1$-dimensional manifold as a function of S effective control parameters, where $S \ll N$. Jiang *et.al.* [42] and Zhang *et.al.* [84] proposed dimensional reduction approaches to predict the tipping points in bipartite mutualistic dynamics. Naseri *et.al.* [85] focused on preserving synchronization in dimension-reduced systems by using the eigenvalue decomposition method and Gram-Schmidt orthogonalization.

Those dimension-reduction approaches simplify the analysis of system states for large-scale networks, but most of them rely on the assumption that node degrees are homogeneous (i.e., with low-degree variance), as has been shown in [16], [17]. Unfortunately, such a requirement does not hold in many real-world systems, especially those whose underlying networks have scale-free (SF) degree distributions or networks with multiple communities. For these networks, the one-dimensional reduction approach cannot capture the wide range of node activities, especially when the system approaches the critical thresholds of phase transition. The ubiquity of scale-free property in the real world [5], [6] requires the generalization of the dimension-reduction framework to heterogeneous networks and networks with multiple communities. Recently, Vegué *et.al.* [86] developed a dimension-reduction approach for modular networks based on the spectral graph theory. The nodes are first classified into n communities according to modular structures, and the community state is then represented by one observable through spectral analysis of a series of matrices and appropriate approximations.

Delayed interactions are very common in many dynamical systems in science, and engineering [87], [88], [89] ranging from climate modeling [90] and population dynamics [91], [92] to transportation systems [93] and supply chains [94]. In contrast to single-variable systems [95], [91], [96], stability analysis, consensus formation, or control in multi-component systems with time delays and possible nonlinearities present significant computational challenges as the system size increases [87], [97], [98]. Since time delays experienced by individuals have profound effects on other participants in complex interconnected systems, the insights gained

from low-dimensional systems may not be directly applicable to systems with many components. This has been shown by the effects of times delays on consensus formation [87], [97], [98] and noisy network synchronization problems [99], [100], [101], [102]. Therefore, one needs to investigate the complex interaction topology to understand the system's evolution and stability.

We proposed a generalized dimension-reduction approach for heterogeneous complex networks and networks with multiple communities. This approach consists of two steps. First, the original network of N nodes is clustered into m clusters of nodes with similar degrees based on the assumption that node states are highly correlated with node degrees. The weighted average state of each cluster is obtained by the mean-field theory, causing the dimension-reduced system to follow the identical evolution mechanism. As a result, it can be described by only m representatives, where $m \ll N$. The system evolution can be well approximated with just a few representatives for systems with various dynamics and a wide range of degree distributions. We find that the number of required clusters peaks when the system approaches the tipping point. More importantly, for the first time, we demonstrate that our generalized dimension reduction approach theoretically enables us to analyze the system with time delays. Therefore, it reduces computational complexity while preserving the essential information of time-delayed system structures, enabling us to convert systems of any size to a low-dimensional version before we apply the corresponding theoretical frameworks.

3.2 Results

3.2.1 Generalized dimension reduction approach

Let us consider a networked system consisting of N nodes where the evolution of node activities, $x = (x_1, x_2, ..., x_N)^T$, can be generally described by Eq. (3.1),

$$\frac{\mathrm{d}x_i}{\mathrm{d}t} = F(x_i) + w \sum_{j=1}^{N} A_{ij} G(x_i, x_j). \tag{3.1}$$

The term "dimension" used here is to refer to "the number of nodes" in the original system or "the number of clusters" in the simplified system. The time-dependent state of node i is represented by a scalar variable $x_i(t) \in R$. Each node follows the same self-dynamics

$F(x_i)$ and is also influenced by its neighboring node j according to the pairwise interaction $G(x_i, x_j)$. The element of the adjacency matrix A is either 0 or 1, indicating the connectivity between components and the network topology. The edge weight w represents the uniform interaction strength of the entire system.

To analyze the system evolution for a given dynamics and network topology, one can numerically solve the coupled ordinary differential equations for all nodes according to Eq. (3.1). However, this approach is often computationally expensive or even infeasible for exceptionally large-scale networks. It is reasonable to assume that nodes of similar topological features have similar evolution patterns. Therefore, one may use only a small number of representatives to describe the system state. This is the main principle behind the dimension-reduction approach to tame the computational cost. This strategy has been proven effective by the one-dimension reduction framework. For homogeneous networks where all nodes share similar connectivity properties, one observable can represent the average state of the entire system by the appropriate choice of reduction approaches. However, for networks with heterogeneous connectivity, we cannot expect that one representative is sufficient to describe the entire system state, as the node states are much more diverse than homogeneous networks. In this study, we generalize the one-dimension reduction framework by introducing more than one observable, making it applicable to heterogeneous networks.

Because of the high correlation between node states and node degrees [12], [40], we partition the network into multiple clusters based on node degrees such that nodes of similar degrees are in the same cluster and their average state is represented by one observable. Therefore, one only needs to numerically solve the dimension-reduced networks with a few number of components. First, we obtain the node features from node degrees distribution. For SF networks where node degrees follow a power-law distribution, we take the logarithm of the node degree k_i and define the normalized variable $v_i = \frac{\log(k_i)}{\log(k_{\max})}$ as the node feature, whereas for homogeneous ER networks, we normalize the node degree $v_i = \frac{k_i}{k_{\max}}$ as the node feature. Based on the feature v_i, the K-means clustering algorithm is applied to partition the network into m clusters such that nodes in the same cluster have similar node features, including node degrees. The next step is to construct m macroscopic variables and the corresponding parameters for each cluster state. The operator $\mathcal{L}^{(a)}(x) \quad (a = 1, 2, ..., m)$ is introduced in Eq. (3.2) to calculate the average state of the cluster a, $y^{(a)} = \mathcal{L}^{(a)}(x)$, and the average interaction strength $\beta_{ab} = \mathcal{L}^{(a)}(k^{(b)})$ from the cluster g_b to the cluster g_a. Here, $k^{(b)}$

is a vector of incoming connections from the cluster g_b.

$$\mathcal{L}^{(a)}(x) = \frac{u^{(a)^T} K x}{u^{(a)^T} A 1} = \frac{\sum_{i=1, i\in g_a}^{N} k_i x_i}{\sum_{i=1, i\in g_a}^{N} k_i}. \tag{3.2}$$

In Eq. (3.2), K is a diagonal matrix with the element $K_{ii} = k_i$ representing the degree of node i, $1 = (1, 1, ..., 1)^T$ is the unit vector, and $u^{(a)} = (u_1^{(a)}, u_2^{(a)}, ..., u_N^{(a)})^T$ is a binary vector indicating that the node i belongs to the cluster g_a if $u_i^{(a)} = 1$, otherwise $u_i^{(a)} = 0$. Thus, the operator $\mathcal{L}^{(a)}$ takes the degree-weighted average of the quantity x_i over all nodes in the cluster g_a. By applying the operator $\mathcal{L}^{(a)}$ to Eq. (3.1) and assuming $\mathcal{L}^{(a)}(f(x)) \approx f(\mathcal{L}^{(a)}(x))$,

$$\frac{\mathrm{d}y^{(a)}}{\mathrm{d}t} = F(y^{(a)}) + w \sum_{b=1}^{m} \beta_{ab} G(y^{(a)}, y^{(b)}). \tag{3.3}$$

one can derive the dimension-reduction framework defined by Eq. (3.3), where $y^{(a)}$ represents the average state of the cluster g_a. Compared with Eq. (3.1), the dynamics of the simplified system preserves the form of the original dynamics, and only the interaction topology changes. This framework maps the dynamics of the N-dimensional complex system into an effective m-dimensional equation, and such mapping can significantly reduce the computational cost and enable the use of theoretical tools developed for low-dimensional systems.

We use the cluster state $y^{(a)}$ to approximate the state of each node in this cluster, $(x_i = y^{(a)}, i \in g_a)$, and thus all node states x are accessible by the dimension-reduced system. To understand the overall evolution at the system level, we define the operator $\mathcal{L}^{(\mathrm{gl})}$ in Eq. (3.4) that converts the N-node states to a global state $y^{(\mathrm{gl})} = \mathcal{L}^{(\mathrm{gl})}(x)$, which enables us to compare dynamics of the simplified system to the original one.

$$\mathcal{L}^{(\mathrm{gl})}(x) = \frac{1^T A x}{1^T A 1} = \frac{\langle k^{\mathrm{out}} x \rangle}{\langle k \rangle} \tag{3.4}$$

To illustrate the efficiency of this dimension-reduction framework, we first apply it to the mutualistic dynamics embedded in different network structures and compare the node states of the m-dimensional system with the original network and the one-dimensional system studied in Ref. [16] as well.

3.2.2 The stable state approximation

We use Eq. (3.5) and Eq. (3.6) to model the deterministic dynamics of the mutualistic system, which tracks the abundance of its species [68]. The self-dynamics $F(x_i)$ defines the growth of each species as following the logistic law with the Allee effect, while the dynamics defined by $G(x_i, x_j)$ accounts for the mutualistic interaction between pairs of species, i and j, with the interaction strength A_{ij} defined in Eq. (3.1).

$$F(x_i) = B_i + x_i \left(1 - \frac{x_i}{K_i}\right)\left(\frac{x_i}{C_i} - 1\right) \tag{3.5}$$

$$G(x_i, x_j) = \frac{x_i x_j}{D_i + E_i x_i + H_j x_j} \tag{3.6}$$

The parameters are node-uniform and set as $B_i = B = 0.1$, $C_i = C = 1$, $D_i = D = 5$, $E_i = E = 0.9$, $H_j = H = 0.1$, $K_i = K = 5$. As reported by Ref. [16], such dynamics exhibit alternative stable states, the high-stable state, and the low-stable states, which depend on the initial states and coupling strength.

We study three types of network topology, SF, ER, and SBM-ER (ER network with communities constructed by the stochastic block model [103]) and the phase diagram of the stable states for dimension-reduced systems with different values of m in Fig. 3.1. The equilibrium states of each node in Fig. 3.1 c are more diverse for the heterogeneous network and the modular network than the homogeneous ER network, and this partly verifies the correlation between the node states and node degrees. As expected, the one-dimensional reduction system cannot accurately represent the average state of the heterogeneous network, especially when the system is close to the tipping point of phase transition. The tipping point is the critical value of a system parameter, in this case, the edge weight w, at which the system undergoes a substantial change in its state (A more rigorous definition of the tipping point is provided in Section II C). As illustrated in Fig. 3.1 e, g, i, k, the system exhibits the transition from low-stable state to high-stable states. In contrast, the one-dimensional reduction system produces reasonable approximations for the homogeneous ER network. Most importantly, it can also capture the critical transition and threshold. In Fig. 3.1 f – k, m-dimensional reduction systems are constructed by the degree-based network partition and degree-weighted mean-field approach. The simplified network topology and phase transition of the global state versus the interaction strength are compared with different values of m

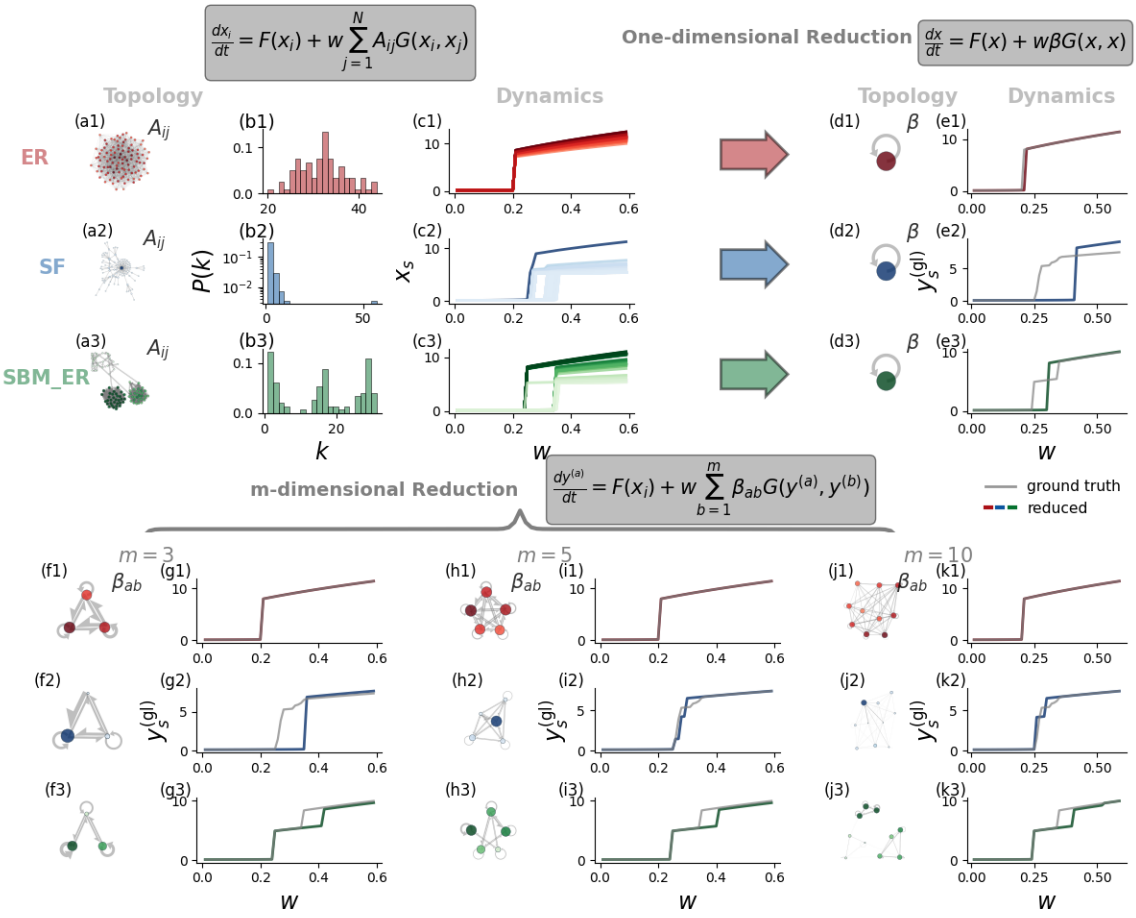

Figure 3.1: The illustration of the network partition and system dynamics defined by the generalized dimension reduction approach. The system follows mutualistic dynamics. We consider three types of network structures, (1) ER in red ($\langle k \rangle = 32$), (2) SF in blue (the power-law exponent $\gamma = 2.1$, the minimal degree $k_{\min} = 1$), (3) SBM-ER in green (link probabilities for each community are $p_1 = 0.9$, $p_2 = 0.5$, $p_3 = 0.05$, while between communities, it is $q = 0.001$). Each network consists of $N = 100$ nodes. We show the equilibrium states under different dimension-reduction strategies. (a) The topology of the original network, where the node color transparency and size are proportional to the node degree. (b) The degree distribution of the original network. (c) The stable state changes with the edge weight w for all individual nodes. (d) The topology of the one-dimensional system. (e) The stable state changes with the edge weight w for the single node. (f), (h), (j) show the topology of the m-dimensional system ($m = 3, 5, 10$ respectively), and (g), (i), (k) are the corresponding global stable states versus edge weights w. The grey curves are the global state obtained from the numerical solution of the original network.

and complexity. For an SF network with $N = 100$ nodes, the state evolution of the five-dimensional reduction system is very close to the ground truth. For the SBM-ER network with three communities, the three-dimensional system captures two substantial changes in the system state out of three, and the global state is accurately predicted when the system is not close to the critical thresholds. One can notice that there is no significant improvement with more clusters divided, which indicates that the community structure, apart from degree attributes, may impact the performance of the dimension-reduced system.

Next, we examine the dimension-reduction framework for a larger SF network in depth and evaluate the approximation accuracy of the state evolution for different coupling strengths and different values of m. In Fig. 3.2 c – e, the uniform interaction strength is set as $w = 0.2$ for the original network, and all nodes stabilize at the active (high-stable) state. However, the one-dimensional reduction system predicts that the entire system evolves to the undesired (low-stable) state, which is a misrepresentation of the original system, in contrast with the successful prediction of the four-dimensional reduction system. As the interaction strength w increases in Fig. 3.2 f – h, one can use the system with smaller m to qualitatively capture the original system state (whether the system is in the high-stable state or in the low-stable state). This is because the system moves away from the tipping point of phase transition. It can be verified by Fig. 3.2 i – k, which displays the phase transition of the global state and the qualitative precision against the interaction strength. As the coupling strength approaches the tipping point of the original system, larger m is required to qualitatively capture the system state. To quantitatively evaluate the approximation accuracy of this formalism, we compare the global state of the dimension-reduced system with the original network and introduce the relative error of the global state in Eq. 3.7. In addition, one can set an error threshold R_e to determine the optimal m, which is defined as the smallest number of clusters required to produce the relative error less than R_e with the assumption that the prediction accuracy increases with m. In Fig. 3.2 l – m, the relative error of the global state increases as the interaction strength approaches the tipping point for a fixed m, and the optimal m_{opt} increases in a similar fashion. Fig. 3.2 shows the performance of the dimension-reduction theory for one SF network, from which one can observe that the approximation accuracy strongly depends on the network coupling strength (the position in the phase diagram).

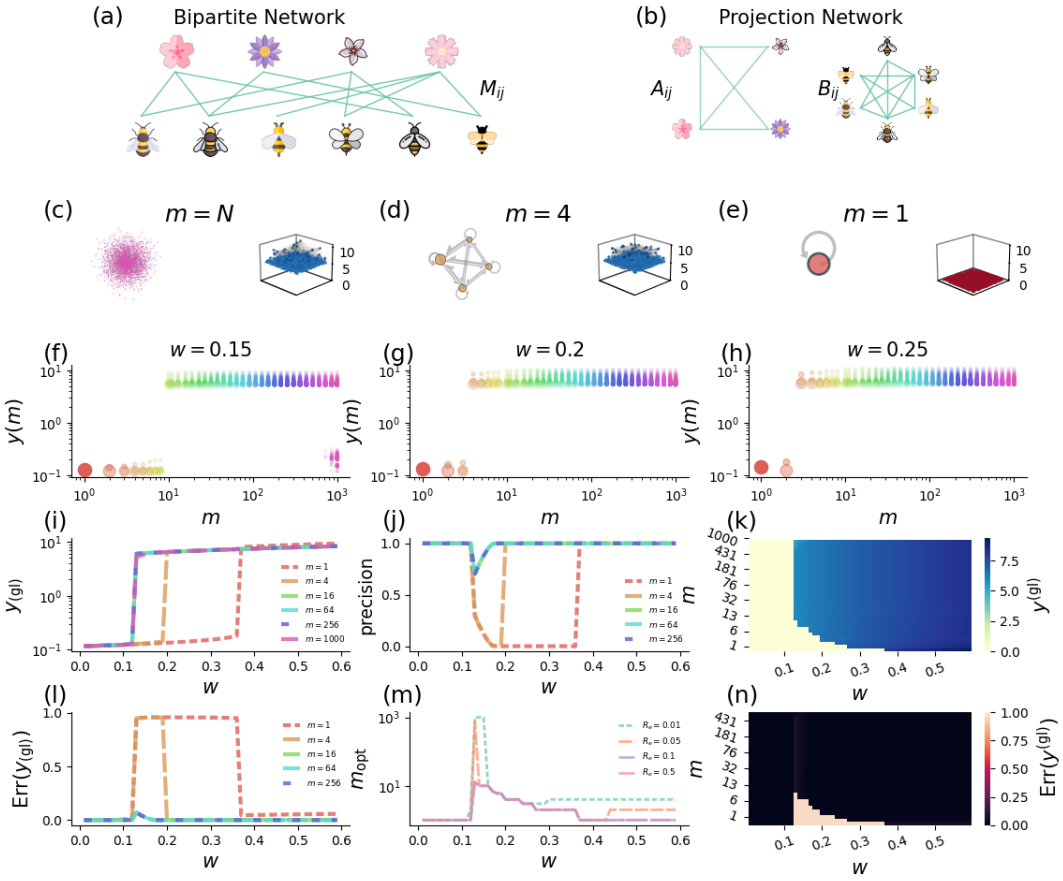

Figure 3.2: **A SF network with $N = 1000$ nodes following mutualistic dynamics. The entire system starts from the low states, $x_i(t = 0) = 0.1$. (a) The bipartite network M_{ij} describes the connection between pollinators and plants. (b) From M_{ij}, two mutualistic projection networks (A_{ij} and B_{ij}) are constructed. (c) – (e) The network topology and the stable states for $m = N$(the original system), $m = 4$, and $m = 1$ with the edge weight $w = 0.2$. For different edge weights (f) $w = 0.15$, (g) $w = 0.2$, (h) $w = 0.25$, the stable states of each cluster are exhibited against the number of clusters m. (i) The global state $y^{(\mathrm{gl})}$ changes with the edge weight w for different values of m. (j) The ratio of the qualitatively correct prediction, which counts the fraction of nodes at either high-stable states or low-stable states predicted by both the original network and the dimension-reduced system. The state threshold separating the two stable states is set as $R_y = 1$. (k) The heatmap of the global state $y^{(\mathrm{gl})}$ as a function of w and m. (l) The relative error of the stable state for different values of m compared to the ground truth. (m) The optimal m changes with w for different values of thresholds R_e, and m_{opt} is defined as the minimal value of m that produces the error smaller than the threshold R_e. (n) The heatmap of relative errors of global states compared with the ground truth.**

$$\mathrm{Err}(\mathrm{y}^{(\mathrm{gl})}) = \frac{|y^{(\mathrm{gl},N)} - y^{(\mathrm{gl},m)}|}{|y^{(\mathrm{gl},N)}| + |y^{(\mathrm{gl},m)})|} \tag{3.7}$$

For SF networks with different heterogeneities, one can observe the phase diagram of the original network and dimension-reduced systems are different from the one-dimensional system. When we include more components (larger m), the equilibrium state approximation improves in Fig. 3.3. For the systems far away from the tipping point of phase transition, one-dimensional systems ($m = 1$) are already sufficient to represent the system state.

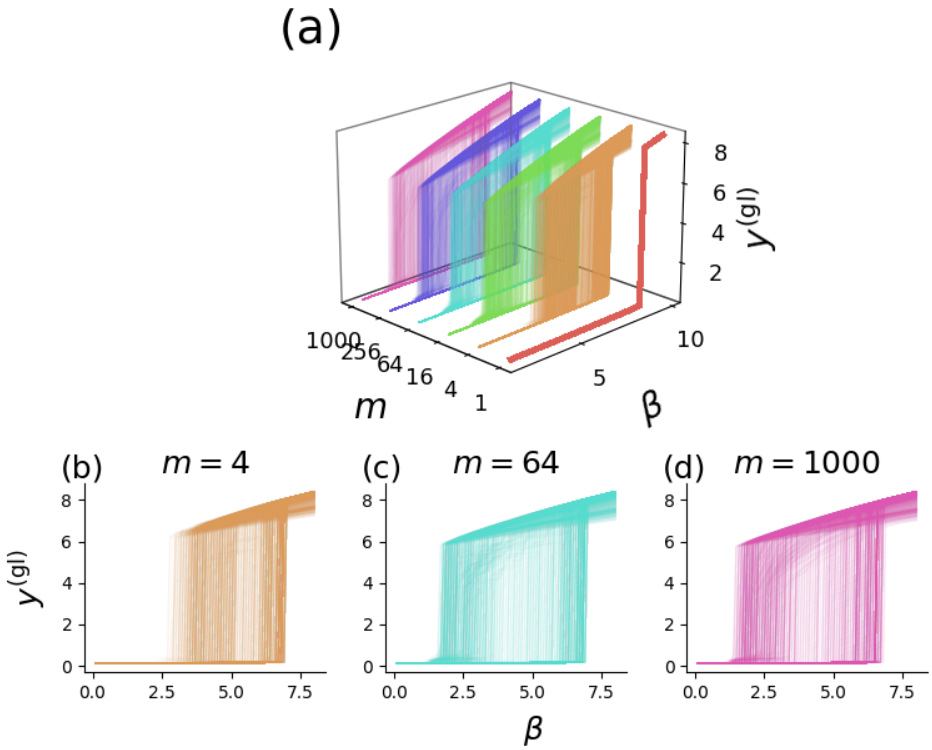

Figure 3.3: The phase diagram of the global state for SF networks following the mutualistic dynamics. The stable states are obtained from $L = 900$ networks (the exponent γ ranges from 2.1 to 5, and the minimal degree k_{min} is 3, 4, or 5), and all of them start from the low states, $x_i(t = 0) = 0.1$. (a) shows the phase diagram for different values of m. The parameter β is calculated by the one-dimensional reduction theory. In each subplot (b) – (d), the phase diagram of the global state against the parameter β for the same system dimensionality (the same m) and each curve represents one individual network.

To systematically validate the proposed framework, we apply it to two more dynamical models, neuronal dynamics [104] and gene regulatory dynamics [105], [106], which also exhibit phase transitions between alternative stable states.

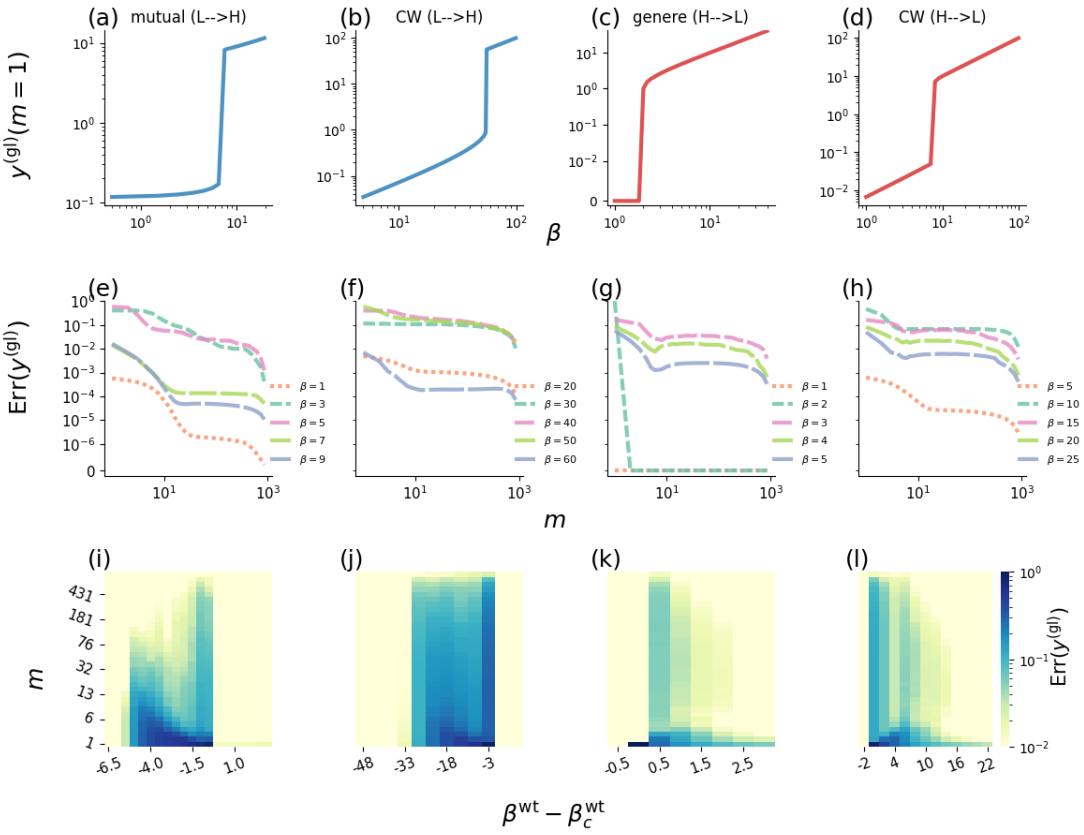

Figure 3.4: The relative error of the global state for different dynamics. Evolution data is collected from $L = 900$ networks (the exponent γ ranges from 2.1 to 5, and the minimal degree k_{min} is 3, 4, or 5). (a) – (d) display the phase diagram of the stable states against the effective interaction strength β, which is calculated by a single-dimension reduction system. For (a) mutualistic dynamics starting from the low state $x_i(t = 0) = 0.1$, the tipping point of phase transition $\beta_c^{(m=1)} = 7$, (b) Wilson-Cowan (CW) neuronal dynamics starting from the low state $x_i(t = 0) = 0.0$, $\beta_c^{(m=1)} = 56$, (c) gene regulatory dynamics starting from the high state $x_i(t = 0) = 100$, $\beta_c^{(m=1)} = 2$, and (d) CW neuronal dynamics starting from the high state $x_i(t = 0) = 100$, $\beta_c^{(m=1)} = 8$. (e) -(h) The error of the global state is calculated for m-dimensional systems in the comparison of the original networks. (i) – (l) are heatmaps of the error as a function of dimensionality m and the distance to the tipping point $\beta_c^{(m)}$.

The Wilson-Cowan neuronal dynamics in Eq. (3.8) describes the firing-rate activity of a population of neurons. Although the Wilson-Cowan equations are already an approximation by mean-field theory [107], [108], they can still exhibit very complicated behavior for the large system. Our approach provides an alternative and complementary way to simplify the

neural dynamics,

$$\frac{\mathrm{d}x_i}{\mathrm{d}t} = -x_i + \sum_{j=1}^{N} A_{ij} \frac{1}{1 + e^{\theta - \delta x_j}}, \tag{3.8}$$

where the parameters $\theta = 5$ and $\delta = 1$ control the firing-rate threshold and the steepness of the activation function, respectively.

We also apply our approach to biological networks. The gene regulatory dynamics are governed by the Michaelis-Menten equation (3.9),

$$\frac{\mathrm{d}x_i}{\mathrm{d}t} = -Bx_i^f + \sum_{j=1}^{N} A_{ij} \frac{x_j^h}{x_j^h + 1}, \tag{3.9}$$

where the parameters are also node-uniform and set as $B = 1$, $f = 1$, $h = 2$. The first term on the right-hand side describes the degradation of each gene, and the second term captures genetic activation, indicating the level of cooperation between genes.

In Fig. 3.4, one can observe that the prediction accuracy depends on the coupling strengths. For different dynamics, the relative error of $y^{(\mathrm{gl})}$ behaves in a similar fashion. As the system interaction strength approaches the tipping point of the one-dimensional system, the error increases in most cases. Therefore, more clusters are needed to correctly understand the system states.

3.2.3 Tipping point approximation

For heterogeneous networks, the m-dimensional reduction strategy achieves a much better approximation accuracy than the one-dimensional reduction model. In many cases, a small number of clusters can capture the system evolution. The only exception is that as the system approaches the tipping point of phase transition, the number of clusters should be increased to help qualitatively predict the system state and identify critical thresholds. Fig.3.4 also shows that the prediction accuracy depends on the distance to the tipping points. Hence, locating the tipping point of phase transition is important for distinguishing the active state from the dead state. To determine the critical point of either the dimension-reduced system or the original networked system, appropriate criteria need to be chosen. Here, we introduce two types of thresholds, the survival ratio threshold R_s (nodes with a state above a certain value are considered to be in a surviving state), and the global state threshold R_y. The tipping point w_c is defined as the smallest interaction strength at which the ratio of survival

nodes or the global state exceeds the predefined threshold (R_s or R_y). In addition, one can quantify the approximation accuracy by calculating the relative difference of the tipping points between the dimension-reduced system and the original network using Eq. (3.10). To demonstrate the improvement of including more than one component, the normalized distance of the critical point in $h^{\mathrm{wt}} - \langle k\rangle^{\mathrm{wt}}$ space is introduced in Eq. (3.11), which is used to represent the difference of thresholds between the one-dimensional reduction system and the m-dimensional system. Here, h^{wt} is the weighted degree heterogeneity defined as $h^{\mathrm{wt}} = wh = w\frac{\langle k^2\rangle - \langle k\rangle^2}{\langle k\rangle}$, $\langle k\rangle^{\mathrm{wt}} = w\langle k\rangle$ is the weighted average degree, and $\beta^{\mathrm{wt}} = w\frac{\langle k^2\rangle}{\langle k\rangle} = h^{\mathrm{wt}} - \langle k\rangle^{\mathrm{wt}}$ is the weighted effective interaction strength of the one-dimensional reduction system.

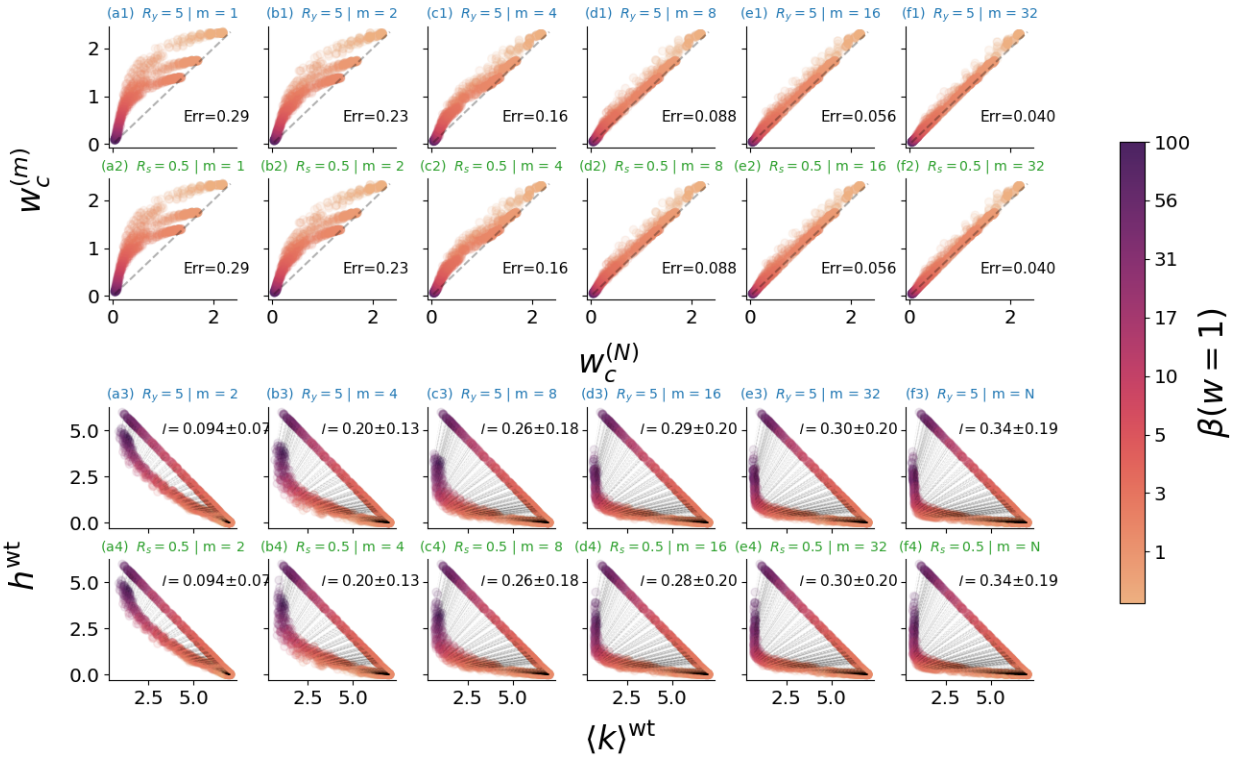

Figure 3.5: The tipping point approximation of the dimension-reduction framework. The results are obtained from $L = 900$ SF networks. (a1) – (f2) compare the tipping points between dimension-reduced systems and the original networks. (a3) – (f4) are the comparisons of the tipping points between multi-dimensional systems and one-dimensional systems in $h^{\mathrm{wt}} - \langle k\rangle^{\mathrm{wt}}$ space. Two error thresholds, R_y and R_s, measure the difference of the global state and the survival ratio, respectively.

In the one-dimensional reduction framework, all networks with different degree distri-

butions share the universal tipping point β_c^{wt} if they follow the same dynamical mechanism [16]. As we have already noticed in Fig. 3.1 and 3.2, the tipping points of heterogeneous networks depend on network topology and they cannot be accurately captured by the one-dimensional systems. In Fig. 3.5, we quantitatively compare the tipping points between the m-dimensional reduction system and the original network and demonstrate that the difference typically decreases as m increases. We also show that the tipping points predicted by the one-dimensional reduction system significantly deviate from the ground truth, and the difference depends on the network topology. From Fig. 3.6, one can observe that the average accuracy of SF network ensembles increases as the number of clusters increases, and such results hold for different types of dynamics.

$$\mathrm{Err} = \frac{|w_c^{(m)} - w_c^{(N)}|}{w_c^{(m)} + w_c^{(N)}} \tag{3.10}$$

$$l = |w_c^{(m)} - w_c^{(N)}| \frac{\sqrt{\langle k \rangle^2 + h^2}}{\beta_c^{wt}} \tag{3.11}$$

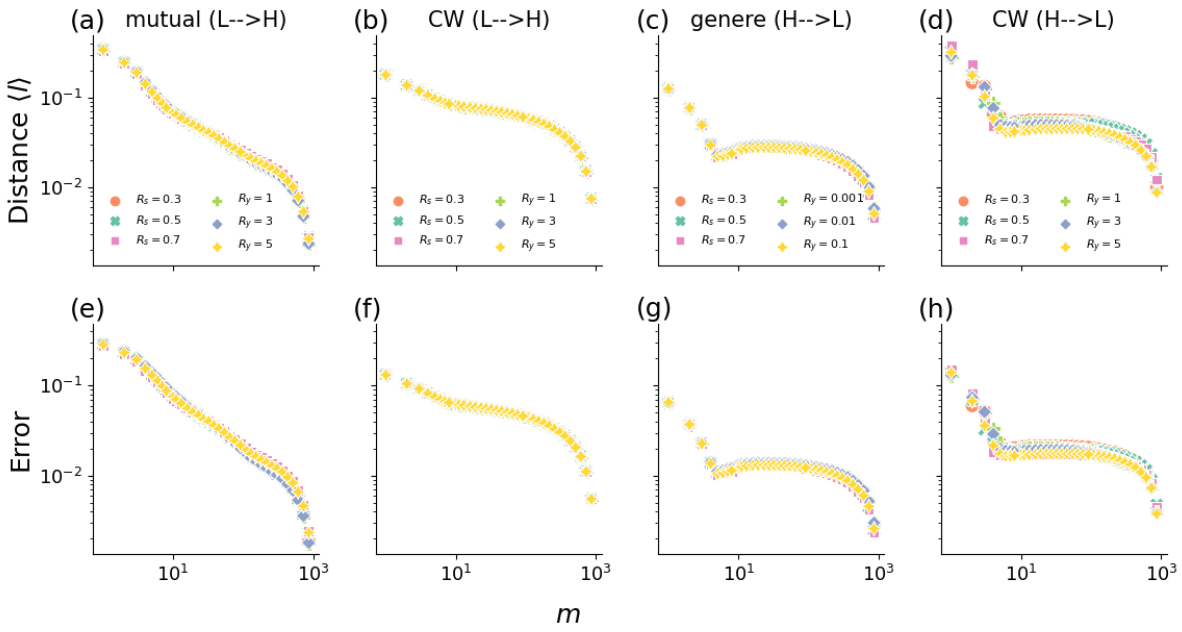

Figure 3.6: The difference of the critical point changes with the number of clusters for SF networks with different dynamics. For each system, the results are obtained from $L = 900$ SF networks. (a) – (d) show the distance of tipping points between the original systems and the dimension-reduction systems, and (e) – (h) show the relative errors. Different symbols represent different threshold types and values.

3.3 The application to time-delay systems

In this section, we use this framework to study the dynamical networks in the presence of time delays and further analyze the critical time delay in terms of stability.

Delayed interactions are quite common in many dynamical systems and have been extensively studied in terms of stability and synchronization [87], [88], [89], [99], [100], [101], [102], [109]. The key early results were published by Hutchinson [95] and May [91], who discussed the time delay and stability in the single-variable ecological systems [91], [95], [96], [110]. As the time delay occurring on one individual has profound effects on its neighboring components in the interconnected systems, one cannot capture the collective phenomena or global dynamics by only investigating one or two components. Therefore, one might need to investigate the complex interaction topology to understand the system evolution and stability. On the other hand, serious computational issues arise for simulating large networked systems. In this case, one can resort to the dimension-reduction framework to reduce computational complexity while preserving key information about the interactions between components.

The network dynamics in the presence of delays can be mathematically characterized by the delay differential equations (DDE). In this study, we focus on the dynamics with constant time delay and the delay effects are incorporated into the self-interaction term. Correspondingly, the time-delayed dynamics of the system composed of N interacting nodes is described by Eq. (3.12). As before, the term "dimension" refers to "the number of nodes" in the original system or "the number of clusters" in the simplified system.

$$\frac{\mathrm{d}x_i}{\mathrm{d}t} = f_i(x_i, x_i(t-\tau), x_j) = F(x_i, x_i(t-\tau)) + w\sum_{j=1}^{N} A_{ij}G(x_i, x_j). \tag{3.12}$$

We apply the degree-based dimension-reduction approach to the delayed system and obtain the m-dimensional system defined by Eq. (3.13), where y_a is the average node state of the cluster g_a, and β_{ab} is the interaction strength from the cluster g_b to the cluster g_a,

$$\frac{\mathrm{d}y_a}{\mathrm{d}t} = f_a(y_a, y_a(t-\tau), y_b) = F(y_a, y_a(t-\tau)) + w\sum_{b=1}^{m} \beta_{ab}G(y_a, y_b). \tag{3.13}$$

Fig. 3.7 shows the impact of time delays on the dynamical stability for a SF network and its corresponding dimension-reduced versions. As the time delay increases, the system

takes longer time to converge to the stable state. If the time delay exceeds a certain threshold, the system will either go to the limit cycle for the low-dimension systems (Fig. 3.7 a1–a3) or diverge (Fig. 3.7 b2 b3, c3, d3), so that one can determine the critical time delay in terms of stability based on the system evolution.

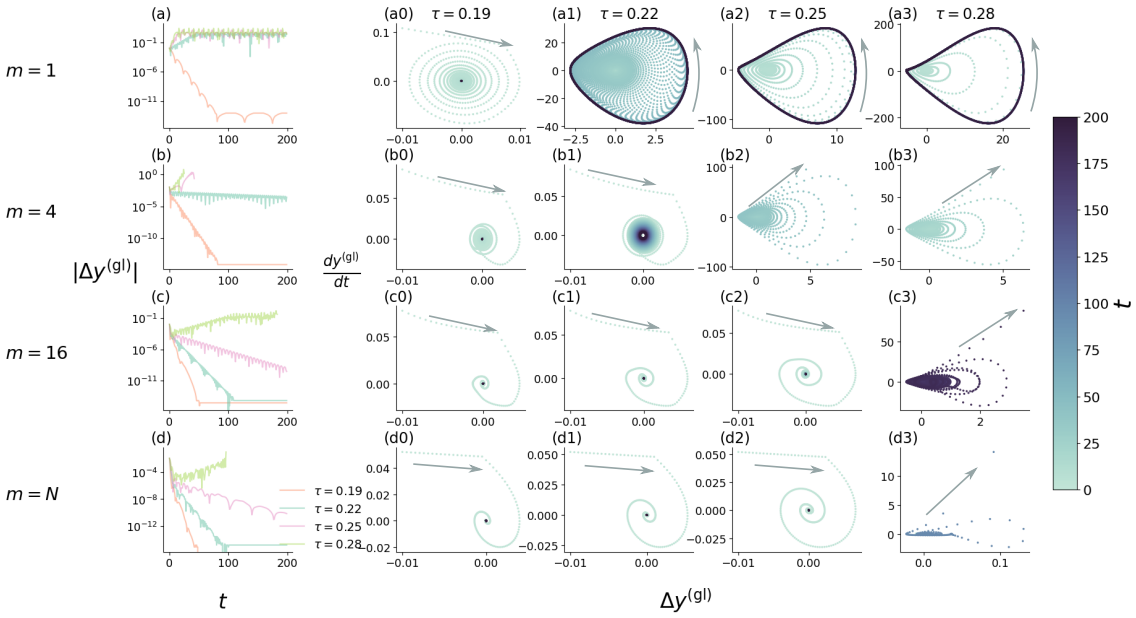

Figure 3.7: A SF network of $N = 1000$ nodes and its corresponding dimension-reduced systems under different time delays. This SF network is constructed by the configurational model with the exponent parameter $\gamma = 2.5$, and the minimal degree $k_{\min} = 3$. The edge weight $w = 0.1$. (a) – (d) The evolution of the global state difference $|\Delta y^{(\mathrm{gl})}|$ for different values of time delay $\tau = 0.19, 0.22, 0.25, 0.28$ and the system dimension $m = 1, 4, 16, N$. $\Delta y^{(\mathrm{gl})}$ is the difference between the system global state at time t and the stable state without time delay. Other figures show the phase space $\frac{\mathrm{d}y^{(gl)}}{\mathrm{d}t}$ versus $\Delta y^{(gl)}$respectively.

One can notice that the low-dimensional system ($m = 1$ or $m = 4$) does not only yield quantitative deviations from the ground truth, but can also qualitatively miss the actual behavior [limit cycle vs. stationary value], as shown in Fig. 3.7. One needs to employ a higher-m ($m = 16$ in this example) reduction scheme to at least qualitatively capture the nature of the steady state, and progressively higher ones for further quantitative improvements. To determine this critical threshold, one can numerically simulate the system evolution under different values of time delays. By using the binary search algorithm, one can find the largest time delay with which the system still converges to a steady stable. For large

networked systems, this method requires substantial computational resources. Hence, one can instead use the dimension-reduction framework to reduce the system complexity. One can observe that the global state evolution becomes more accurate compared to the ground truth (the evolution of the original system) as the number of clusters increases (Fig. 3.7 c and d).

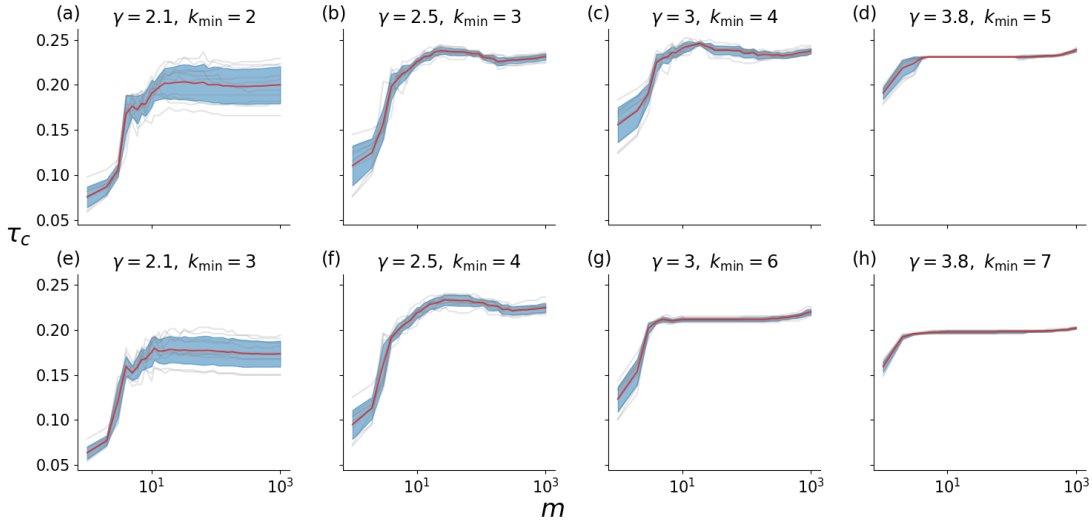

Figure 3.8: The critical time delay τ_c determined by dynamical evolution for SF networks using the dimension-reduction approach. All networks are created by configuration model and they consist of $N = 1000$ nodes. For each parameter choice, there are 10 realizations. The edge weights are the same, $w = 0.6$. (a) – (d) The average degree $\langle k \rangle \sim 6$, and (e) – (h) $\langle k \rangle \sim 10$.

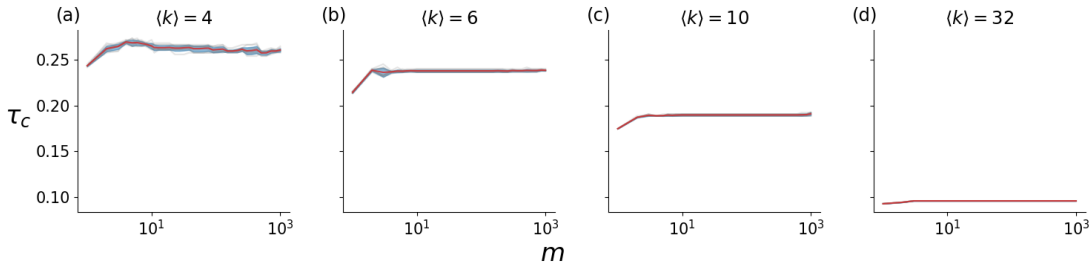

Figure 3.9: The critical time delay τ_c determined by dynamical evolution for ER networks using the dimension-reduction approach. All networks are created by configuration model and they consist of $N = 1000$ nodes. The edge weights are the same, $w = 0.6$. The average degrees are set (a) $\langle k \rangle = 4$, (b) $\langle k \rangle = 6$, (c) $\langle k \rangle = 10$, and (d) $\langle k \rangle = 32$. For each setup, there are 10 realizations.

Furthermore, the critical time delay can be predicted by the dimension-reduced sys-

tems for different network topologies as shown in Fig. 3.8 and 3.9, and the error decreases dramatically as more clusters are included. The more heterogeneous the network is (smaller γ for SF networks), the larger number of clusters may be needed. This approach proves to be very efficient since even for very heterogeneous networks, the system with $m = 10$ clusters can produce reasonable approximations.

Alternatively, one can derive the characteristic equation (3.14) [96], [97] associated with the system (3.12) by exerting a small perturbation $R = ce^{\alpha t}$ ($\alpha = \mu + i\nu$) around the equilibrium and performing the first order approximation to obtain the linear stability

$$\det(M(\alpha;\tau)) = \det\big(\alpha I - J_f(x)|_{x_s} - J_f(x_\tau)|_{x_s} e^{-\alpha\tau}\big) = 0 \tag{3.14}$$

In Eq. (3.14), I is the identity matrix, $J_f(x)$ and $J_f(x_\tau)$ are the Jacobian matrices, $f = (f_1, f_2, ..., f_N)^T$ is a vector of individual dynamical functions, $x = (x_1, x_2, ..., x_N)^T$ is a vector of node states at time t, and $x_\tau = (x_1(t-\tau), x_2(t-\tau), ..., x_N(t-\tau))$ is a vector of node states with delay τ (i.e., at time $t - \tau$). The (i, j) element of matrix $J_f(x)$, for example, is calculated by $\frac{\partial f_i}{\partial x_j}$. The system is asymptotically stable if and only if all roots α of Eq. (3.14) have negative real parts [96]. When the time delay reaches the threshold τ_c, Eq. (3.14) has a pair of purely imaginary roots ($\pm i\nu$), which is the critical condition. Hence, for any delay $\tau < \tau_c$, the real parts of all roots α remain negative, leading to asymptotically stable convergence, and when $\tau > \tau_c$, there is at least one root with positive real part, which destabilizes the system, according to Rouche's theorem and continuity [111].

To determine the critical time delay, one should first set $\alpha = i\nu$, and then solve the characteristic equation (3.14). Because it is essentially a polynomial equation, there are multiple solutions. For the critical condition, only the smallest positive solution is of interest. It turns out to be another challenging numerical problem as the solutions strongly depend on the initial condition shown in Fig. 3.10. The heuristic approach is to increase the search space of (τ_0, ν_0) in order to find out more solutions and choose the smallest one as the critical point. Although the solution obtained by this method is not guaranteed to be the ground truth, it demonstrates the accuracy in comparison to the result from the numerical evolution in Fig. 3.11. In addition, the critical time delays obtained by the dimension-reduced systems are in good agreement with the original system as long as a sufficient number of clusters ($m = 10$) are included.

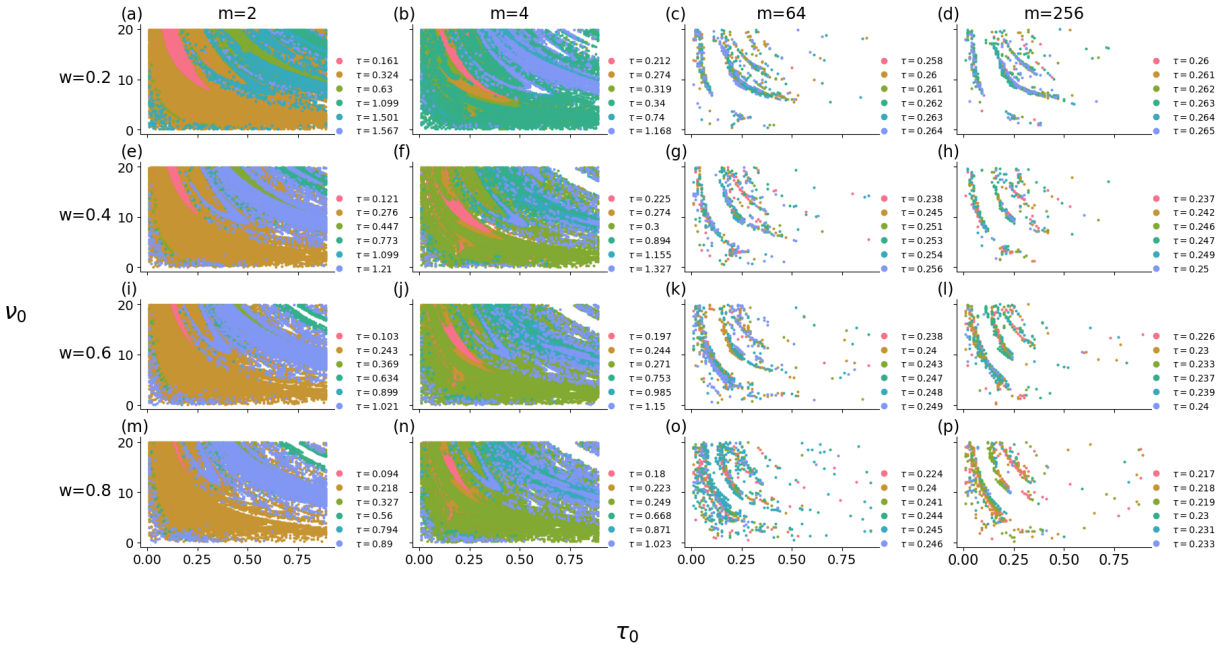

Figure 3.10: Solutions to Eq. (3.14) for different initial parameters (τ_0, ν_0). The system consists of $N = 1000$ nodes. Results are for different edge weights w and system dimensionality m. For (a) – (d) $w = 0.2$, (e) – (h) $w = 0.4$, (i) – (l) $w = 0.6$, and (m) – (p) $w = 0.8$. For (a), (e), (i) and (m) $m = 2$, (b), (f), (j) and (n) $m = 4$, (c), (g), (k) and (o) $m = 64$, and (d), (h), (l) and (p) $m = 256$.

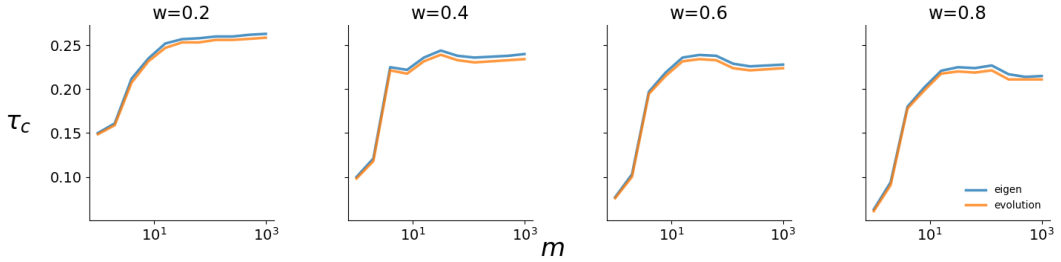

Figure 3.11: The comparison of the critical time delay obtained from the system evolution and the characteristic equation. There are $N = 1000$ nodes in the system.

3.4 Discussions

In this study, we present a mean-field framework to reduce the dimensionality of large complex networks. In this framework, the network is first classified into m clusters based on node degrees such that the nodes in the same cluster share similar degrees with the assumption that nodes of similar degrees have similar dynamical evolutions. For each cluster, one

observable is then introduced to represent the degree-weighted average state. Therefore, an N-dimensional network is described by an m-dimensional system and the dimension-reduced version preserves the original dynamical rules. Compared with the previous one-dimensional mean-field approaches [16], [17], this framework better approximates the state evolutions and tipping points, especially for heterogeneous networks and networks with communities. We find that the approximation accuracy depends on the network topology, the distance to the underlying tipping point of phase transition, and the number of clusters m. Generally, the approximation error increases as the system approaches the tipping point, which indicates that more clusters are needed to have a reasonable understanding of system evolutions. Under different interaction strengths, the number of clusters required to obtain the predefined accuracy (i.e., the value of m_{opt}) differs. It can be determined by comparing the node evolutions of the m-dimensional reduction system with the original network. It turns out that m_{opt} is almost always much smaller than the number of nodes N in the original network. In other words, one can have a reasonable approximation of system evolutions by constructing a much simpler system with m_{opt} representatives instead of investigating the original network. Another advantage of this dimension-reduction framework is that the interpretation is very clear, as each variable in the dimension-reduced system represents the average of node states in that cluster. Further, one can study how the interactions between clusters influence the cluster states and the system evolution, especially around the tipping points of phase transition. This may guide us to recover the dysfunctional systems by controlling certain clusters [40], [112].

This framework can not only be used to approximate the system state, but it also has some other potential applications. Here we show that one can apply this theory to time-delay dynamical systems and evaluate the critical threshold in terms of the system stability. In the presence of time delays, the system becomes unstable if the delay is greater than the critical point. Using this method, one can avoid numerically simulating the dynamics of all components or computing the eigenvalues of characteristic matrices for large networks. We also show that our approach can be universally applied to different types of networks and dynamics or with co-adaptation [113].

Despite the promising results, there are still open questions that need to be addressed in future research. For instance, the impact of network topology and dynamics on the optimal number of clusters remains unclear. Currently, the choice of the number of clusters is

determined empirically for each system. This issue also arises when the dimension-reduction framework is applied to time-delay systems. A theoretical investigation of this issue would provide guidelines for the relationship between the error produced by the mean-field approximation and the system dimension. Our approach will be significantly empowered if the method is developed to compute how many clusters the system should be partitioned into based on the network structure and its dynamics from a more theoretical perspective.

CHAPTER 4
DIVIDE-AND-RULE POLICY IN THE NAMING GAME

4.1 Introduction

Opinion spreading, language evolution, and collective behavior in social systems have been of great interest to researchers and they were investigated from mathematical and so-called sociophysics perspectives for at least four decades [19], [114], [115], [116], [117], [118], [119], [120], [121], [122], [123], [124], [125], [126]. Agent-based models and statistical physics provide powerful tools for studying the opinion dynamics and social influence, often modeled by dyadic agent interactions [23], [127], [128], [129]. When choosing one of the several opinions, some individuals may follow the choices of their peers or acquaintances. However, other individuals in the system may advocate a single opinion and refuse to consider any others, to which we refer as committed agents or zealots. The presence of zealotry strongly biases the evolution of the opinions towards those held by the committed minorities. Even the presence of one group with committed agents of modest size may convert all the uncommitted agents to adopting the opinion of committed agents [20], [21], [22], [24], [130], [131], [132].

Here, we focus on the Naming Game (NG) to study the opinion dynamics in the presence of committed minorities. Introduced as a linguistic evolution model, the NG was initially used as a model for the formation of a vocabulary from different observations, and it demonstrated how a population of agents can collectively converge to a single unique word for labeling different objects or observations in their environment [23], [128], [133], [134]. Recently, it has been used as a mathematical model for the dynamics of social influence, which describes the evolution of competing opinions through the dyadic interactions between agents. A number of theoretical studies have been done to investigate the spread and evolution of opinions on various regular and complex networks in the presence of committed agents [135], [136], [137], [138], [139], [140], [141]. Yet many of them focus on the models with two competing opinions. To gain a general understanding of this model, the scenario with multiple opinions deserves more attention. In such systems, agents can hold a variety of opinions, and the dynamics of opinion evolution can be more complex and diverse than in the two-opinion scenario.

Portions of this chapter previously appeared as: C. Ma, G. Korniss, and B. K. Szymanski, "Divide-and-rule policy in the Naming Game," Jun. 2023. arXiv:*2306.15922*.

In our study, we consider the Naming Game with an arbitrarily large number of competing opinions and examine the influence of committed members on opinion evolution. Given the presence of mixed states that involve more than a single opinion, monitoring the state of the system with m distinct single opinions becomes extremely challenging, as there are $2^m - 1$ possible combinations of opinions which are proportional to the number of state variables needed to write the equations for the state evolution of the system. Such exponential growth of state variables makes this problem intractable even for the system of size m larger than 10 for both numerical simulation and analytical derivation of the solution.

There are also a limited number of studies discussing the system with multiple competing opinions [142], [143], [144], [145]. For some special scenarios, one may reduce the system complexity by inspecting symmetry and making appropriate approximations [142]. We adapt this approach to investigate the influence of committed agents and phase transition in the quasi-symmetric setup. However, the approximation might fail if no symmetry is preserved. Our strategy is to focus on the key features of the system. Since the system state is determined by the density evolution of each single opinion, it is not necessary to distinguish or record all mixed states. Instead, one can just keep track of the density distribution and spreading probability of each single opinion. By anonymizing mixed states, the number of states to be monitored is reduced, making the analysis of the system more manageable. This approach is general and can be applied to a wide range of scenarios.

The rest of the study is organized as follows. Section II provides an overview of the interaction mechanism of the Naming Game and its variants, as well as its evolution from the perspective of mean-field theory. Section III focuses on the original model on complete graphs and uses the mean-field differential equations to investigate opinion evolution. This section considers systems with different numbers of opinions, including two opinions, three opinions, and an arbitrarily large number of opinions. We also discuss phase transitions for different allocations of committed agents among multiple groups and the conditions under which the critical points arise, as well as two simplified systems of symmetrical setups designed to approximate the critical thresholds of the arbitrary initial conditions. Section IV studies the listen-only variant of the Naming Game on complete graphs and presents a recursive approach to reduce the system's complexity. In Section V, we investigate the original Naming Game model on Erdős-Rényi ER networks and show that for the given simplified scenario, the system evolution makes the divide and rule policy observable.

4.2 Model description and mean-field approximation

In the Naming Game (NG) model [23], [128], [137] using several distinct opinions, each agent holds a subset of opinions that defines its state. This state may change as a result of this agent's interaction with other agents when it acts as a speaker or listener in the NG current state.

In the original NG dynamics, at each NG state, a randomly chosen agent becomes a speaker and sends a random opinion from its opinion state to a randomly chosen neighbor to be a listener. If the listener already has the sent opinion in its opinion state, both speaker and listener retain only this opinion, otherwise, the listener adds it to its opinion state. There is a special type of agent whose opinion state contains only one opinion, and it never acts as a listener, so it holds its opinion unchanged during the entire NG. In other words, such agents are immune to any influence but can still spread their opinions to their neighbors when acting as a speaker. We refer to them as committed agents or zealots. In addition to this original model, there are two variants, which limit changes to only one of the two interacting nodes, named the "listener-only" and "speaker-only" versions. For the "listener-only" type, only the opinion state of the listeners can be modified. Here, we focus on the original NG model and its "listener-only" variant.

For the opinion dynamics on the complete graph, mean-field theory can be applied to systematically study the evolution of opinion states. For the general scenario with m unique single opinions, an uncommitted agent can hold at most $M = 2^m - 1$ opinion states in total. For instance, when $m = 3$, the possible opinion states are A, B, C, AB, AC, BC, and ABC. Under the condition of homogeneous mixing, the mean-field differential equations are written as

$$\frac{\mathrm{d}x_k}{\mathrm{d}t} = \sum_{i=1}^{M}\sum_{j=1}^{M} U_{ij}^{(k)} x_i x_j + \sum_{i=1}^{M}\sum_{j=1}^{m} V_{ij}^{(k)} x_i P_j + \sum_{i=1}^{m}\sum_{j=1}^{M} W_{ij}^{(k)} P_i x_j. \tag{4.1}$$

Such equations describe the changes in the density of uncommitted agents holding different opinion states as well as the interactions between the uncommitted agents and committed agents. The density $x_i (i = 1, 2, ..., m)$ represents the fraction of uncommitted agents holding the single opinion state i, and the density x_i $(i = m+1, m+2, ..., M)$ represents the fraction of agents holding the mixed opinion state i. It represents the fraction of agents in this system that have opinion i in their opinion state. $P_i (i = 1, 2, ..., m)$ is the density of zealots committed to the single opinion i, which does not change over time. The matrices U, V, and

W contain the coefficients determined by the interaction mechanism and they differ for the three versions of the interaction rules. Specifically, $U_{ij}^{(k)}$ is the probability that the interaction between the uncommitted speaker with the opinion state i and the uncommitted listener with j gives rise to the opinion state k. $V_{ij}^{(k)}$ is the probability that results in the speaker adopting the opinion state k for the interaction between the uncommitted speaker holding the opinion state i and the committed listener with j. Similarly, $W_{ij}^{(k)}$ is the probability that results in the listener adopting the opinion state k for the interaction between the committed speaker holding the opinion state i and the uncommitted listener with j. The densities x_i and P_i must sum up to 1, so we have $\sum_{i=1}^{M} x_i + \sum_{i=1}^{m} P_i = 1$.

For the system with a small number of single opinions, m, the numerical integration of the mean-field differential equation, Eq. (4.1), can be performed to obtain the density evolution of each opinion state in the NG model. However, as the number of all opinion states, M, which includes both single and mixed opinions, increases exponentially with m, performing direct numerical simulations becomes computationally infeasible and impractical for large values of m.

4.3 Original version

First, the original NG dynamics are analyzed using mean-field differential equations, with a focus on the density evolution of each opinion state in the presence of committed minorities. This section includes the study of three scenarios varying in complexity., the first with two single opinions, the second with three single opinions, and the third with m single opinions in general.

4.3.1 The two-opinion scenario

In the scenario of $m = 2$, there are two opinions, A and B, in the system competing against each other. Eq. (4.1) reduces to two mean-field equations,

$$\frac{\mathrm{d}x_A}{\mathrm{d}t} = -x_A x_B + x_{AB}^2 + x_{AB}x_A + \frac{3}{2}P_A x_{AB} - P_B x_A \tag{4.2}$$

$$\frac{\mathrm{d}x_B}{\mathrm{d}t} = -x_A x_B + x_{AB}^2 + x_{AB}x_B + \frac{3}{2}P_B x_{AB} - P_A x_B \tag{4.3}$$

By definition, $x_A + x_B + x_{AB} + P_A + P_B = 1$. Together with Eq. (4.2) and Eq. (4.3), the two-opinion model can be analytically and numerically solved.

We are interested in the scenario in which one opinion (let us say A) has a higher fraction of committed agents than the other opinion, B, but the latter is initially supported by all uncommitted agents, making it the majority opinion. Committed agents of opinion A can assimilate uncommitted agents, thus causing opinion A to eventually become the majority opinion. Previous studies [21], [131] have shown that there exists a minimal fraction of committed agents, denoted by $P_A^{(c)}$, which is required for a fast phase transition of the dominant opinion from B to A. Below this threshold, the waiting time for such a transition grows exponentially with the number of agents, making it infeasible to observe in practical cases. To understand the final dominant state of the system, a new variable, n_i, is introduced, which represents the total fraction of agents holding opinion i in equilibrium. This fraction includes both the committed and uncommitted agents for a single opinion, $n_i = x_i^{(s)} + P_i$, whereas for mixed opinion states, n_i only accounts for the uncommitted agents, $n_i = x_i^{(s)}$, because committed agents only advocate their single opinions.

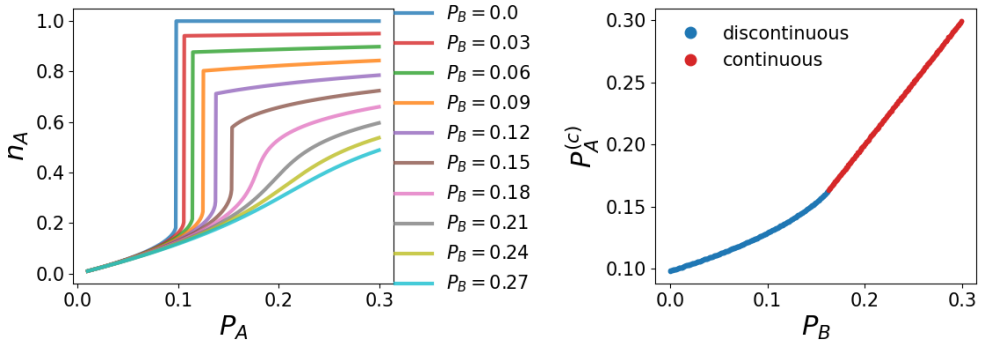

(a) (b)

Figure 4.1: Phase transition and the tipping point for $m = 2$. (a) The stable density of agents with opinion A n_A as a function of their committed fraction P_A for different values of P_B. (b) The critical point $P_A^{(c)}$ changes with P_B. The blue dots represent the discontinuous transition of n_A versus P_A, while the red ones represent the continuous change.

Previous studies [21] have shown that in the absence of committed agents advocating opinion B ($P_B = 0$, $P_A > 0$), a minimal fraction of committed agents advocating opinion A ($P_A^{(c)}$) of approximately 0.098 is required to trigger a fast transition from the majority opinion B to A. As Fig. 4.1a shows, when both committed groups, opinions A and B, are

present, there are two types of transitions, the discontinuous transition and the continuous one, that may occur depending on the committed fractions. They are separated by the point $(P^{(c)}, P^{(c)}) \approx (0.162, 0.162)$ [131]. For $P_B > P^{(c)}$, the fraction of agents holding opinion A increases continuously with P_A, and the critical points lie on the line $P_A^{(c)} = P_B$.

4.3.2 Three-opinion scenario

A slightly more complex system arises with three opinions. Let us consider three opinions A, B, and C, where opinions A and C are committed by two minor fractions of committed agents, and initially, all uncommitted agents, which form the majority of all agents, hold opinion B. We ask a similar question as in the previous example. For the scenario of $P_A > P_C$, to enable opinion A to dominate the system, what is the minimal fraction of committed agents, $P_A^{(c)}$, and how does this threshold depend on the committed fraction of the opinion C?

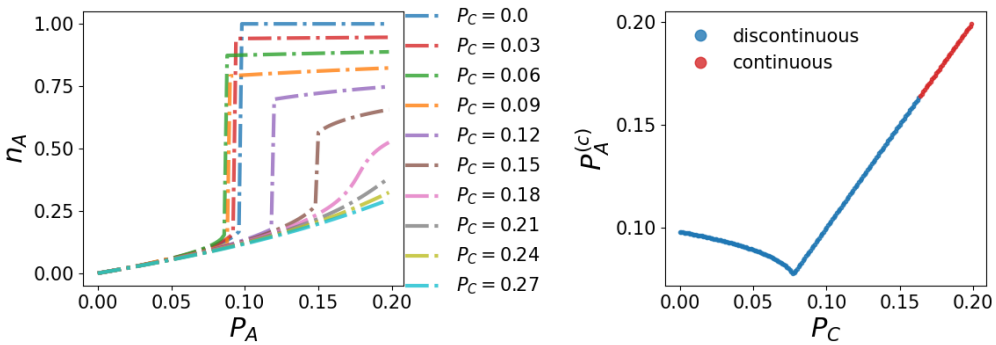

(a) (b)

Figure 4.2: Phase transition and tipping point for $m = 3$. (a) The stable density of agents with opinion A n_A as a function of their committed fraction P_A for different values of P_C. (b) The critical point $P_A^{(c)}$ changes with P_C. The blue dots represent the discontinuous transition of n_A versus P_A, while the red ones represent the continuous change.

According to Eq. (4.1), the evolution of each state variable can be numerically integrated. For small values of P_C, the fraction of agents holding opinion A, n_A, exhibits a discontinuous transition with respect to P_A (Fig. 4.2a), and beyond the critical point $P_A^{(c)}$, opinion A wins the majority of supporters. The relationship between the critical point $P_A^{(c)}$

and P_C is non-monotonic. In the regime of discontinuous transition, $P_A^{(c)}$ first decreases with P_C and then increases linearly with P_C, indicating that increasing the latter is beneficial for the agents committed to opinion A to dominate the majority of uncommitted agents given that P_C is smaller than a certain value ($P_C \approx 0.077$ at the lowest point in Fig. 4.2b). However, for $P_C > 0.077$, $P_A^{(c)}$ increases linearly with P_C and this regime includes both the discontinuous transition and the continuous one, different from the previous two-opinion scenario. The critical point separating two types of transitions remains the same as the two-opinion scenario.

4.3.3 The general scenario – multi-opinion model

For the general scenario with m single opinions (A, B, C_1, C_2, C_3, ..., C_{m-2}), it is of interest to understand the impact of committed agents on the majority of uncommitted agents and potential for one single opinion to dominate over other competitors. Consider a scenario where the majority of uncommitted agents support a single opinion, denoted as B, while the remaining agents are committed to $m-1$ single opinions. Among these $m-1$ opinions, the one with the largest committed fraction, denoted as A, has the potential to reverse the majority of uncommitted agents from supporting B to supporting A. The question then arises as to the minimum fraction of committed agents, $P_A^{(c)}$, required for such a transition to occur. To streamline the analysis, the committed agents supporting opinions other than A are grouped into a single category, referred to as $\tilde{A}$, with a combined committed fraction of $P_{\tilde{A}}$. This simplification is justified as none of the single opinions in the group $\tilde{A}$ can prevail in the competition. However, the number of competing opinions in the group $\tilde{A}$, $m-2$, their total committed fraction, $P_{\tilde{A}}$, and the allocation of these committed agents, P_i, may all potentially affect the critical point, $P_A^{(c)}$.

We, therefore, investigate the impact of such factors on the dominance transition of opinion dynamics by constructing three different scenarios for allocating committed agents within the group $\tilde{A}$.

1. **Scenario S_0: randomly distributed.** The committed fraction, P_i, of each single opinion in the group $\tilde{A}$ can be any value between 0 and $P_{\tilde{A}}$, but their total adds up to $P_{\tilde{A}}$.

2. **Scenario S_1: perfectly symmetric.** $m-2$ opinions in the group $\tilde{A}$ share the equal

fraction of committed agents, $P_i = p_0 = P_{\tilde{A}}/(m-2)$. The quantity, p_0, in the later context also refers to the average committed fractions of agents advocating the single opinion state in the group $\tilde{A}$.

3. **Scenario S_2: extremely polarized.** In contrast to the scenario S_1, we maximize the deviation of P_i in the group $\tilde{A}$ to establish the highly uneven distribution of committed fractions. Provided that the single opinion A has the largest committed fraction in the system, the largest committed fraction in the group $\tilde{A}$ should be smaller than P_A. To set up the numerical simulation, we chose $\max\{P_i\} = p_1 = P_A - 10^{-3}$, and the number of opinions with the committed fraction p_1 is also maximized, which is $n_1 = \lfloor P_{\tilde{A}}/p_1 \rfloor$. The rest of committed agents, $p_2 = P_{\tilde{A}} - n_1 p_1 (< p_1)$, are assigned to one single opinion. In this scenario, there are $m - n_1 - 3$ (≥ 0) single opinions in the group $\tilde{A}$ without any committed followers. In the group $\tilde{A}$, P_i can take three values, p_1, p_2, and 0. As there are no uncommitted agents assigned to the group $\tilde{A}$, some single opinions may end up with no supporters. One should note that the number of single opinions is still considered as m when compared with the scenarios S_0 and S_1.

The mean-field equations (4.1) can be directly integrated to analyze the opinion dynamics for a system with a limited number of single opinions. However, for a system with many opinions m, this method becomes computationally infeasible because the number of variables, M, increases exponentially with m. To overcome this challenge, simpler scenarios are considered, as described in the scenarios S_1 and S_2. The simplified structures of scenarios S_1 and S_2 allow for a more efficient and manageable study of the critical transition in comparison to direct numerical integration for the scenario S_0 with arbitrary initial conditions. In the scenario S_1, a collection of single opinions (denoted as the group $\tilde{A}$) are designed to have the same fraction of committed agents and no uncommitted supporters. Under the homogeneous mixing condition, the number of supporters for these opinions is expected to evolve in the same fashion. In this scenario, the number of state variables to be monitored is reduced from $2^m - 1$ to $4m - 5$. For example, when $m = 5$ where single opinions are A, B, C_1, C_2, C_3. Opinions C_1, C_2, and C_3 are assigned the same fraction of committed agents, so the fraction of uncommitted agents they can assimilate to themselves is expected to be the same by symmetry. Further, some mixed opinion states, such as C_1C_2, C_1C_3, and C_2C_3, or AC_1, AC_2, and AC_3 also have the same uncommitted supporters as time progresses. This

results in a reduction in the number of state variables that need to be monitored. A similar argument also applies to the scenario S_2.

Next, we study the fraction of supporters of opinion A which is assigned the largest committed fraction, and the critical transition in which this opinion assimilates the majority of uncommitted individuals to itself for the three scenarios.

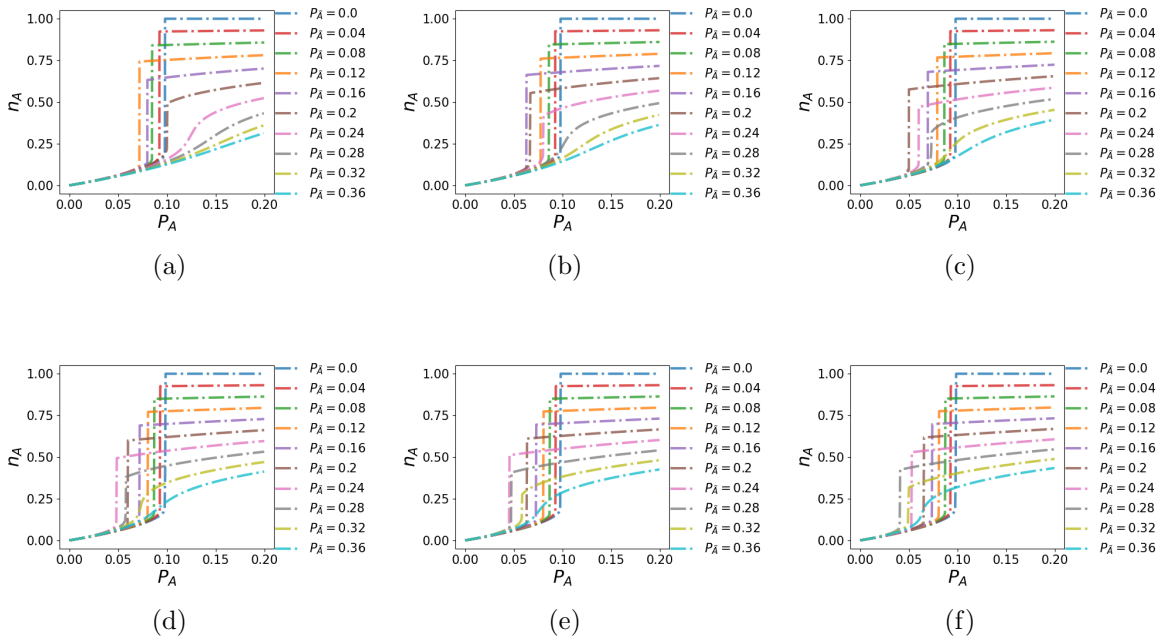

Figure 4.3: Scenario S_1. The fraction n_A holding the opinion A changes with P_A for different values of $P_{\tilde{A}}$. (a) $m = 4$, (b) $m = 5$, (c) $m = 6$, (d) $m = 7$, (e) $m = 8$, (f) $m = 9$.

In the scenario S_1, the total fraction of supporters of opinion A, n_A exhibits a discontinuous transition with P_A for small values of $P_{\tilde{A}}$ shown in Fig. 4.3. Also, as seen Fig. 4.4, in the critical point $P_A^{(c)}$ displays a non-monotonic behavior as $P_{\tilde{A}}$ or p_0 increases. The presence of a small committed group plays a key role in the formation of a dominant opinion. The initial decrease in the critical value $P_A^{(c)}$ as the committed fraction p_0 of the smaller groups increases suggests that as the number of committed individuals in these groups grows, they become more effective in facilitating the dominance of the opinion with the largest committed fraction. The initial decrease in $P_A^{(c)}$ can be attributed to the increased potential for interactions and conversions between the committed individuals in the smaller groups and the uncommitted individuals in the system. Moreover, the non-monotonic behavior of $P_A^{(c)}$

with increasing $P_{\tilde{A}}$ or p_0 also indicates the presence of a threshold effect. Beyond a certain value of $P_{\tilde{A}}$ or p_0, the critical value $P_A^{(c)}$ begins to increase, indicating that the positive influence of the smaller committed groups on the dominant opinion's growth becomes weaker. The linear relationship instead shows the competition between opinion A and other opinions with a smaller committed fraction.

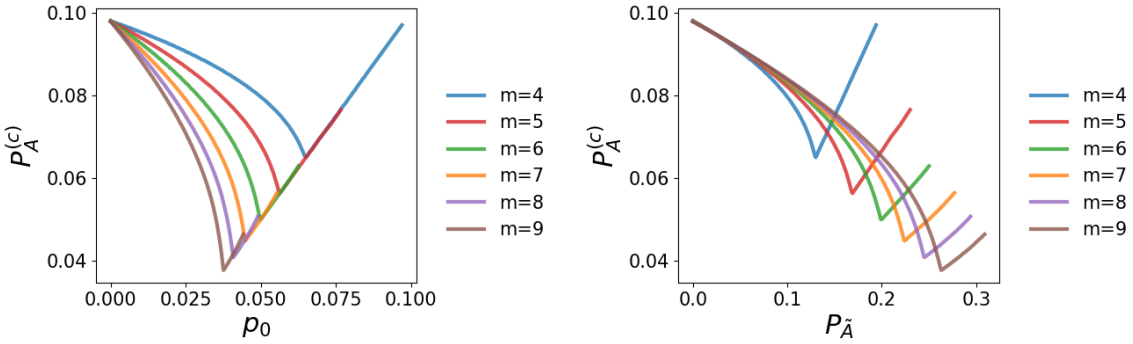

(a) (b)

Figure 4.4: Scenario S_1 for $m = 4, 5, 6, 7, 8, 9$. The critical point $p_A^{(c)}$ changes with (a) p_0 and (b) $P_{\tilde{A}}$. It only includes discontinuous transitions. The continuous transition follows the relationship $P_A^{(c)} = p_0$.

To explore how the value of the tipping point $P_A^{(c)}$ depends on the distribution of committed agents in the group $\tilde{A}$, we manipulate the committed fraction P_i while preserving $P_{\tilde{A}}$ in the scenario S_0. Results displayed in Fig. 4.5(a)–(c) show a non-monotonic behavior of the critical point $P_A^{(c)}$ as a function of the maximum value of P_i in group $\tilde{A}$. The initial decrease of $P_A^{(c)}$ indicates that the presence of a large fraction of committed agents within group $\tilde{A}$ is beneficial for opinion A to dominate the system compared to when the committed agents are uniformly distributed among the $m - 2$ single opinions.

This conclusion can also be confirmed by observing how $P_A^{(c)}$ changes with the standard deviation of P_i. However, it is worth noting that a higher P_i does not always result in a favorable outcome in terms of the dominance of opinion A. For opinion A to become dominant, its committed fraction P_A must be greater than any other committed fraction in the group $\tilde{A}$, which explains the linear increase of $P_A^{(c)}$ observed in the results. The non-monotonic behavior of the critical value of $P_A^{(c)}$ highlights the importance of considering the effects of different distributions of committed fractions on the overall dynamics of the system,

especially the dominance transition.

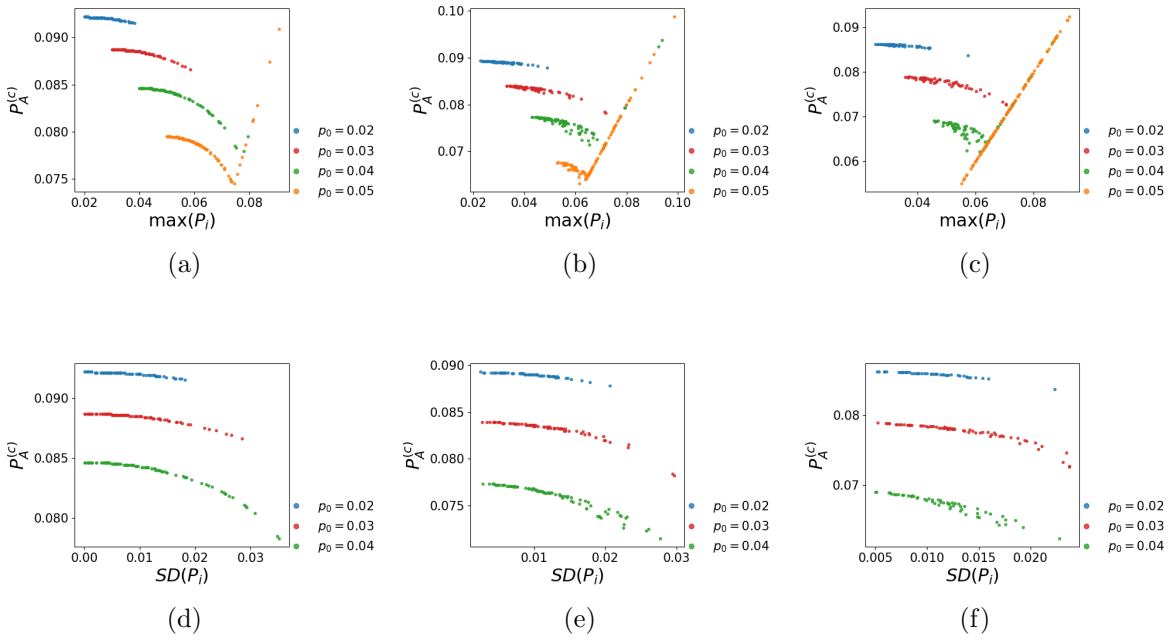

Figure 4.5: Scenario S_0. (a)–(c) The critical point $P_A^{(c)}$ changes with the maximum of P_i in the group $\tilde{A}$ with an initial decrease followed by a linear increase. (d)–(f) only include the data of the decrease regime, which shows that $P_A^{(c)}$ changes with the standard deviation (SD) of P_i. (a) and (d) $m = 4$, (b) and (e) $m = 5$, (c) and (f) $m = 6$.

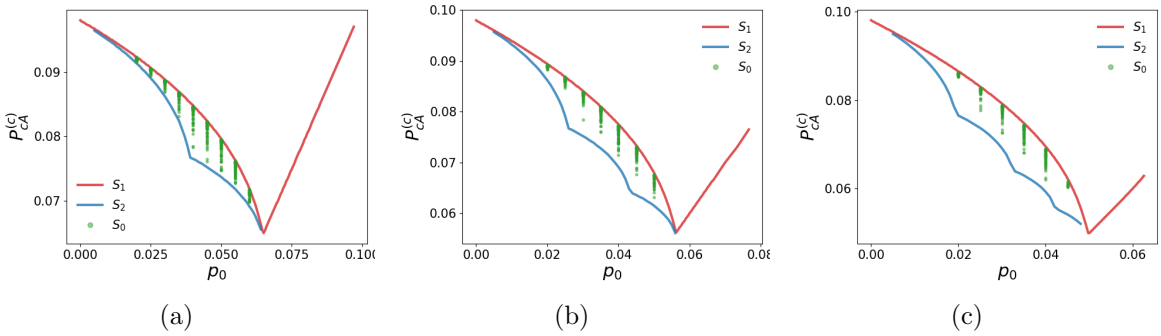

Figure 4.6: The critical point $P_A^{(c)}$ changes with p_0 in three scenarios S_0, S_1, and S_2. For the scenario S_0, only the data where $P_A^{(c)}$ is along the decreasing branch with $\max\{P_i\}$ in Fig. 4.5 is included. (a) $m = 4$, (b) $m = 5$, (c) $m = 6$.

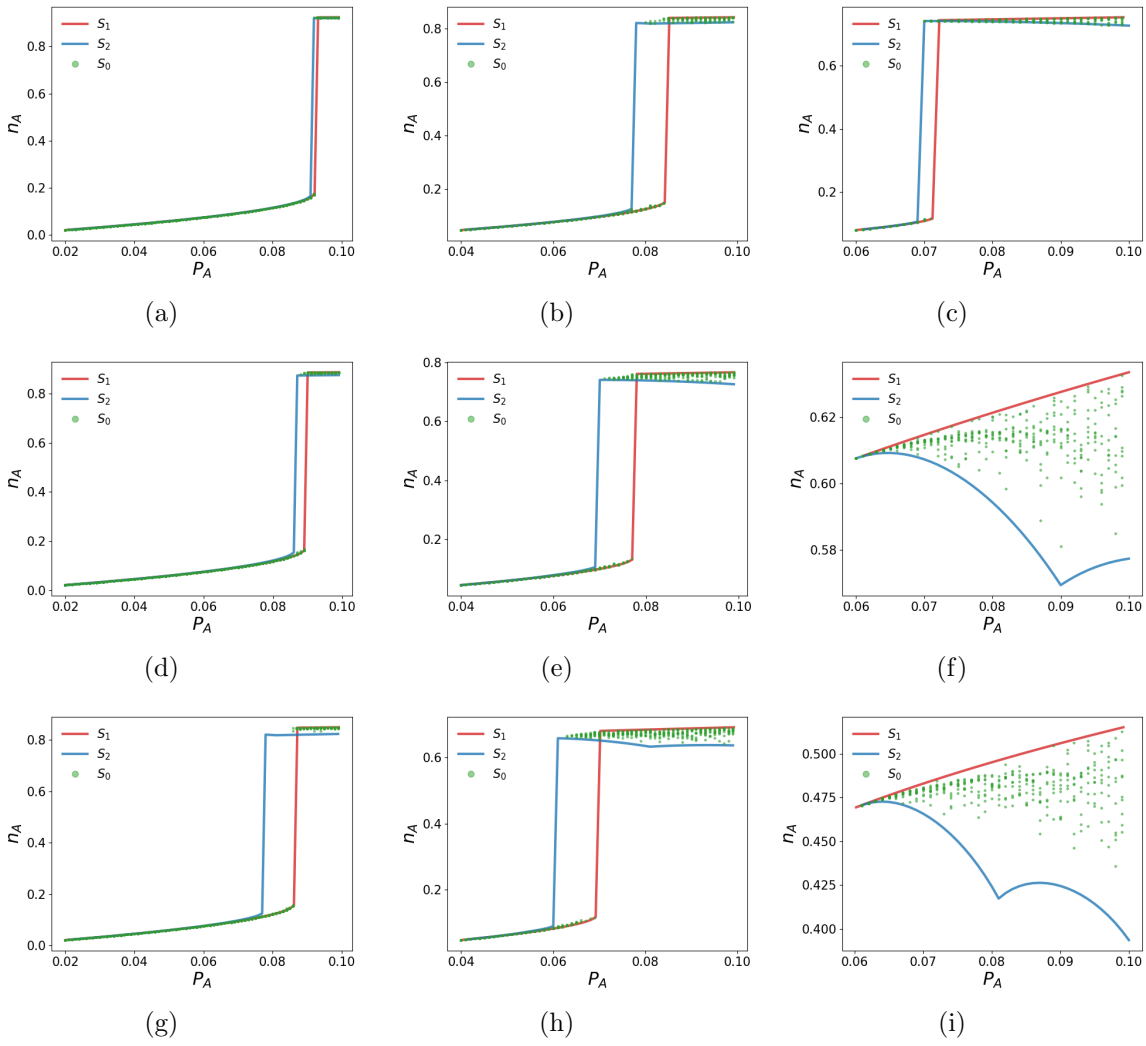

Figure 4.7: The steady state n_A changes with P_A in three scenarios S_0, S_1, and S_2. (a)–(c) $m = 4$, (d)–(f) $m = 5$, (g)–(i) $m = 6$. (a), (d), and (g), $p_0 = 0.02$; (b), (e), and (h), $p_0 = 0.04$; (c), (f), and (i), $p_0 = 0.06$.

As seen in Fig. 4.5, the scenario S_2 is expected to have a smaller critical point $P_A^{(c)}$ than S_1 given the fraction of committed agents in group $\tilde{A}$ is small enough, which can be confirmed from Fig. 4.6. The critical points obtained from two scenarios, S_1 and S_2, provide the upper bound and the lower bound, respectively, for the scenario S_0. Additionally, one can compare the steady states of the three scenarios in Fig. 4.7. The scenarios S_1 and S_2 also provide a good approximation for the steady state n_A in the scenario S_0. It is observed that the critical point $P_A^{(c_1)}$ in the scenarios S_1 is always greater than $P_A^{(c_2)}$ in the scenario S_2, and the two critical points $P_A^{(c_1)}$ and $P_A^{(c_2)}$ divide the parameter space into three parts. For values of P_A less than $P_A^{(c_2)}$, the scenario S_1 yields the lower bound of n_A while S_2 provides

the upper bound. For $P_A^{(c_2)} < P_A < P_A^{(c_1)}$, both scenarios establish the lower bound. For $P_A > P_A^{(c_1)}$ or the scenario when there are no critical points, the scenario S_1 corresponds to the upper limit of n_A while S_2 corresponds to the lower limit. By investigating the scenarios S_1 and S_2, the critical points and the steady states of the single opinion A with the largest committed fraction in the scenario S_0 are well estimated.

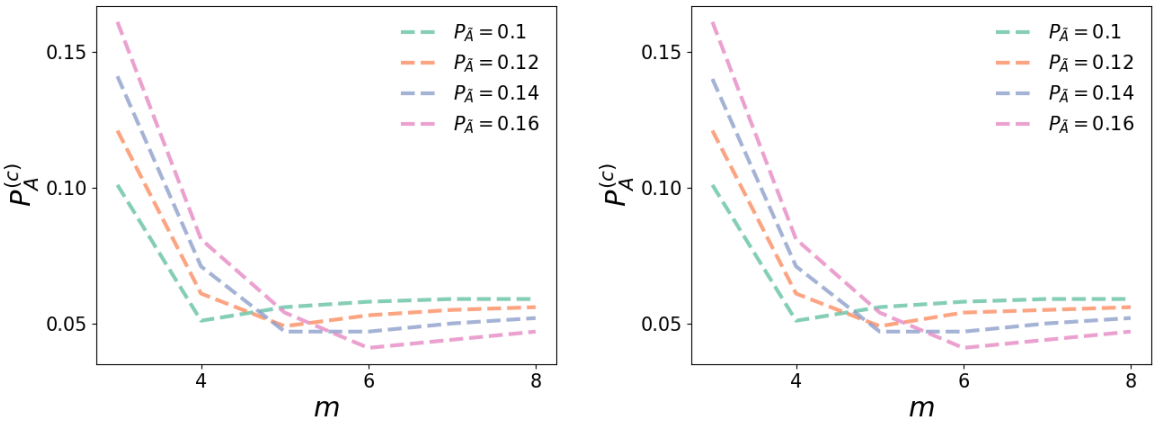

(a) (b)

Figure 4.8: Divide and rule. The critical point $P_A^{(c)}$ in the scenario S_1 is obtained by the recursive approach in (a), and the integration of the differential equations in (b). The critical point, $P_A^{(c)}$, has a non-monotonic relationship with the number of single opinions, m. Dividing the committed agents into a moderate number of competing minorities can aid in the domination of uncommitted agents by opinion A in the system. The parameter is set as $P_{\tilde{A}} = 0.1, 0.12, 0.14, 0.16$.

We now analyze the opinion competition from another perspective. The key question is to determine the dynamics of opinion A as it competes against opinions B and $\tilde{A}$. As shown in Fig. 4.8a, the critical point, $P_A^{(c)}$, in the scenario S_1 has a non-monotonic relationship with the number of single opinions, m. Given a fixed committed fraction, $P_{\tilde{A}}$, as m increases, the individual committed fraction, p_0 $(= P_{\tilde{A}}/(m-2))$, in group $\tilde{A}$ decreases, weakening the opposition from this group. The initial decrease of $P_A^{(c)}$ reveals the validity of divide and rule policy, whereby the more opinions splits among themselves the committed agents of the group $\tilde{A}$, the easier it is for opinion A to dominate uncommitted agents in the system. Reversing this rule reveals that the major obstacle to the opinion A dominance is the small number of opinions in the group $\tilde{A}$. However, if m continues to increase, the critical point

$P_A^{(c)}$ also increases, suggesting that opinion B becomes the major threat. In this scenario, the strong opponent, $\tilde{A}$, (large p_0) can be helpful for opinion A to dominate the system, thus making group $\tilde{A}$ a friend of opinion A, in line with the Heider balance theory rule [146] that states "The enemy of my enemy is my friend".

The critical point $P_A^{(c)}$ in the scenario S_0 can differ depending on the distribution of the committed agents. However, the scenarios S_1 and S_2 serve as an approximation by providing the upper and lower bounds, respectively, for this critical value. Additionally, the symmetry exhibited in the scenarios S_1 and S_2 results in identical evolution for opinion states with the same committed fraction in the group $\tilde{A}$ under the homogeneous mixing condition. This reduction in complexity allows for a more efficient analysis of the system dynamics, as a satisfactory approximation can be obtained by considering the scenarios S_1 and S_2.

4.4 Simplification by recursive relationship

In the previous section, we discussed how one can establish the symmetrical distribution of committed agents to reduce the complexity and approximate the opinion dynamics in more arbitrary scenarios. In this section, we will present a more general approach to reducing the system's complexity.

Since the largest committed opinion defines the system state, it is sufficient to focus on this opinion density evolution. We introduce a quantity $Q_i^{(t)}$, which represents the probability of a single opinion i being communicated at step t from the population [142], and we establish an iteration function for the opinion density at step t based on the state at step $t-1$. It has been shown that the original NG dynamics and the listener-only version on the complete graph have qualitatively similar results [147]. As it is easier to derive the iterative function by considering only the state change of listeners, we develop our framework for the listener-only version. For an uncommitted node to adopt a single opinion i at step t, it must have held the opinion i in its list at step $t-1$ and received opinion i at step t. Eq. (4.4) describes such conditions, where x_{i+} is the total fraction of all mixed states containing the opinion i. The first term of Eq. (4.4) represents the scenario when a listener holding the single opinion i receives the signal i, and the second term corresponds to the scenario when a listener in the mixed state containing the single opinion i hears the opinion i. After the interaction, the listener in both scenarios either remains in the single state i or adapts to it. Eq. (4.5) establishes the recursive relationship of the mixed state containing two opinions, i and j.

Specifically, if a listener initially supports opinion i (j) and subsequently receives signal j (i), it will switch to the mixed state, ij. This equation accounts for the scenario where a listener holds one opinion but is influenced by the received opinion through interaction with other agents. Similarly, the recursive relationship of the mixed state containing three single opinions is derived in Eqs. (4.6). One can easily generalize the iteration function of the mixed state containing n single opinions as Eq. (4.7), where $\mathcal{S}_n(i_1, i_2, ..., i_n)$ represents all permutations of a set containing n elements.

$$x_i^{(t)} = x_i^{(t-1)} Q_i^{(t-1)} + x_{i+}^{(t-1)} Q_i^{(t-1)} \tag{4.4}$$

$$x_{ij}^{(t)} = x_i^{(t-1)} Q_j^{(t-1)} + x_j^{(t-1)} Q_i^{(t-1)} \tag{4.5}$$

$$\begin{aligned} x_{ijk}^{(t)} =& x_{ij}^{(t-1)} Q_k^{(t-1)} + x_{ik}^{(t-1)} Q_j^{(t-1)} + x_{jk}^{(t-1)} Q_i^{(t-1)} \\ =& x_i^{(t-2)} Q_j^{(t-2)} Q_k^{(t-1)} + x_j^{(t-2)} Q_i^{(t-2)} Q_k^{(t-1)} \\ &+ x_i^{(t-2)} Q_k^{(t-2)} Q_j^{(t-1)} + x_k^{(t-2)} Q_i^{(t-2)} Q_j^{(t-1)} \\ &+ x_j^{(t-2)} Q_k^{(t-2)} Q_i^{(t-1)} + x_k^{(t-2)} Q_j^{(t-2)} Q_i^{(t-1)} \\ =& \sum_{(i',j',k') \in \mathcal{S}_3(i,j,k)} x_{i'}^{(t-2)} Q_{j'}^{(t-2)} Q_{k'}^{(t-1)} \end{aligned} \tag{4.6}$$

$$x_{i_1 i_2 ... i_n}^{(t)} = \sum_{(i'_1, i'_2, ..., i'_n) \in \mathcal{S}_n(i_1, i_2, ..., i_n)} x_{i'_1}^{(t-n+1)} Q_{i'_2}^{(t-n+1)} Q_{i'_3}^{(t-n)} ... Q_{i'_{n-1}}^{(t-2)} Q_{i'_n}^{(t-1)}. \tag{4.7}$$

To simplify the computation and focus on the density distribution of single opinions, x_i, the need to calculate or record all mixed states is eliminated. Instead, only Q_i and x_{i+} need to be tracked. The density evolution of mixed states containing opinion i, such as $x_{i\tilde{i}}$, $x_{i\tilde{i}\tilde{i}}$, $x_{i\tilde{i}\tilde{i}\tilde{i}}$, can be derived using Eq. (4.7), where $\tilde{i}$ refers to any single opinion other than opinion i. In this way, the number of variables is reduced from $2^m - 1$ to m^2.

By summing up Eq. (4.5) over a subset that includes any single opinion j other than i, one can obtain $x_{i\tilde{i}}^{(t)}$ as Eq. (4.8), where $\mathcal{M}$ is the set of m single opinions, and $\mathcal{M} \setminus i$ represents the set of all single opinions excluding the opinion i.

$$x_{i\tilde{i}}^{(t)} = x_i^{(t-1)} \sum_{j\in\mathcal{M}\setminus i} Q_j^{(t-1)} + Q_i^{(t-1)} \sum_{j\in\mathcal{M}\setminus i} x_j^{(t-1)} \tag{4.8}$$

Similarly, one can derive the general formula for the mixed state of length $n+1$ with opinion i and other n opinions, $x_{i\underbrace{\tilde{i}\,...\,\tilde{i}}_{n}}^{(t)}$,

$$x_{i\underbrace{\tilde{i}\,...\,\tilde{i}}_{n}}^{(t)} = \sum_{j\in\mathcal{M}} x_j^{(t-n)} \sum_{i\in(j_1,...,j_n)\in\mathcal{M}\setminus j} Q_{j_1}^{(t-n)}...Q_{j_n}^{(t-1)} \tag{4.9}$$

In Eq. (4.9), j_1, ..., j_n are n distinct integers, representing n different single opinions. By definition, opinion i must be one of n distinct single opinions $j_1, ..., j_n$. The ultimate objective is to track the evolution of single opinions over time, as captured by Eq. (4.4). This requires computing the probability of transmitting opinion i, $Q_i^{(t)}$, and the density of mixed states, $x_{i+}^{(t)}$, $(i = 1, 2, ..., m)$ at each interaction step t. According to the interaction rule, only speakers with a single opinion i in their list can communicate opinion i. Additionally, for the mixed state, each single opinion in the list has an equal probability of being transmitted. Therefore, $Q_i^{(t)}$ and $x_{i+}^{(t)}$ are expressed as Eqs. (4.10) and (4.11), respectively.

$$Q_i^{(t)} = x_i^{(t)} + P_i^{(t)} + \frac{1}{2}x_{i\tilde{i}}^{(t)} + \frac{1}{3}x_{i\tilde{i}\tilde{i}}^{(t)} + ... + \frac{1}{m}x_{i\underbrace{\tilde{i}\tilde{i}\tilde{i}\,...\,\tilde{i}}_{n}}^{(t)} \tag{4.10}$$

$$x_{i+}^{(t)} = x_{i\tilde{i}}^{(t)} + x_{i\tilde{i}\tilde{i}}^{(t)} + x_{i\tilde{i}\tilde{i}\tilde{i}}^{(t)} + ... + x_{i\underbrace{\tilde{i}\tilde{i}\tilde{i}\,...\,\tilde{i}}_{n}}^{(t)} \tag{4.11}$$

By employing recursive functions (4.4), (4.9), (4.10), and (4.11), one can calculate the density evolution of single opinions for any initial condition. One can further simplify the computation if the system's stable state is of primary interest, which means that the probabilities of communicating opinion i at different time steps are the same. Therefore, these probabilities $Q_i^{(t)}$, $Q_i^{(t-1)}$,..., $Q_i^{(t-n)}$ can be represented by one quantity $Q_i^{(s)}$. Comparing the system evolution obtained by the recursive approach and differential equations in Fig. 4.9, we find that the results are nearly identical, validating the recursive approach.

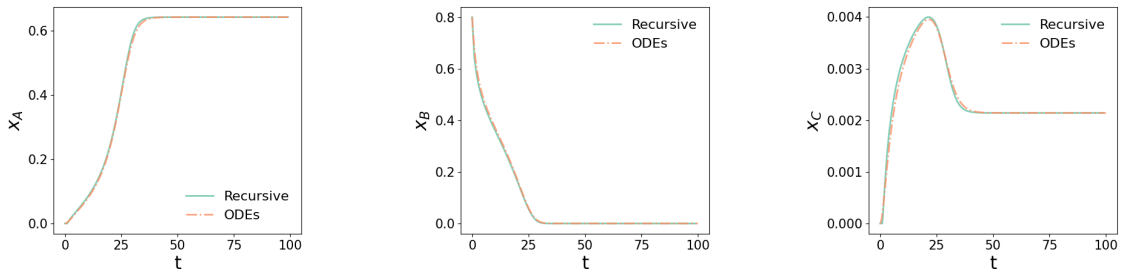

(a) (b) (c)

Figure 4.9: The evolution of the uncommitted fraction for the opinions A, B and C_1 (same as C_2, C_3, C_4, thus denoted as C) obtained by the recursive approach and the differential equations. The number of opinions $m = 6$, $P_A = 0.1$, and $P_{C_1} = P_{C_2} = P_{C_3} = P_{C_4} = 0.025$. Initially, all the uncommitted agents support the opinion B, $x_B(t = 0) = 0.8$.

4.5 The multi-opinion system on random networks

While, in principle, it is possible to develop a heterogeneous (degree-based) mean-field approximation scheme [120], [148], we do not pursue that approach here. Instead, we resort to the original agent-based simulation of the Naming Game (i.e., using node-based local update rules) to study the density evolution of agents supported by different opinions. We consider a similar problem discussed in the previous sections, and the difference is that all the single opinions are supported by committed agents. The opinion with the largest committed fraction is denoted as A. For simplicity, the other $m - 1$ opinions share the same fraction of committed fraction, p_0, and are initially supported by the same number of uncommitted agents. Hence, they are classified into one group, $\tilde{A}$ with the total committed fraction $P_{\tilde{A}} = (m - 1)p_0$. For the finite networked system, either the opinion A or one of the opinions in $\tilde{A}$ would dominate the system in the steady state. We are interested in the critical point, $P_A^{(c)}$, that enables the dominance by the opinion A, and the influence of the number of single opinions, m on the critical point.

4.5.1 The impact of random communication topology – ER networks

Networks generated by the Erdős-Rényi (ER) model [4] used with the same parameter may have different connectivities. As seen in Fig. 4.10, in some cases, the evolution of the system and the dominant opinion in the stable state differs from one realization to another. This variability arises due to the differences in the connectivity structure among agents across

realizations and the random selection order of agents as speakers and listeners. These factors introduce randomness in finite systems, leading to variations in the system's behavior.

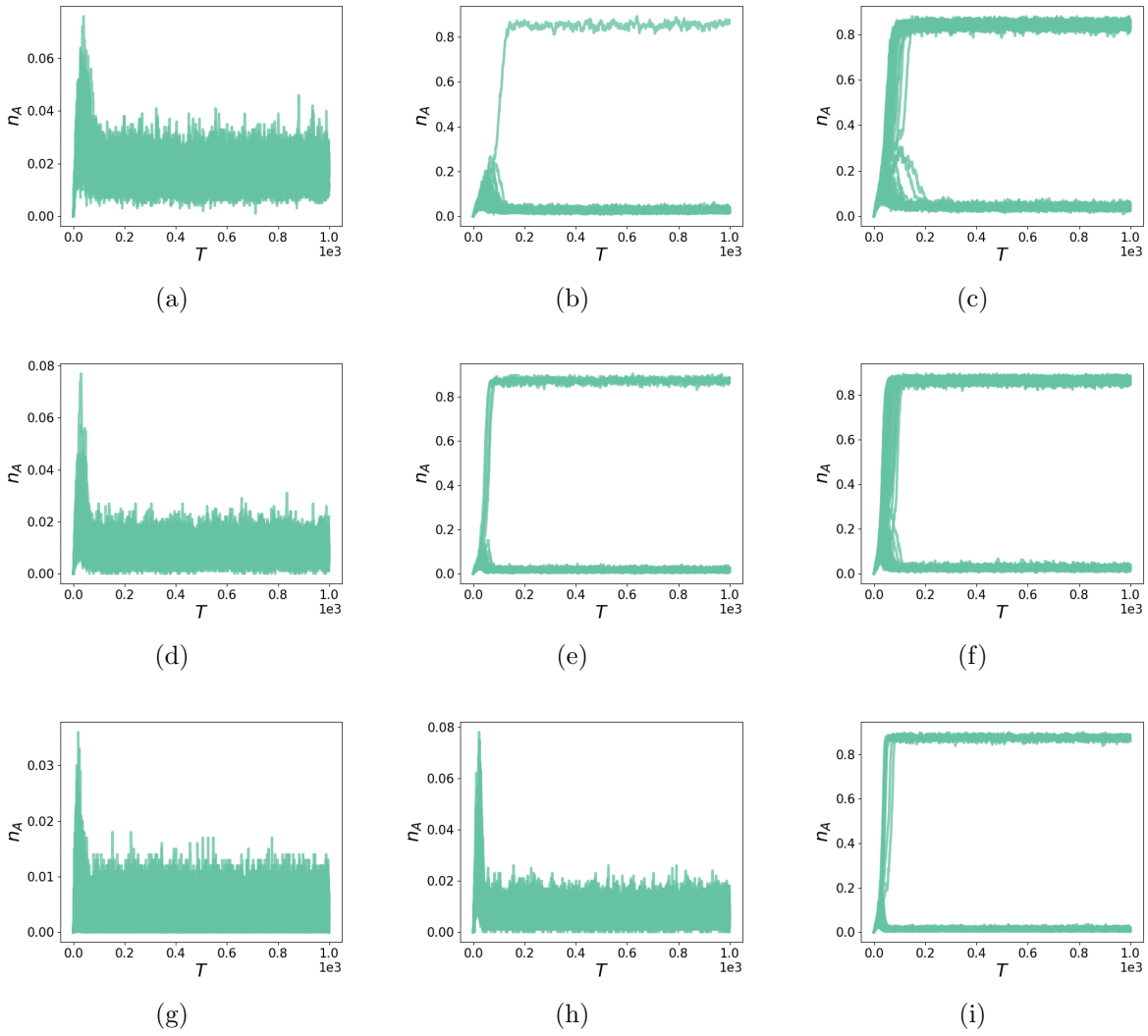

Figure 4.10: The fraction of agents supporting the opinion A changes with the interaction time on ER networks with $N = 1000$ agents. The number of single opinions $m = 5$, and the committed fraction of each opinion in the group $\tilde{A}$ is $p_0 = 0.01$. There are 50 realizations for each parameter setting. The average degrees are $\langle k \rangle = 6$ in panels (a) – (c), $\langle k \rangle = 8$ in panels (d) – (f), and $\langle k \rangle = 16$ in panels (g) – (i). For the committed size, in (a), (d), and (g), $P_A = 0.02$, in (b), (e), and (h), $P_A = 0.03$, in (c), (f), and (i), $P_A = 0.04$.

To represent the system state, the average fraction $\langle n_i \rangle$ of agents supporting the opinion i is defined in Eq. (4.12), where L is the number of realizations. Additionally, we introduce

the ratio R_i as the fraction of realizations that end up being dominated by the opinion i.

$$\langle n_i \rangle = \frac{1}{L} \sum_{j=1}^{L} n_i^{(j)} \tag{4.12}$$

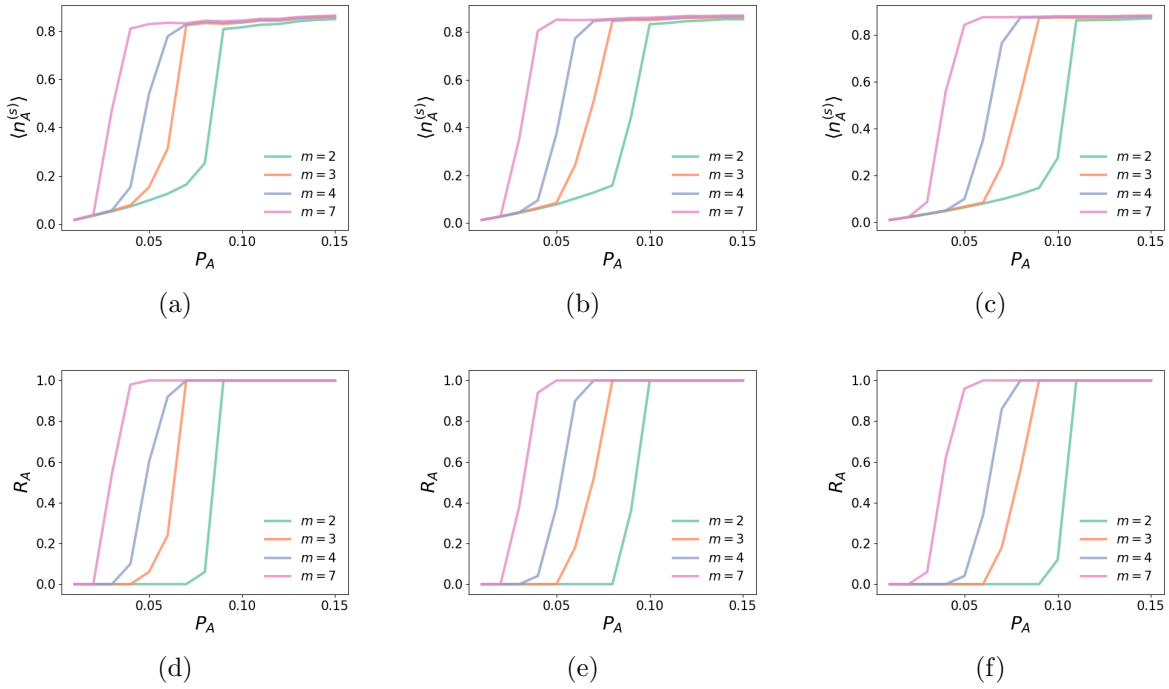

Figure 4.11: The system stable states change with the committed fraction P_A on ER networks with $N = 1000$ agents. $P_{\tilde{A}} = 0.06$. (a) – (c) $\langle n_A^{(s)} \rangle$ is the fraction of agents supporting A in the steady state, which is averaged over $L = 50$ realizations. (d) – (f) R_A is the fraction of realizations that end up with A dominant state. The average degrees are $\langle k \rangle = 6$ in (a) and (d), $\langle k \rangle = 8$ in (b) and (e), and $\langle k \rangle = 16$ in (c) and (f).

Fig. 4.11 shows that as the committed fraction P_A increases, there is a critical transition from a low density to the dominant state for the average number of agents holding opinion A, $\langle n_A^{(s)} \rangle$, as well as for the ratio R_A. To further investigate the transition on networks, we define the critical point on random networks, denoted by $P_A^{(c)}$, as the smallest committed fraction that enables the transition ratio R_A to exceed $\frac{1}{2}$ (Note that our chosen conventional cutoff value $\frac{1}{2}$ does not affect the findings). To analyze the relationship between the average degree $\langle k \rangle$ and the critical point $P_A^{(c)}$ on random networks, we examined complete graphs

and networks with varying $\langle k \rangle$, as shown in Figure 4.12. Our results indicate that as the number of single opinions m increases, the critical point $P_A^{(c)}$ decreases, in line with the divide and rule policy. Additionally, we observed that the critical point decreases as the average network degree decreases, suggesting that sparse random communication topologies may amplify the impact of committed members on the system, such that opinion A with the largest committed fraction is easier to dominate the system [148].

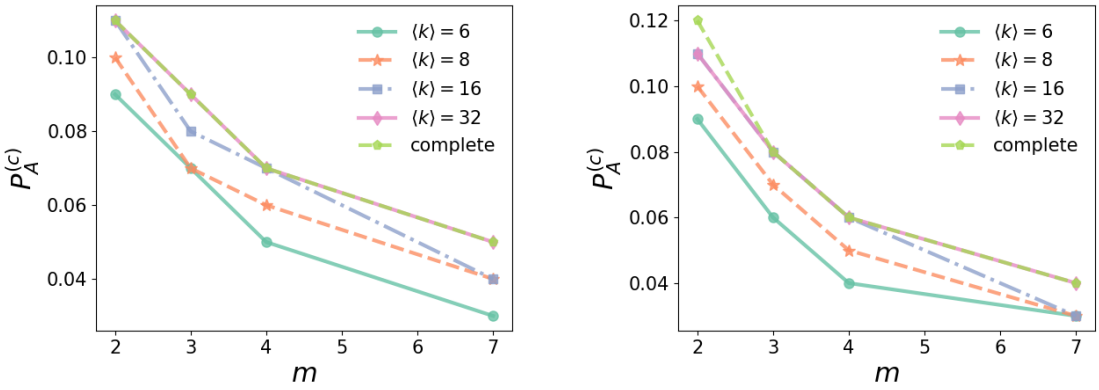

(a) (b)

Figure 4.12: The critical point $P_A^{(c)}$ changes with the number of single opinions on ER networks and is compared with complete graphs. The number of agents is $N = 1000$ in (a), and $N = 10000$ in (b). The total fraction of committed agents in the group $\tilde{A}$ is $P_{\tilde{A}} = 0.06$. The critical point is the smallest committed fraction which enables half of the realizations to stabilize with opinion A as a dominant state. The critical point increases as the average degree increases.

4.6 Discussions

In this study, we focus on the competition of the opinion with the largest fraction of committed agents against other opinions with committed agents and the opinion with the majority of uncommitted supporters. We study such competition using the original NG dynamics and its listener-only version. While continuous-time mean-field differential equations can accurately describe the opinion evolution for complete graphs in the infinite-size limit, the complexity of systems with multiple opinions grows exponentially, making direct integration of the corresponding differential equations impractical.

To address this challenge, we introduce two simplified scenarios, S_1 and S_2, which fea-

ture more symmetric setups. These scenarios significantly reduce computation complexity and they can provide upper and lower bounds for the critical point ($P_A^{(c)}$) of dominance transition in the scenario with an arbitrary distribution of committed agents. Through comparative analysis of critical transitions across the three scenarios, we highlight the significant influence of the distribution of committed agents within the minority committed group, $\tilde{A}$, in determining $P_A^{(c)}$. Specifically, the number of opinions and the distribution pattern of committed agents within group $\tilde{A}$ can either facilitate or hinder the propagation and eventual dominance of opinion A over uncommitted agents. When opinion B without committed followers is the primary competitor, augmenting the number of committed agents in $\tilde{A}$ can lower $P_A^{(c)}$ by diminishing the support for opinion B. Conversely, if agents committed to opinions other than A are the main opponents, increasing their number requires a higher fraction of agents committed to A, thereby raising the critical point.

Furthermore, to enhance the accuracy of depicting the NG opinion dynamics and capture critical transitions across various initial conditions in a computationally manageable manner, we develop the discrete-time recursive approach. This method focuses more on the evolution of single opinions by consolidating mixed states with the same opinion into a single variable and introducing the probability of a randomly chosen speaker communicating any single opinion. By streamlining computations while preserving the system's dynamics, this framework offers an efficient representation of NG dynamics in a complete graph.

Additionally, to gain insights into real-world opinion evolution, we conducted agent-based simulations to understand system dynamics and capture critical transitions across various finite-sized networks. In our experimental setup, the primary committed group advocates for opinion A, while the remaining agents, both committed and uncommitted, are evenly distributed among other minor committed opinions. Our observations reveal a strategy akin to the "divide and rule" policy, where dividing agents into more minor groups results in a reduced critical fraction of agents committed to A required for system dominance. This phenomenon suggests that segmenting agents facilitates the easier domination of the opinion with the largest committed size in the system.

While we presented two frameworks to simplify the multi-opinion NG model, there are some limitations to this work. Firstly, extending the theoretical analysis to networks of various topologies would provide a more comprehensive understanding of opinion dynamics in real-world scenarios. Secondly, we can introduce varied commitments to allow individuals

to stick to a single opinion temporarily while maintaining their long-term flexibility, particularly relevant for moderately committed agents. Thirdly, we would also like to extend the original Naming Game model from pairwise interactions to group interactions, allowing for the consideration of discussions within groups of friends, which is common in real-life situations.

CHAPTER 5
CONCLUSIONS AND OUTLOOK

In this thesis, we have investigated the realm of critical transitions, a phenomenon found ubiquitously across diverse systems. Leveraging the tools of network science, our explorations have spanned various aspects of network dynamics and critical phenomena. Specifically, we have explored the system resilience and dimension reduction within ecological systems, alongside investigating opinion dynamics within social systems.

Within the domain of ecological systems, our research has been primarily focused on understanding system resilience in response to external perturbations. Through our analysis, we have identified two distinct cluster modes associated with different system sizes and noise intensities, each exhibiting unique evolutionary patterns and statistical characteristics. The single-cluster phase exhibits random individual recovery lifetimes and exponential waiting time distributions, contrasting with the more deterministic evolution observed in the multi-cluster mode. We have further revealed the dependence of recovery time on system size and noise strength. Employing nucleation theory, we have discovered a universal scaling law, offering a framework to predict critical transitions and guide resilience restoration in complex dynamical systems. However, challenges remain in leveraging mean-field theory to simplify the study of critical transitions in noisy environments and addressing the complex interactions of real-world ecosystems. Future research efforts will concentrate on investigating diverse network topologies and fluctuation signals, as well as exploring stochastic switching phenomena to advance our understanding of critical transitions in ecological systems.

In our exploration of complex networks, computational challenges arise as the systems scale up. Dimension reduction has emerged as a powerful tool for simplifying complex network dynamics while preserving essential features. We have developed a degree-based mean-field framework to reduce the complexity of large networked systems. This framework involves classifying the network into clusters based on node degrees, where nodes within the same cluster exhibit similar degrees and dynamical evolutions. Each cluster is represented by one observable, capturing the degree-weighted average state. Consequently, the original network is described as an dimension-reduced system, preserving the original dynamical rules. Unlike previous one-dimensional mean-field approaches, this framework provides a more accurate approximation of state evolutions and tipping points of critical transitions,

particularly for heterogeneous networks and those with communities. We observe that the approximation accuracy improves as one increases network homogeneity, the distance to the tipping point of phase transition, and the number of clusters. Though the optimal number of clusters varies under different interaction strengths, it is consistently much smaller than the number of nodes in the original network. Moreover, this framework offers clear interpretation, with each variable in the dimension-reduced system representing the average of node states in its respective cluster. Beyond state approximation, the framework demonstrates potential applications in evaluating critical thresholds for system stability in time-delay dynamical systems, avoiding the need for numerical simulations or computing characteristic matrix eigenvalues. While promising, future research should address open questions regarding the impact of network topology and dynamics on the optimal number of clusters, and the development of theoretical guidelines for cluster partition.

Turning our attention to social systems, we have explored the dynamics of opinion spreading in the Naming Game model and observed critical transitions within such model. We focus on scenarios involving committed agents (or referred to as zealots) and uncommitted supporters, and examine how the opinion with the largest fraction of committed agents contends against other committed opinions and the majority uncommitted opinion. Leveraging mean-field theory, we have described the opinion dynamics for evolution on a complete graph in the infinite-size limit. To address computational complexities inherent in multi-opinion systems, we have devised two simplified scenarios and developed a recursive approach. Our comparisons of critical transitions across the two scenarios have revealed that committed agents within the minority group can either facilitate or impede the dominance of the largest committed group, depending on the initial opinion status. Moreover, these scenarios provide upper and lower bounds for estimating the critical threshold of the original system. Through agent-based simulations on random finite-sized networks, we have further elucidated the dynamics, highlighting how the divide-and-rule strategy influences the critical fraction required for opinion dominance. Additionally, our study serves as an abstract model of political contests, wherein the large committed group symbolizes government supporters, and minor committed groups represent divided opposition factions, which can be used to analyze significant social-political transformations. While our proposed frameworks can simplify the multi-opinion NG model, making it computationally easier to track the opinion evolution and capture tipping points, there are also some revenues for future explorations, including ex-

tending the theoretical analysis to networks of real-world characteristics, introducing varied commitments to allow committed individuals to only stick to a single opinion temporarily, and incorporating group interactions to allow for the consideration of discussions within groups of friends, which is common in real-life situations.

Across diverse systems ranging from ecological networks to biological dynamics and social opinion spreading, we have uncovered and examined the presence and importance of critical transitions. The identification of tipping points of such transitions has consistently been a focal point of our investigations, which enables us to comprehend and anticipate abrupt changes within systems, providing insights into their resilience and stability.

REFERENCES

[1] M. E. J. Newman, *Networks: An Introduction.* New York, NY, USA: Oxford University Press, 2010.

[2] A.-L. Barabási, *Network Science.* Cambridge, U.K.: Cambridge University Press, 2016.

[3] B. Bollobás, *Modern Graph Theory.* New York, NY, USA: Springer, 1998.

[4] P. Erdős and A. Rényi, "On the evolution of random graphs," *Publ. Math. Inst. Hungary. Acad. Sci.*, vol. 5, pp. 17–61, May 1960.

[5] A.-L. Barabási and R. Albert, "Emergence of scaling in random networks," *Science*, vol. 286, no. 5439, pp. 509–512, Oct. 1999.

[6] A.-L. Barabási and E. Bonabeau, "Scale-free networks," *Sci. Am.*, vol. 288, no. 5, pp. 60–69, May 2003.

[7] R. Albert and A.-L. Barabási, "Statistical mechanics of complex networks," *Rev. Mod. Phys.*, vol. 74, no. 1, pp. 47–97, Jan. 2002.

[8] D. J. Watts and S. H. Strogatz, "Collective dynamics of 'small-world' networks," *Nature*, vol. 393, no. 6684, pp. 440–442, Jun. 1998.

[9] S. H. Strogatz, "Exploring complex networks," *Nature*, vol. 410, no. 6825, pp. 268–276, Mar. 2001.

[10] M. Girvan and M. E. J. Newman, "Community structure in social and biological networks," *Proc. Natl. Acad. Sci. U.S.A.*, vol. 99, no. 12, pp. 7821–7826, Jun. 2002.

[11] G. Palla, I. Derényi, I. Farkas, and T. Vicsek, "Uncovering the overlapping community structure of complex networks in nature and society," *Nature*, vol. 435, no. 7043, pp. 814–818, Jun. 2005.

[12] B. Barzel and A.-L. Barabási, "Universality in network dynamics," *Nat. Phys.*, vol. 9, no. 10, pp. 673–681, Oct. 2013.

[13] X. Liu, D. Li, M. Ma, B. K. Szymanski, H. E. Stanley, and J. Gao, "Network resilience," *Phys. Rep.*, vol. 971, pp. 1–108, Aug. 2022.

[14] R. Cohen, K. Erez, D. Ben-Avraham, and S. Havlin, "Resilience of the internet to random breakdowns," *Phys. Rev. Lett.*, vol. 85, no. 21, pp. 4626–4628, Nov. 2000.

[15] C. S. Holling, "Resilience and stability of ecological systems," *Annu. Rev. Ecol. Evol. Syst.*, vol. 4, no. 1, pp. 1–23, Nov. 1973.

[16] J. Gao, B. Barzel, and A.-L. Barabási, "Universal resilience patterns in complex networks," *Nature*, vol. 530, no. 7590, pp. 307–312, Feb. 2016.

[17] E. Laurence, N. Doyon, L. J. Dubé, and P. Desrosiers, "Spectral dimension reduction of complex dynamical networks," *Phys. Rev. X*, vol. 9, no. 1, Mar. 2019, Art. no. 011042.

[18] A. Vespignani, "Modelling dynamical processes in complex socio-technical systems," *Nat. Phys.*, vol. 8, no. 1, pp. 32–39, Jan. 2012.

[19] C. Castellano, S. Fortunato, and V. Loreto, "Statistical physics of social dynamics," *Rev. Mod. Phys.*, vol. 81, no. 2, pp. 591–646, May 2009.

[20] M. Mobilia, A. Petersen, and S. Redner, "On the role of zealotry in the voter model," *J. Stat. Mech.: Theory Exp.*, vol. 2007, no. 08, Aug. 2007, Art. no. P08029.

[21] J. Xie, S. Sreenivasan, G. Korniss, W. Zhang, C. Lim, and B. K. Szymanski, "Social consensus through the influence of committed minorities," *Phys. Rev. E*, vol. 84, no. 1, Jul. 2011, Art. no. 011130.

[22] G. Verma, A. Swami, and K. Chan, "The impact of competing zealots on opinion dynamics," *Physica A*, vol. 395, pp. 310–331, Feb. 2014.

[23] A. Baronchelli, M. Felici, V. Loreto, E. Caglioti, and L. Steels, "Sharp transition towards shared vocabularies in multi-agent systems," *J. Stat. Mech.: Theory Exp.*, vol. 2006, no. 06, Jun. 2006, Art. no. P06014.

[24] X. Niu, C. Doyle, G. Korniss, and B. K. Szymanski, "The impact of variable commitment in the naming game on consensus formation," *Sci. Rep.*, vol. 7, no. 1, Feb. 2017, Art. no. 41750.

[25] M. Scheffer, S. Carpenter, J. A. Foley, C. Folke, and B. Walker, "Catastrophic shifts in ecosystems," *Nature*, vol. 413, no. 6856, pp. 591–596, Oct. 2001.

[26] M. Scheffer, S. R. Carpenter, V. Dakos, and E. H. van Nes, "Generic indicators of ecological resilience: Inferring the chance of a critical transition," *Annu. Rev. Ecol. Evol. Syst.*, vol. 46, no. 1, pp. 145–167, Dec. 2015.

[27] I. Dobson, B. A. Carreras, V. E. Lynch, and D. E. Newman, "Complex systems analysis of series of blackouts: Cascading failure, critical points, and self-organization," *Chaos*, vol. 17, no. 2, Jun. 2007, Art. no. 026103.

[28] R. M. May, S. A. Levin, and G. Sugihara, "Ecology for bankers," *Nature*, vol. 451, no. 7181, pp. 893–894, Feb. 2008.

[29] T. M. Lenton *et al.*, "Tipping elements in the Earth's climate system," *Proc. Natl. Acad. Sci. U.S.A.*, vol. 105, no. 6, pp. 1786–1793, Feb. 2008.

[30] I. A. van de Leemput *et al.*, "Critical slowing down as early warning for the onset and termination of depression," *Proc. Natl. Acad. Sci. U.S.A.*, vol. 111, no. 1, pp. 87–92, Jan. 2014.

[31] R. M. May, "Thresholds and breakpoints in ecosystems with a multiplicity of stable states," *Nature*, vol. 269, no. 5628, pp. 471–477, Oct. 1977.

[32] U. Feudel, "Complex dynamics in multistable systems," *Int. J. Bifurcation Chaos*, vol. 18, no. 06, pp. 1607–1626, Jun. 2008.

[33] V. Guttal and C. Jayaprakash, "Impact of noise on bistable ecological systems," *Ecol. Model.*, vol. 201, no. 3, pp. 420–428, Mar. 2007.

[34] B. Walker, C. S. Holling, S. R. Carpenter, and A. Kinzig, "Resilience, adaptability and transformability in social–ecological systems," *Ecol. Soc.*, vol. 9, no. 2, Dec. 2004, Art. no. 5.

[35] J. M. White and J. C. Stromberg, "Resilience, restoration, and riparian ecosystems: Case study of a dryland, urban river," *Restor. Ecol.*, vol. 19, no. 1, pp. 101–111, Jan. 2011.

[36] M. Devoto, S. Bailey, P. Craze, and J. Memmott, "Understanding and planning ecological restoration of plant–pollinator networks," *Ecol. Lett.*, vol. 15, no. 4, pp. 319–328, Jan. 2012.

[37] T. Yang *et al.*, "Delay and noise induced regime shift and enhanced stability in gene expression dynamics," *J. Stat. Mech.: Theory Exp.*, vol. 2014, no. 12, Dec. 2014, Art. no. P12015.

[38] C. Zeng *et al.*, "Noises-induced regime shifts and -enhanced stability under a model of lake approaching eutrophication," *Ecol. Complex.*, vol. 22, pp. 102–108, Jun. 2015.

[39] P. D'Odorico, F. Laio, and L. Ridolfi, "Noise-induced stability in dryland plant ecosystems," *Proc. Natl. Acad. Sci. U.S.A.*, vol. 102, no. 31, pp. 10 819–10 822, Aug. 2005.

[40] H. Sanhedrai, J. Gao, A. Bashan, M. Schwartz, S. Havlin, and B. Barzel, "Reviving a failed network through microscopic interventions," *Nat. Phys.*, vol. 18, no. 3, pp. 338–349, Mar. 2022.

[41] J. Liang, Y. Hu, G. Chen, and T. Zhou, "A universal indicator of critical state transitions in noisy complex networked systems," *Sci. Rep.*, vol. 7, no. 1, pp. 1–9, Feb. 2017.

[42] J. Jiang *et al.*, "Predicting tipping points in mutualistic networks through dimension reduction," *Proc. Natl. Acad. Sci. U.S.A.*, vol. 115, no. 4, pp. E639–E647, Jan. 2018.

[43] C. Tu, P. D'Odorico, and S. Suweis, "Dimensionality reduction of complex dynamical systems," *Iscience*, vol. 24, no. 1, Jan. 2021, Art. no. 101912.

[44] A. N. Kolmogorov, "A statistical theory for the recrystallization of metals," *Bull. Acad. Sci. USSR*, vol. 1, pp. 355–359, Jan. 1937.

[45] W. Johnson and R. Mehl, "Reaction kinetics in processes of nucleation and growth," *Trans. Am. Inst. Min. Metall. Eng.*, vol. 135, pp. 416–442, Dec. 1939.

[46] M. Avrami, "Kinetics of phase change. I General theory," *J. Chem. Phys.*, vol. 7, no. 12, pp. 1103–1112, Dec. 1939.

[47] J. Lothe and G. M. Pound, "Reconsiderations of nucleation theory," *J. Chem. Phys.*, vol. 36, no. 8, pp. 2080–2085, Apr. 1962.

[48] P. A. Rikvold, H. Tomita, S. Miyashita, and S. W. Sides, "Metastable lifetimes in a kinetic ising model: Dependence on field and system size," *Phys. Rev. E*, vol. 49, pp. 5080–5090, Jun. 1994.

[49] R. A. Ramos, P. A. Rikvold, and M. A. Novotny, "Test of the kolmogorov-johnson-mehl-avrami picture of metastable decay in a model with microscopic dynamics," *Phys. Rev. B*, vol. 59, pp. 9053–9069, Apr. 1999.

[50] Y. Ishibashi and Y. Takagi, "Note on ferroelectric domain switching," *J. Phys. Soc. Jpn.*, vol. 31, no. 2, pp. 506–510, Aug. 1971.

[51] H. M. Duiker and P. D. Beale, "Grain-size effects in ferroelectric switching," *Phys. Rev. B*, vol. 41, pp. 490–495, Jan. 1990.

[52] A. Gandhi, S. Levin, and S. Orszag, "Nucleation and relaxation from meta-stability in spatial ecological models," *J. Theor. Biol.*, vol. 200, no. 2, pp. 121–146, Sep. 1999.

[53] G. Korniss and T. Caraco, "Spatial dynamics of invasion: The geometry of introduced species," *J. Theor. Biol.*, vol. 233, no. 1, pp. 137–150, Mar. 2005.

[54] L. O'Malley, J. Basham, J. A. Yasi, G. Korniss, A. Allstadt, and T. Caraco, "Invasive advance of an advantageous mutation: Nucleation theory," *Theor. Popul. Biol.*, vol. 70, no. 4, pp. 464–478, Dec. 2006.

[55] A. Allstadt, T. Caraco, and G. Korniss, "Ecological invasion: Spatial clustering and the critical radius," *Evol. Ecol. Res.*, vol. 9, pp. 375–394, Aug. 2007.

[56] T. K. Michaels, M. B. Eppinga, and J. D. Bever, "A nucleation framework for transition between alternate states: Short-circuiting barriers to ecosystem recovery," *Ecology*, vol. 101, Jun. 2020, Art. no. e03099.

[57] C. Zeng, Q. Han, T. Yang, H. Wang, and Z. Jia, "Noise- and delay-induced regime shifts in an ecological system of vegetation," *J. Stat. Mech.: Theory Exp.*, vol. 2013, no. 10, Oct. 2013, Art. no. P10017.

[58] E. Forgoston and R. O. Moore, "A primer on noise-induced transitions in applied dynamical systems," *SIAM Review*, vol. 60, no. 4, pp. 969–1009, Jan. 2018.

[59] D. V. Alexandrov, I. A. Bashkirtseva, and L. B. Ryashko, "Noise-induced transitions and shifts in a climate–vegetation feedback model," *R. Soc. Open Sci.*, vol. 5, no. 4, Apr. 2018, Art. no. 171531.

[60] H. L. Richards, S. W. Sides, M. A. Novotny, and P. A. Rikvold, "Magnetization switching in nanoscale ferromagnetic grains: Description by a kinetic Ising model," *J. Magn. Magn. Mater.*, vol. 150, no. 1, pp. 37–50, Sep. 1995.

[61] C. H. Waddington, *The Strategy of the Genes*. London, U.K.: George Allen and Unwin, 1957.

[62] D. K. Wells, W. L. Kath, and A. E. Motter, "Control of stochastic and induced switching in biophysical networks," *Phys. Rev. X*, vol. 5, no. 3, Sep. 2015, Art. no. 031036.

[63] L. Xu, K. Zhang, and J. Wang, "Exploring the mechanisms of differentiation, dedifferentiation, reprogramming and transdifferentiation," *PLOS ONE*, vol. 9, no. 8, Aug. 2014, Art. no. e105216.

[64] H. Kramers, "Brownian motion in a field of force and the diffusion model of chemical reactions," *Physica*, vol. 7, no. 4, pp. 284–304, Apr. 1940.

[65] L. S. Tsimring and A. Pikovsky, "Noise-induced dynamics in bistable systems with delay," *Phys. Rev. Lett.*, vol. 87, no. 25, Nov. 2001, Art. no. 250602.

[66] C. Jiang, J. Gao, and M. Magdon-Ismail, "True nonlinear dynamics from incomplete networks," *AAAI*, vol. 34, no. 01, pp. 131–138, Apr. 2020.

[67] L. O'Malley, "The advance of an advantageous allele: nucleation, front propagation, and seasonal effects," Ph.D. dissertation, Rensselaer Polytechnic Institute, Troy, NY USA, 2008.

[68] J. N. Holland, D. L. DeAngelis, and J. L. Bronstein, "Population dynamics and mutualism: Functional responses of benefits and costs," *Am. Nat.*, vol. 159, no. 3, pp. 231–244, Mar. 2002.

[69] S. Suweis, F. Simini, J. R. Banavar, and A. Maritan, "Emergence of structural and dynamical properties of ecological mutualistic networks," *Nature*, vol. 500, no. 7463, pp. 449–452, Aug. 2013.

[70] W. Allee, O. Park, A. E. Emerson, T. Park, and K. P. Schmidt, *Principles of Animal Ecology*. Philadelphia, PA, USA: Saunders, 1949.

[71] V. Dakos, E. H. van Nes, R. Donangelo, H. Fort, and M. Scheffer, "Spatial correlation as leading indicator of catastrophic shifts," *Theor. Ecol.*, vol. 3, no. 3, pp. 163–174, Aug. 2010.

[72] S. Chen, E. B. O'Dea, J. M. Drake, and B. I. Epureanu, "Eigenvalues of the covariance matrix as early warning signals for critical transitions in ecological systems," *Sci. Rep.*, vol. 9, no. 1, Dec. 2019, Art. no. 2572.

[73] C. S. Holling, "Some characteristics of simple types of predation and parasitism," *Can. Entomol.*, vol. 91, no. 7, pp. 385–398, Jul. 1959.

[74] S. R. Carpenter, D. Ludwig, and W. A. Brock, "Management of eutrophication for lakes subject to potentially irreversible change," *Ecol. Appl.*, vol. 9, no. 3, pp. 751–771, Aug. 1999.

[75] M. Scheffer, *Ecology of Shallow Lakes*. London, U.K.: Chapman and Hall, 1998.

[76] S. Havlin *et al.*, "Challenges in network science: Applications to infrastructures, climate, social systems and economics," *Eur. Phys. J. Spec. Top.*, vol. 214, no. 1, pp. 273–293, Nov. 2012.

[77] J. Gao, A. Bashan, L. Shekhtman, and S. Havlin, *Introduction to Networks of Networks*. Bristol, U.K.: IOP Publishing, 2022.

[78] S. H. Strogatz, "From Kuramoto to Crawford: Exploring the onset of synchronization in populations of coupled oscillators," *Physica D*, vol. 143, no. 1, pp. 1–20, Sep. 2000.

[79] R. Pastor-Satorras and A. Vespignani, "Epidemic spreading in scale-free networks," *Phys. Rev. Lett.*, vol. 86, no. 14, pp. 3200–3203, Apr. 2001.

[80] L. M. Pecora, F. Sorrentino, A. M. Hagerstrom, T. E. Murphy, and R. Roy, "Cluster synchronization and isolated desynchronization in complex networks with symmetries," *Nat. Commun.*, vol. 5, no. 1, Jun. 2014, Art. no. 4079.

[81] M. T. Schaub, N. O'Clery, Y. N. Billeh, J.-C. Delvenne, R. Lambiotte, and M. Barahona, "Graph partitions and cluster synchronization in networks of oscillators," *Chaos*, vol. 26, no. 9, Sep. 2016, Art. no. 094821.

[82] D. Eroglu, M. Tanzi, S. van Strien, and T. Pereira, "Revealing dynamics, communities, and criticality from data," *Phys. Rev. X*, vol. 10, no. 2, Jun. 2020, Art. no. 021047.

[83] T. Pereira, S. van Strien, and M. Tanzi, "Heterogeneously coupled maps: Hub dynamics and emergence across connectivity layers," *J. Eur. Math. Soc.*, vol. 22, no. 7, pp. 2183–2252, Apr. 2020.

[84] H. Zhang, Q. Wang, W. Zhang, S. Havlin, and J. Gao, "Estimating comparable distances to tipping points across mutualistic systems by scaled recovery rates," *Nat. Ecol. Evol.*, vol. 6, no. 10, pp. 1524–1536, Aug. 2022.

[85] N. Naseri, F. Parastesh, F. Ghassemi, S. Jafari, E. Schöll, and J. Kurths, "Converting high-dimensional complex networks to lower-dimensional ones preserving synchronization features," *EPL*, vol. 140, no. 2, Oct. 2022, Art. no. 21001.

[86] M. Vegué, V. Thibeault, P. Desrosiers, and A. Allard, "Dimension reduction of dynamics on modular and heterogeneous directed networks," *PNAS Nexus*, vol. 2, May 2023, Art. no. 150.

[87] R. Olfati-Saber, J. A. Fax, and R. M. Murray, "Consensus and cooperation in networked multi-agent systems," *Proc. IEEE*, vol. 95, no. 1, pp. 215–233, Jan. 2007.

[88] T. Erneux, *Applied Delay Differential Equations*. New York, NY, USA: Springer, 2009.

[89] A. Otto, W. Just, and G. Radons, "Nonlinear dynamics of delay systems: An overview," *Philos. Trans. R. Soc. A*, vol. 377, no. 2153, pp. 1 – 6, Sep. 2019.

[90] A. Keane, B. Krauskopf, and C. M. Postlethwaite, "Climate models with delay differential equations," *Chaos*, vol. 27, no. 11, Nov. 2017, Art. no. 114309.

[91] R. M. May, "Time-delay versus stability in population models with two and three trophic levels," *Ecology*, vol. 54, no. 2, pp. 315–325, Mar. 1973.

[92] Y. Kuang, *Delay Differential Equations: With Applications in Population Dynamics*. Boston, MA, USA: Academic Press, 1993.

[93] M. Bando, K. Hasebe, A. Nakayama, A. Shibata, and Y. Sugiyama, "Dynamical model of traffic congestion and numerical simulation," *Phys. Rev. E*, vol. 51, no. 2, pp. 1035–1042, Feb. 1995.

[94] C. E. Riddalls and S. Bennett, "The stability of supply chains," *Int. J. Prod. Res.*, vol. 40, no. 2, pp. 459–475, Jan. 2002.

[95] G. E. Hutchinson, "Circular causal systems in ecology," *Ann. N. Y. Acad. Sci.*, vol. 50, no. 4, pp. 221–246, Dec. 1948.

[96] S. Ruan, "Absolute stability, conditional stability and bifurcation in Kolmogorov-type predator-prey systems with discrete delays," *Quart. Appl. Math.*, vol. 59, no. 1, pp. 159–173, Mar. 2001.

[97] R. Sipahi, S. Niculescu, C. T. Abdallah, W. Michiels, and K. Gu, "Stability and stabilization of systems with time delay," *IEEE Control Syst. Mag.*, vol. 31, no. 1, pp. 38–65, Feb. 2011.

[98] W. Qiao and R. Sipahi, "Rules and limitations of building delay-tolerant topologies for coupled systems," *Phys. Rev. E*, vol. 85, Jan 2012, Art. no. 016104.

[99] D. Hunt, G. Korniss, and B. K. Szymanski, "Network synchronization in a noisy environment with time delays: Fundamental limits and trade-offs," *Phys. Rev. Lett.*, vol. 105, no. 6, Aug. 2010, Art. no. 068701.

[100] D. Hunt, B. K. Szymanski, and G. Korniss, "Network coordination and synchronization in a noisy environment with time delays," *Phys. Rev. E*, vol. 86, no. 5, Nov. 2012, Art. no. 056114.

[101] D. Hunt, G. Korniss, and B. K. Szymanski, "The impact of competing time delays in coupled stochastic systems," *Phys. Lett. A*, vol. 375, no. 5, pp. 880–885, Jan. 2011.

[102] D. Hunt, F. Molnár, B. K. Szymanski, and G. Korniss, "Extreme fluctuations in stochastic network coordination with time delays," *Phys. Rev. E*, vol. 92, no. 6, Dec. 2015, Art. no. 062816.

[103] P. W. Holland, K. B. Laskey, and S. Leinhardt, "Stochastic blockmodels: First steps," *Soc. Netw.*, vol. 5, no. 2, pp. 109–137, Jun. 1983.

[104] H. R. Wilson and J. D. Cowan, "Excitatory and inhibitory interactions in localized populations of model neurons," *Biophys. J.*, vol. 12, no. 1, pp. 1–24, Jan. 1972.

[105] U. Alon, *An Introduction to Systems Biology: Design Principles of Biological Circuits*. New York, NY, USA: Chapman and Hall/CRC, 2006.

[106] G. Karlebach and R. Shamir, "Modelling and analysis of gene regulatory networks," *Nat. Rev. Mol. Cell Biol.*, vol. 9, no. 10, pp. 770–780, Oct. 2008.

[107] M. A. Buice and C. C. Chow, "Beyond mean field theory: Statistical field theory for neural networks," *J. Stat. Mech.: Theory Exp.*, vol. 2013, no. 03, Mar. 2013, Art. no. P03003.

[108] C. Bick, M. Goodfellow, C. R. Laing, and E. A. Martens, "Understanding the dynamics of biological and neural oscillator networks through exact mean-field reductions: A review," *J. Math. Neurosc.*, vol. 10, no. 1, May 2020, Art. no. 9.

[109] E. Pigani, D. Sgarbossa, S. Suweis, A. Maritan, and S. Azaele, "Delay effects on the stability of large ecosystems," *Proc. Natl. Acad. Sci. U.S.A.*, vol. 119, no. 45, Nov. 2022, Art. no. e2211449119.

[110] S. Ruan, "Delay differential equations in single species dynamics," *NATO ASI*, vol. 205, pp. 477 – 517, Dec. 2006.

[111] J. Dieudonne, *Foundations of Modern Analysis*. New York, NY, USA: Academic, 1969.

[112] C. Ma, G. Korniss, B. K. Szymanski, and J. Gao, "Universality of noise-induced resilience restoration in spatially-extended ecological systems," *Commun. Phys.*, vol. 4, no. 1, pp. 1–12, Dec. 2021.

[113] H. Zhang, X. Liu, Q. Wang, W. Zhang, and J. Gao, "Co-adaptation enhances the resilience of mutualistic networks," *J. R. Soc. Interface.*, vol. 17, no. 168, Jul. 2020, Art. no. 20200236.

[114] M. H. Degroot, "Reaching a consensus," *J. Am. Stat. Assoc.*, vol. 69, no. 345, pp. 118–121, Mar. 1974.

[115] M. Granovetter, "Threshold models of collective behavior," *Am. J. Sociol.*, vol. 83, no. 6, pp. 1420–1443, May 1978.

[116] S. Galam, "Application of statistical physics to politics," *Physica A*, vol. 274, no. 1, pp. 132–139, Dec. 1999.

[117] M. Anghel, Z. Toroczkai, K. E. Bassler, and G. Korniss, "Competition-driven network dynamics: Emergence of a scale-free leadership structure and collective efficiency," *Phys. Rev. Lett.*, vol. 92, no. 5, Feb. 2004, Art. no. 058701.

[118] V. Sood and S. Redner, "Voter model on heterogeneous graphs," *Phys. Rev. Lett.*, vol. 94, no. 17, May 2005, Art. no. 178701.

[119] M. Kitsak *et al.*, "Identification of influential spreaders in complex networks," *Nat. Phys.*, vol. 6, no. 11, pp. 888–893, Nov. 2010.

[120] A. Vespignani, "Modelling dynamical processes in complex socio-technical systems," *Nat. Phys.*, vol. 8, no. 1, pp. 32–39, Jan. 2012.

[121] Y. Dong, M. Zhan, G. Kou, Z. Ding, and H. Liang, "A survey on the fusion process in opinion dynamics," *Inform. Fusion*, vol. 43, pp. 57–65, Sep. 2018.

[122] G. Toscani, A. Tosin, and M. Zanella, "Opinion modeling on social media and marketing aspects," *Phys. Rev. E*, vol. 98, no. 2, Aug. 2018, Art. no. 022315.

[123] D. Bhat and S. Redner, "Nonuniversal opinion dynamics driven by opposing external influences," *Phys. Rev. E*, vol. 100, no. 5, Nov. 2019, Art. no. 050301.

[124] F. Baumann, I. M. Sokolov, and M. Tyloo, "A Laplacian approach to stubborn agents and their role in opinion formation on influence networks," *Physica A*, vol. 557, Nov. 2020, Art. no. 124869.

[125] V. C. Yang, M. Galesic, H. McGuinness, and A. Harutyunyan, "Dynamical system model predicts when social learners impair collective performance," *Proc. Natl. Acad. Sci. U.S.A.*, vol. 118, no. 35, Aug. 2021, Art. no. e2106292118.

[126] I. Iacopini, G. Petri, A. Baronchelli, and A. Barrat, "Group interactions modulate critical mass dynamics in social convention," *Commun. Phys.*, vol. 5, no. 1, pp. 1–10, Mar. 2022.

[127] K. Li, H. Liang, G. Kou, and Y. Dong, "Opinion dynamics model based on the cognitive dissonance: An agent-based simulation," *Inform. Fusion*, vol. 56, pp. 1–14, Apr. 2020.

[128] A. Baronchelli, V. Loreto, and L. Steels, "In-depth analysis of the naming game dynamics: The homogeneous mixing case," *Int. J. Mod. Phys. C*, vol. 19, no. 05, pp. 785–812, May 2008.

[129] M. Ye *et al.*, "Collective patterns of social diffusion are shaped by individual inertia and trend-seeking," *Nat. Commun.*, vol. 12, no. 1, Sep. 2021, Art. no. 5698.

[130] S. Galam and F. Jacobs, "The role of inflexible minorities in the breaking of democratic opinion dynamics," *Physica A*, vol. 381, pp. 366–376, Jul. 2007.

[131] J. Xie, J. Emenheiser, M. Kirby, S. Sreenivasan, B. K. Szymanski, and G. Korniss, "Evolution of opinions on social networks in the presence of competing committed groups," *PLOS ONE*, vol. 7, no. 3, Mar. 2012, Art. no. 33215.

[132] D. Centola, J. Becker, D. Brackbill, and A. Baronchelli, "Experimental evidence for tipping points in social convention," *Science*, vol. 360, no. 6393, pp. 1116–1119, Jun. 2018.

[133] L. Steels, "A self-organizing spatial vocabulary," *Artif. Life*, vol. 2, no. 3, pp. 319–332, Apr. 1995.

[134] Q. Lu, G. Korniss, and B. K. Szymanski, "Naming games in two-dimensional and small-world-connected random geometric networks," *Phys. Rev. E*, vol. 77, no. 1, Jan. 2008, Art. no. 016111.

[135] R.-R. Liu, C.-X. Jia, H.-X. Yang, and B.-H. Wang, "Naming game on small-world networks with geographical effects," *Physica A*, vol. 388, no. 17, pp. 3615–3620, Sep. 2009.

[136] Q. Lu, G. Korniss, and B. K. Szymanski, "The naming game in social networks: Community formation and consensus engineering," *J. Econ. Interact. Coord.*, vol. 4, no. 2, pp. 221–235, Nov. 2009.

[137] X. Castelló, A. Baronchelli, and V. Loreto, "Consensus and ordering in language dynamics," *Eur. Phys. J. B*, vol. 71, no. 4, pp. 557–564, Oct. 2009.

[138] A. M. Thompson, B. K. Szymanski, and C. C. Lim, "Propensity and stickiness in the naming game: Tipping fractions of minorities," *Phys. Rev. E*, vol. 90, no. 4, Oct. 2014, Art. no. 042809.

[139] Y. Gao, G. Chen, and R. H. M. Chan, "Naming game on networks: Let everyone be both speaker and hearer," *Sci. Rep.*, vol. 4, no. 1, Aug. 2014, Art. no. 6149.

[140] C. Doyle, S. Sreenivasan, B. K. Szymanski, and G. Korniss, "Social consensus and tipping points with opinion inertia," *Physica A*, vol. 443, pp. 316–323, Feb. 2016.

[141] G. Marchetti, M. Patriarca, and E. Heinsalu, "A bayesian approach to the naming game model," *Front. Phys.*, vol. 8, Feb. 2020, Art. no. 10.

[142] A. Waagen, G. Verma, K. Chan, A. Swami, and R. D'Souza, "Effect of zealotry in high-dimensional opinion dynamics models," *Phys. Rev. E*, vol. 91, no. 2, Feb. 2015, Art. no. 022811.

[143] W. Pickering, B. K. Szymanski, and C. Lim, "Analysis of the high-dimensional naming game with committed minorities," *Phys. Rev. E*, vol. 93, no. 5, May 2016, Art. no. 052311.

[144] J. Zhou, Y. Lou, G. Chen, and W. K. S. Tang, "Multi-language naming game," *Physica A*, vol. 496, pp. 620–634, Apr. 2018.

[145] Y. Lou, G. Chen, and J. Hu, "Communicating with sentences: A multi-word naming game model," *Physica A*, vol. 490, pp. 857–868, Jan. 2018.

[146] F. Heider, "Attitudes and cognitive organization," *J. Psychol.*, vol. 21, no. 1, pp. 107–112, Jan. 1946.

[147] A. Baronchelli, "Role of feedback and broadcasting in the naming game," *Phys. Rev. E*, vol. 83, no. 4, Apr. 2011, Art. no. 046103.

[148] W. Zhang, C. Lim, and B. K. Szymanski, "Analytic treatment of tipping points for social consensus in large random networks," *Phys. Rev. E*, vol. 86, Dec 2012, Art. no. 061134.